IN REPLY
REFER TO: WLO-72-60

Copy 6

DATE: 18 August 1960

TO: A. C. Angel

SUBJECT: Report of Preliminary Pitch Axis Analysis

Enclosure: Report of Preliminary Pitch Axis Analysis

Gentlemen:

Results of preliminary analyses of the pitch axis control system are presented in the enclosure. These results are subject to changes as dictated by simulator and aeroelastic studies now in progress. Additional analysis results are available at WLO if desired, however, the enclosed report covers the significant results.

STAT

Project Engineer

STAT

Senior Account Administrator

JBM:dll

Report of Preliminary Pitch Analysis

SECTION 1

ABSTRACT

This document contains results of preliminary analyses to determine suitable configurations for the pitch axis stability augmentation system and autopilot. Results are included for studies covering:

- A completely linear airplane - damper system.
- A linear damper controlling an airplane with non-linear static stability and non-linear manual control system.
- An autopilot with pitch attitude hold and Mach hold modes and automatic trim.
- Failsafety through redundant damper mechanization.

In each of these areas, configurations have been established which meet or exceed performance requirements with minimum complexity. Failsafety studies verify satisfactory vehicle protection for stability augmentation servo, gyro, or electronics ramp type failures. Preliminary estimates indicate adequate protection against autopilot failures except in the low altitude, high q region.

INTRODUCTION

Objectives

Preliminary analysis and design have been conducted to meet three basic design objectives:

1. Failsafety - Design the system such that one failure known to the pilot plus a second unknown failure will not result in a maneuver from which the pilot cannot recover.

   Primary effort toward this objective has been design and analysis of the redundant stability augmentation system. Continuing analysis of the autopilot and auto-trim systems will verify compliance with the objective or delineate action necessary to meet the objective.

2. Scheduling Complexity - Endeavor to achieve satisfactory performance with a minimum of air data scheduling in order to enhance system reliability.

   Due to the wide variations in aircraft dynamics, some system parameter scheduling has been necessary to meet the minimum performance requirements outlined in objective Number 3. At the same time however, the parameter scheduling has allowed the minimum performance requirements to be exceeded without additional complexity. Presently a total of 7 scheduling potentiometers and three altitude switches are required in the pitch axis, (includes damper redundancy). This represents a considerable reduction over similar systems with narrower aircraft dynamic variations.

3. Performance - Optimize performance at the design flight conditions; augment static stability during the approach and landing condition. Vehicle must possess reasonable handling qualities at all other flight conditions, but need not possess optimum performance.

As stated in Item 2, this objective has been reached and exceeded for the rigid vehicle. Most of the significant variations in performance which remain are due to large variations in weight and C.G. location which cannot be easily compensated for by scheduling.

Scope

The scope of analytical work at WLO has thus far been restricted mostly to small perturbation studies including only the rigid body aircraft equations of motion. In view of these restrictions, the configurations and results included herein are subject to changes delineated by aeroelastic studies and simulator results.

SECTION 3

SYSTEM CONFIGURATION

The pitch axis automatic control system consists of a redundant stability augmentation system working through series servos, and a single channel autopilot working through a parallel servo. Each available mode of the system will be discussed in terms of single channel operation, with aspects of multiple channel operation being discussed separately.

(a) Modes

(1) Stability Augmentation

The free airplane frequency and damping are augmented by a q'_c (pitot differential pressure) scheduled proportional pitch rate feedback to the series servo.

At high altitudes (above 62,000 feet) the static stability is further augmented by a lagged pitch rate signal. The gain and time constant of this term are fixed.

The above two terms are sufficient to provide good handling qualities throughout the flight envelope. However, the pitch attitude loop requires better inner loop damping at high altitudes than these two terms provide. This additional damping is obtained by adding more proportional pitch rate at high altitudes. This is easily accomplished by adding a lead term to the lagged pitch rate feedback. Thus, the damper equation is:

$$\delta_e = \dot{\theta}\left\{\delta_{\dot{\theta}} + \left[\frac{5\,(1+s)}{1+12s}\right]_{h \geq 62{,}000}\right\} \quad \text{where: } \delta_{\dot{\theta}} = f(q'_c)$$

The damper block diagram is shown in Figure 3.1.

(2) Attitude Hold

The Pitch Attitude Hold mode configuration is illustrated by a portion of the block diagram in Figure 3.1. The system consists of the stability augmentation system discussed above and a proportional parallel servo driven by lagged pitch attitude error. As noted, the low-pass time constant is scheduled with log Ps as shown in Figure 3.2. The gain of the pitch attitude loop, δ_{θ_L}, is scheduled with both log q'_c and log Ps as shown in Figure 3.3. The control equation for the mode is:

$$\delta_e = \frac{\theta_\varepsilon \, \delta_{\theta_L}}{1 + T_\theta S} + \dot{\theta}\left\{\delta_{\dot{\theta}} + \left[\frac{5\,(1+s)}{1+12s}\right] h \geq 62{,}000\right\}$$

(3) Mach Hold

Mach hold mode, described by the block diagram in Figure 3.1, utilizes the pitch attitude hold mode as an inner loop and two signals, $\Delta \log (R-1)$ and $\dot{\log (R-1)}$ provided by the air data computer. The air data quantities are proportional to Mach error, ΔM, and Mach rate, $\dot{M}$, respectively. The quantity R is the ratio of total pressure to static pressure. The ratio $\frac{\Delta \log (R-1)}{\Delta M}$ (in effect a variable gain in the Mach loop) is a function of Mach number which decreases as Mach increases.

The Mach signals are summed into the autopilot bridge such that they command lagged pitch attitude changes. An electromechanical integrator is used to provide an integrated Mach error signal necessary for accurate control of Mach number regardless of varying trim requirements.

Mach error and integral gains Θ_R and $\Theta\int_R$ are scheduled with log Ps as shown in Figure 3.4.

Mach rate gain is constant at 50 $\frac{\text{degrees pitch attitude}}{\text{unit of } \frac{\log (R-1)}{\text{sec}}}$

The control equation for Mach hold is:

$$\delta_e = \delta_{\Theta_L}\left\{\frac{\Theta_\varepsilon}{1+T_\Theta S} - \Delta\log(R-1)\left(\Theta_R + \frac{\Theta_{SR}}{S}\right) - \dot{\log(R-1)}\,\dot{\Theta}_R\right\}$$

$$\pm\dot{\Theta}\left\{\delta_{\dot{\Theta}} + \left[\frac{5(1+5s)}{1+12s}\right]_{h\geq 62{,}000'}\right\}$$

(4) Automatic Trim

The auto-trim system represented in the block diagram of Figure 3.1 consists principally of a switch sensing parallel servo position, an electrical trim actuator and a stability compensator. The switch is represented in the diagram as having a deadspot and hysteresis. A nominal switch deadspot of ±0.25 degrees of equivalent elevator deflection is recommended together with ±0.05° hysteresis. While on duty, the trim actuator will drive at a rate of 0.1 $\frac{\text{deg}}{\text{sec}}$ equivalent surface rate. The function of the auto trim system is to provide changes in trim elevator angle necessary to maintain 1 g flight and at the same time have negligible effect on dynamic response of the other automatic control modes.

(b) Redundant System

A redundant monitoring system was devised for the pitch damper mode to provide failsafe operation throughout the mission profile. The system consists of duplicate channels, A and B, each containing a pitch rate gyro, damper parameters $\delta_{\dot{\Theta}}$ and $\delta_{\dot{\Theta}L}$ and associated electronic circuitry, and the right and left series servos. In addition, the system includes a monitor channel, M, containing a pitch rate gyro, scheduling parameters and electronic circuitry, to monitor the gyro and electronics for Channels A and B. Initial

plans for a servo analog to monitor the redundant series servo channels were discarded because of the difficulty of designing an analog to duplicate the servo characteristics over the entire operative temperature range of the profile. The block diagram of the redundant channels is shown in Figure 3.5.

The redundant monitoring system detects and disengages a faulty channel whenever the following events occur:

(1) The voltage proportional to the displacement from center of a series servo differs from that of its mate in the same channel by the allowable difference $\mathcal{E} = 2.18° = (\delta_R - \delta_L)$.

(2) The voltage proportional to the output of the rate gyro and the gain scheduling electronics of one channel differs from that of another channel by the allowable difference $\mathcal{E} = 2.18° = (\delta_R + \delta_L)$.

The redundant pitch damper configuration was analyzed on an analog computer at fourteen flight conditions which were selected to yield a representative coverage of the mission profile. Series servo malfunctions and gyro and electronic malfunctions were simulated at series servo rates varying from the maximum servo rate of 15°/s down to 0.3°/s (slow, creeping failure). In both single and multiple channel malfunctions, the largest incremental g's resulted from the slow, creeping type of failures. The incremental peak g's obtained at the critical flight conditions 7, 8, and 10 - all high surface effectiveness conditions - are summarized below for failures in straight and level flight at a series servo rate of 0.3°/s:

	1st Failure		2nd Failure	
Malfunction:	Servo X_{AR}	Gyro X_A	Servo X_{BL}	Gyro X_B
Condition 7	.85 g's	.57 g's	1.0 g's	.75 g's
Condition 8	.87 g's	.55 g's	1.1 g's	.7 g's
Condition 10	.85 g's	.6 g's	.95 g's	.78 g's

In the first failure condition, one of the redundant operating channels fails due to a servo or gyro failure while the second channel continues operating. In the second failure condition, an operating channel has failed and been disengaged and a servo or gyro failure then occurs in the remaining operating channel.

Nominal values of $\mathcal{E} = 2.18° = (\delta_R - \delta_L)$ for servo malfunctions and $\mathcal{E} = 2.18° = (\delta_R + \delta_L)$ for gyro malfunctions; system dead time of 35 milliseconds, and servo recentering lag time of 50 milliseconds were used. The effect of varying the nominal values was also checked.

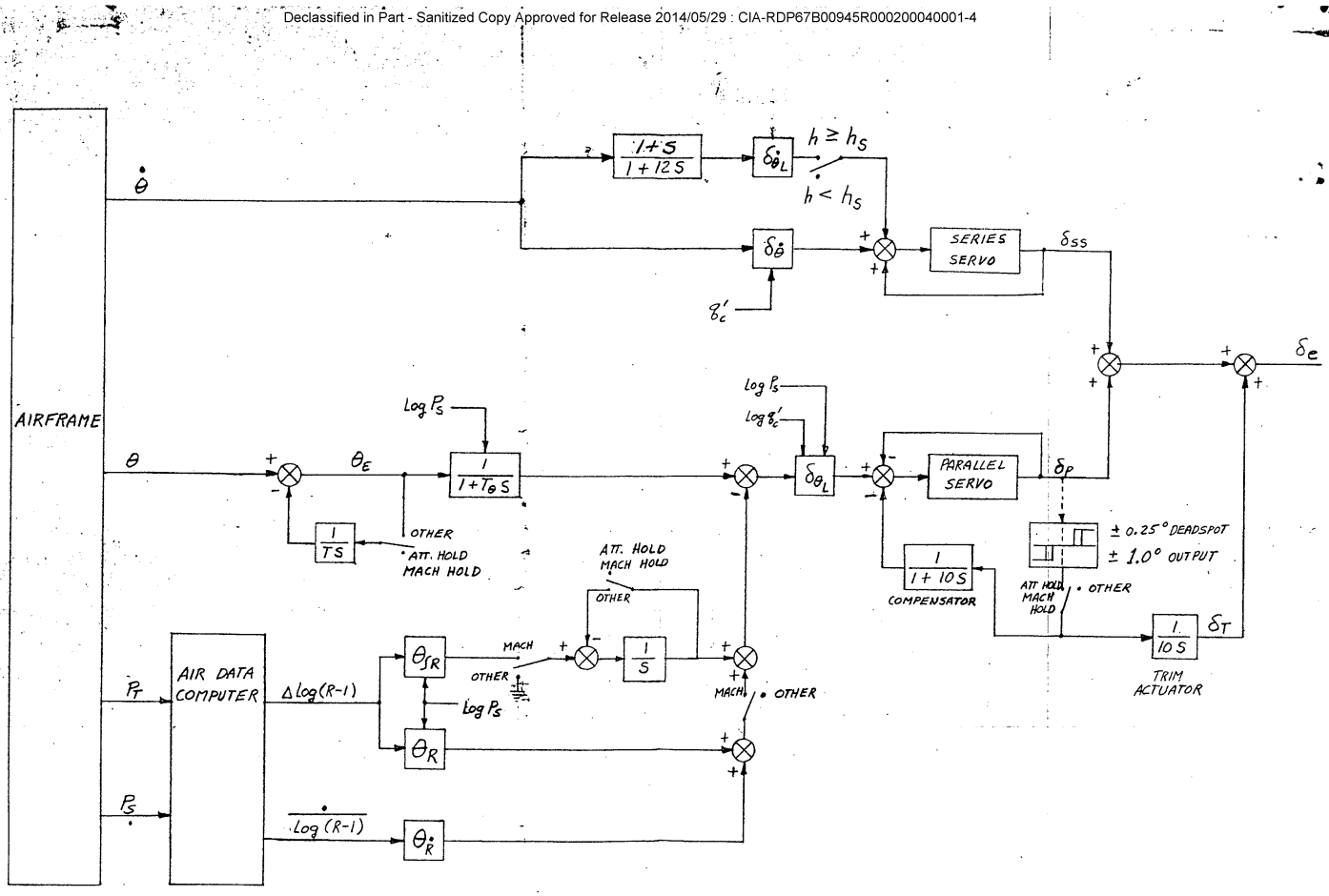

FIGURE 3.1 SINGLE CHANNEL DAMPER AND AUTOPILOT BLOCK DIAGRAM

FIGURE 5.2

PITCH ATTITUDE LOW PASS TIME CONSTANT SCHEDULE

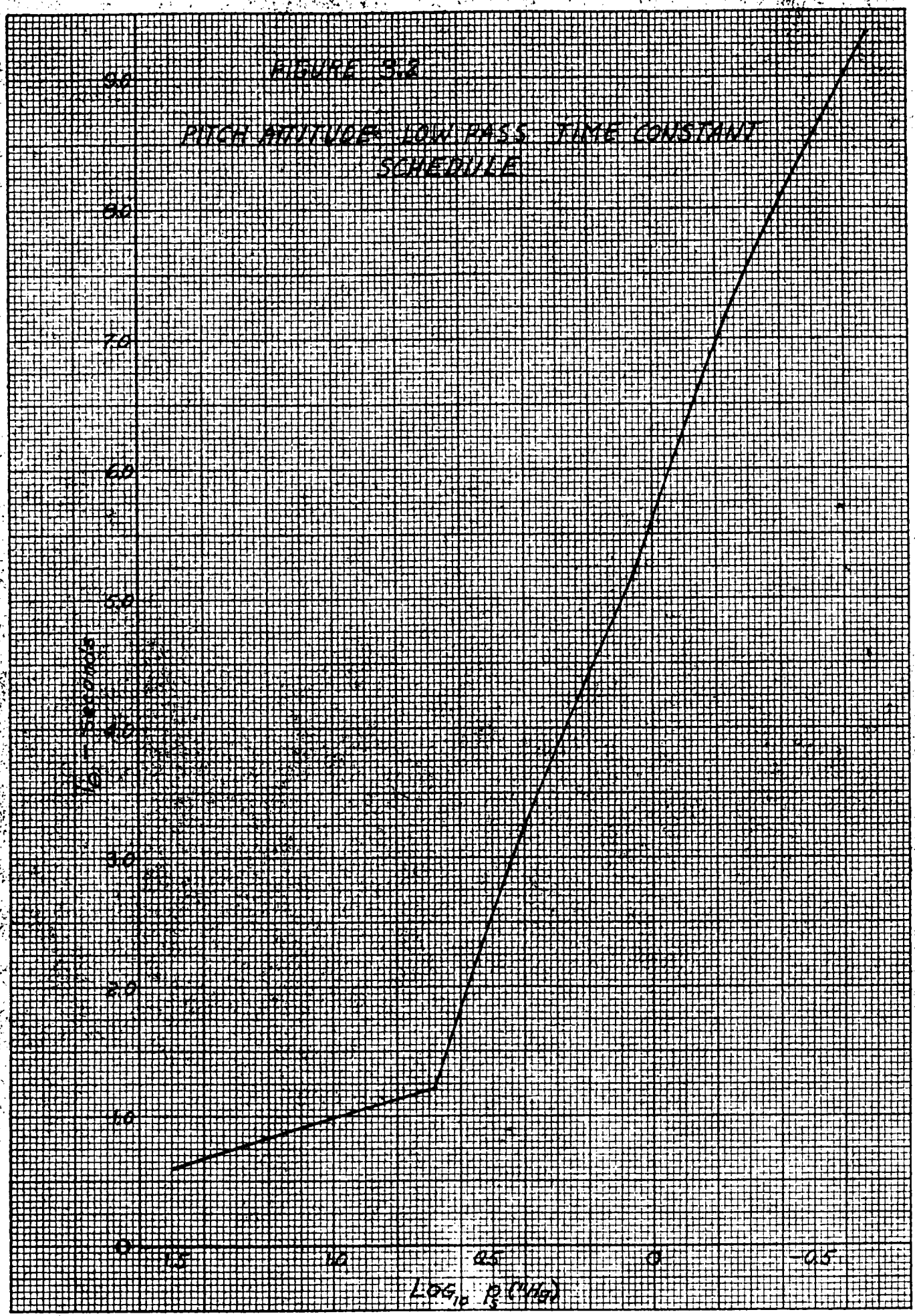

K&E 10 X 10 TO THE ½ INCH 359-11 KEUFFEL & ESSER CO. MADE IN U.S.A.

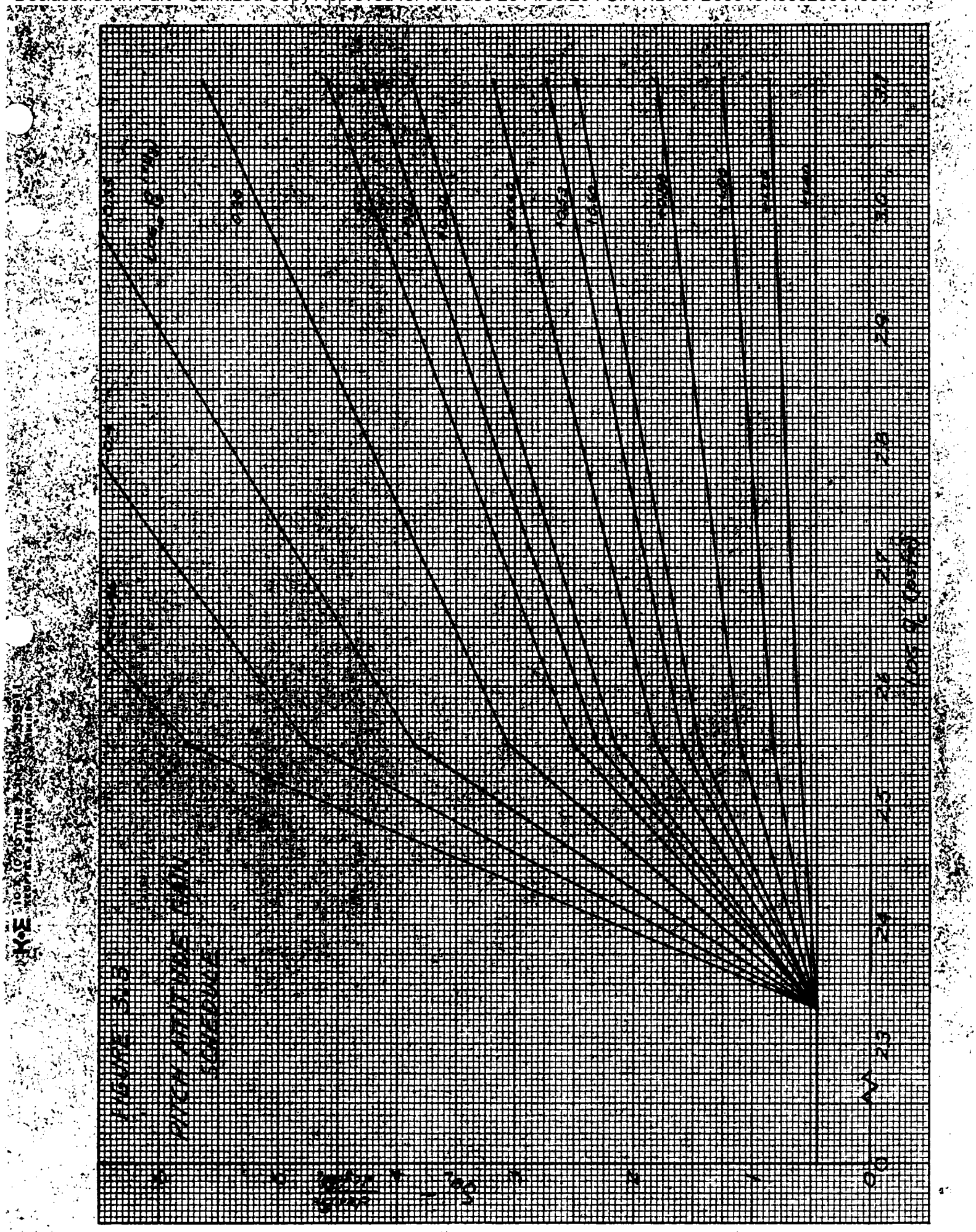

FIGURE 3.6 MACH DISPLACEMENT AND MACH INTEGRAL GAIN SCHEDULES

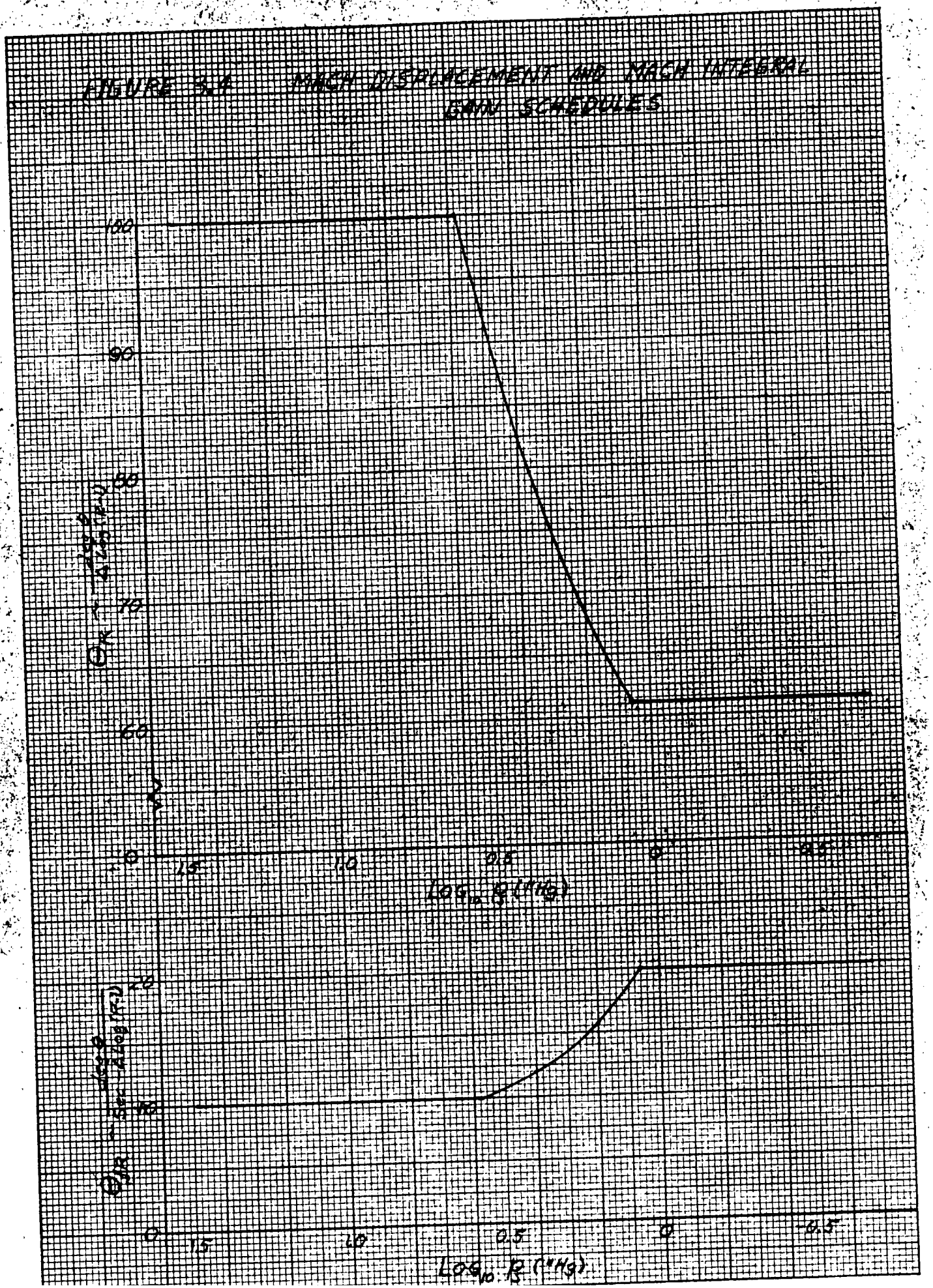

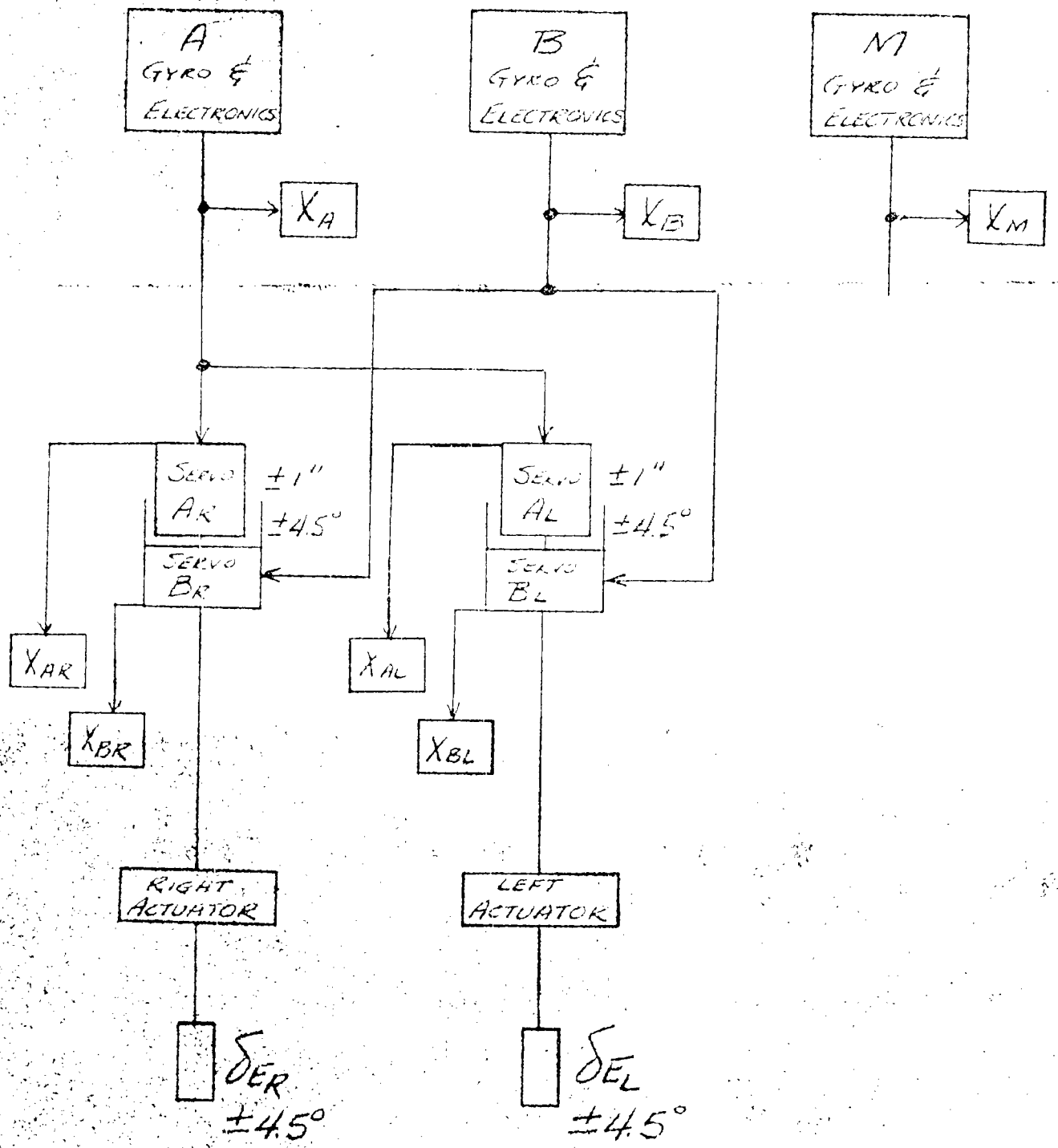

FIGURE 3.5 BLOCK DIAGRAM OF REDUNDANT PITCH DAMPER

PROBLEM AREAS

Three major problem areas are known to exist with this vehicle - pitch-up, speed instability, and aeroelasticity.

(a) Pitch-Up

The aircraft $C_{m_{C_L}}$ curves taken from wind tunnel data reverse slope indicating static instability at high altitudes and high lift coefficients. For this reason static stability is augmented with a lagged pitch rate feedback at altitudes above 62,000 feet. The choice of gain and time constant on this term is based on the assumption that the aircraft will never exceed 1% $\bar{c}$ negative static margin.

If future data shows that a negative static margin of more than 1% $\bar{c}$ can exist, or, that violent static instability can exist at lower altitudes then a damper change may be required.

(b) Speed Instability

The trim elevator versus Mach number curves show a speed instability problem at Mach numbers between 0.5 and 1.1 for altitudes below 36,000 feet. In this region the pilot would be required to pull back on the stick after an increase in speed. This is opposite to normal stick feel.

The problem is common to most high speed aircraft. However, it is accentuated in this case, because it occurs during refueling when the pilot is attempting to maintain precise control.

(b) (Cont'd)

Several schemes are available for providing an elevator trim angle as a function of Mach number.

The seriousness of the problem together with the schemes for alleviating it are currently being studied on a moving cab simulator.

(c) Aeroelasticity

Early structural analyses have shown that the vehicle will have five symmetric bending modes below 10 cps. The lowest frequency (or fundamental) will be in the neighborhood of 2 cps. The highest vehicle short period frequencies will be in the neighborhood of 1 cps. Thus, allowable low frequency phase margin will not permit extensive filtering, and, as a result, selection of a favorable gyro location becomes a necessity.

The analyses shown in this report are based on the assumption of a rigid vehicle and hence the gyro has no structural pickup. As a result the damper is likely to require some modifications once the aeroelastic problems are fully known.

ANALOG COMPUTER SIMULATIONS

Analog computer wiring diagrams used in the various pitch axis studies are included in this section. Separate diagrams are included for the linear damper and autopilot studies, for the non-linear damper study and for the failsafety study. A single list of airframe potentiometer settings, applicable to all of the diagrams, is given in Table 5.1.

(a) Linear Damper and Autopilot

The computer simulation is shown in Figure 5.1. For the linear damper studies, only the lift and pitching moment equations were used to describe the aircraft. The series servo was simulated as a second order system with natural frequency of 14.2 cps and damping ratio of 0.7. Early damper studies used a frequency of 30 cps, but traces included in this report are based on 14.2 cps. Servo authority was set at ±4.5° equivalent surface deflection. Unity gyro dynamics were used, and the power actuator was represented by a first order lag of 0.03 seconds.

Pitch attitude hold studies were also conducted with a two degree-of-freedom airplane. The parallel servo used in the attitude hold mode was simulated as a second order system with a natural frequency of 10 cps and a damping ratio of 0.9.

A third degree of freedom provided by the airspeed equation was included in the Mach hold studies to provide a computation of Mach error. Altitude rate was also computed to provide an additional term in the Mach error computation accounting for the effect of temperature lapse rate on Mach number. Dynamics of the air data computer have thusfar been simulated as a linear second order equation. The ADC has two separate channels, one driven by a q'_c signal and the other by a P_s signal. Although both loops affect

(a) (Cont'd)

Mach error computation, separate simulation of both channels is not justified in a preliminary analysis. The slower of the two channels, the P_S channel, was simulated to be conservative. The natural frequency varies from 2.3 radians/sec. at maximum altitude to 23 radians/sec. at sea level. A damping ratio of 0.8 was used.

Each of the air data pressure sources P_T and P_S has a tubing lag associated with it. It was agreed that this lag should not exceed 3 seconds if good Mach hold performance is to be maintained at maximum altitude. A single lag, Tss, was simulated with a linear variation on a semi-log plot from 3 seconds at maximum altitude through 0.1 seconds at 30,000 feet. Both the pressure source lag and the ADC dynamics were applied to the sum of all of the Mach signals to avoid multiple simulation.

Simulation of the auto-trim switch is accomplished with a pair of relay amplifiers which are biased to energize when parallel servo displacement exceeds the bias. One relay simulates each side of the switch. When a relay is energized, a second bias signal is switched into the circuit to provide switch hysteresis. When either relay is energized it also provides a step input to the trim actuator and the stability compensating lag network.

(b) Non-Linear Damper

The non-linear damper simulation consisted of the linear short period pitch aircraft characteristics at flight conditions 17 and below. At flight conditions 18 and above, the non-linear slope of the variable $M_\alpha \alpha$, (the pitching moment due to angle of attack changes times the angle of attack change,) was simulated on a

(b) (Cont'd)

non-linear function generator. The dynamics of the series servo were mechanized as a second order loop with natural frequency of ω = 30 cps and damping ratio of ζ = 0.8. The servo rate limits of 15°/sec and displacement limits of ±4.5° were included. A first order lag of $\frac{1}{1 + .03\,S}$ represents the actuator dynamics, and the rate gyro dynamics were neglected. The manual control system breakout force of 2.5# stick force was simulated by a deadspot circuit. The coulomb friction of 2.5# stickforce was approximated by a hysteresis circuit. The effect of the bobweight was included in the simulation by feeding a normal acceleration signal at 5#/g into the stick force circuit. A second order loop was used to simulate a spring rate of 3.9#/in. and a viscous damping term sufficient to make ζ = 0.7. A control system mass of 0.3 slugs was used. The non-linear gearing of the stick, δ_c/λ, was simulated on the non-linear function generator.

The computer diagram is shown in Figures 5.2 and 5.2 b.

(c) Failsafety, Redundant System

The pitch aircraft equations of motion for angle of attack and pitching moment variations were used. At flight conditions 17 and below, the variations were linear. At flight conditions 18 and above, the non-linear slope of the variable $M_\alpha \alpha$ was simulated on function generators.

The redundant channels A, B, and M were simulated with identical circuitry on analog computers. The pitch rate gyro, the series servo, and the hydraulic and linkage thresholds were simulated as one lumped system threshold of 0.052 degrees of surface in channel A and in channel B to conserve amplifiers. The gyro

threshold in channel M was neglected. The gyro dynamics were neglected in all channels. The servo dynamics of ω = 30 cps and ζ = .8 were simulated in a second order loop for each redundant servo. The servo rate limit of 15 °/s was included. A first order lag of $\frac{1}{1 + .03\,S}$ was used to approximate the actuator dynamics. The actuator rate limits of 30 °/s were not simulated. Since the manual control system was not simulated, and no manual elevator commands were used in the analysis, the elevator summing amplifier was limited to the series servo authority limits of ±4.5°.

The hardware mechanization of the redundant series servos utilizes a series hook-up between the A and B channel servos in each right and left actuator linkage (Reference Figure 3.5). Here, the two servos track together to drive the associated actuator in normal system operation. The servo output authority is 15°/s and ±4.5°. of actuator motion whether one or both servos are operating. The electrical analog of the mechanical system utilized a parallel hook-up between the A and B channel servos in each right and left actuator simulation to achieve the same servo behavior effect in both normal and malfunctioning operation. Here, each servo shared the load of driving the right and left actuators in normal operation. During malfunctioning operation, the gain of the servo output is doubled to provide full authority to each servo in the malfunctioning channel. The analog computer diagrams are shown in Figure 5.3.a and 5.3.b.

(c) (Cont'd)

The detection and disengagement of a faulty channel was simulated with relay logic. The voltage difference between two servos outputs (for example: X_{AR} and X_{AL} in channel A) was fed to a biased relay amplifier. In the event that a malfunction occurred, this difference exceeded the bias, and the relay energized and fed a fixed voltage into an integrator. After a predetermined time delay or system dead time elapsed, the integrator output exceeded the bias of a second relay amplifier. The second relay then energized and its contacts disengaged the malfunctioning channel by removing the input and recentered the servos in that channel with a first order lag network in the servo simulation. A similar process occurred for gyro and electronic malfunction simulations. In this analysis, a 5:1 time scale (machine time = 5 x real time) was used to minimize the inherent relay lags.

The servo and gyro malfunctions were simulated by feeding ramps of varying rates into the appropriate amplifiers.

TABLE 5.1 CORRECTED ANALOG COMPUTER POT SETTINGS FOR LINEAR DAMPER AND AUTOPILOT STUDIES

Pot	Value	1*	2*	3*	4	5	6	7	8	9	10	11*	12*	13	14	15	16	17	18	19	20	21	22	23	24*	25	26*	27	28*	29	30
A1	$-Z_w/4$	.203	.126	.133	.503	.324	.231	.681	.437	.323	.367	.164	.238	.120	.234	.315	.091	.120	.127	.133	.051	.054	.056	.049	.024	.020	.024	.024	.027	.017	.018
A2	$-Z_\delta/U_1$	.252	.158	.165	.553	.347	.243	.772	.484	.341	.293	.175	.259	.140	.261	.180	.094	.065	.052	.047	.017	.017	.016	.012	.007	.006	.007	.006	.008	.005	.004
A3	$\alpha_g/100$	.782	.782	.524	.526	.526	.526	.386	.386	.386	.283	.360	.377	.585	.352	.245	.336	.253	.189	.151	.138	.112	.095	.086	.094	.111	.093	.085	.092	.091	.083
A4	$T_\delta U_1/57.3g$	.012	.012	.018	.030	.030	.030	.041	.041	.041	.056	.044	.042	.027	.049	.065	.047	.063	.084	.108	.119	.118	.174	.192	.177	.150	.179	.195	.181	.182	.201
A5	$T_\delta U_1/57.3g$	.012	.012	.018	.030	.030	.030	.041	.041	.041	.056	.044	.042	.027	.049	.065	.047	.063	.084	.108	.119	.118	.174	.192	.177	.150	.179	.195	.181	.182	.201
A6	$-M_\delta/4$	.304	.230	.217	.773	.597	.374	1.0	.835	.530	.715	.264	.365	.214	.447	.661	.161	.240	.219	.210	.079	.078	.078	.070	.035	.029	.033	.035	.030	.023	.024
A7	$-M_\dot{\alpha}/4$	.141	.108	.103	.364	.279	.175	.514	.394	.247	0	.123	.169	.101	.208	0	.076	0	0	0	0	0	0	0	0	0	0	0	0	0	0
A8	$+M_\dot{\alpha}$	0	0	0	0	0	0	0	0	0	.145	0	0	0	0	.494	0	.180	.029	.041	.021	.024	.014	.011	.006	.009	.006	.005	.006	.004	.004
A9	$-M_\alpha/20$ $(\Delta n=1)$	0	0	.051	0	0	.147	0	0	.325	.489	.218	0	0	.110	.865	0	.287	.403	.473	.136	.140	.134	.092	0	0	0	0	.076	0	0
A10	$-M_\alpha$ $(\Delta n=1)$	0	0	0	0	0	0	0	0	0	0	0	.758	0	0	0	.832	0	.349	.396	.068	.073	.060	.092	.865	.093	.545	.497	0	.424	.496
A11	$+M_\alpha/10$ $(\Delta n=1)$	.020	.036	0	.124	.227	0	.053	.360	0	0	0	0	.076	0	0	0	0	0	0	0	0	0	.690	0	0	0	0	.492	0	0
A12	$-M_\delta/40$	.061	.052	.070	.343	.264	.165	.670	.517	.326	.574	.184	.241	.092	.361	.416	.121	.144	.161	.184	0	0	0	0	0	0	0	0	0	0	0
B1	$-500\frac{M_\alpha}{T_\delta}g$	0	0	0	.056	.056	.056	.056	.056	.056	.134	.108	.118	.071	.056	.190	0	0	0	0	.083	.080	.086	.082	.039	.031	.037	.041	.034	.026	.027
B2	$-Z_{\dot{w}}$	.293	.292	.198	.123	.122	.124	.099	.097	.098	.135	.096	.097	.136	.092	.042	.096	.054	.028	.022	+ 0	0	0	0	.216	.179	.212	.232	.207	.204	.222
B3	$-M_{\dot{w}}/10$	.002	0	0	0	0	0	.021	.021	.010	.504	.048	.061	0	.151	.099	.157	.105	0	0	.021	.014	.011	.013	.012	.014	.011	.011	.012	.011	.012
B4	$+M_{\dot{w}}$	0	.018	.028	.013	.020	.089	0	0	0	0	0	0	.036	0	0	0	0	.380	.377	0	0	0	0	0	0	0	0	0	0	0
B5	$-10X_{\dot{w}}$	.527	.740	.371	.117	.102	.136	.131	.092	.082	.472	.098	.083	.192	.056	.095	.106	.048	.049	.048	.646	.665	.676	.620	.763	.969	.755	.779	.347	.531	.532
B6	$-10X_w$	.200	1.099	.861	.301	.454	.460	.154	.224	.265	.054	.480	.371	.530	.209	.098	.327	.610	.154	.123	.033	.023	.017	.022	.022	.014	.022	.013	.022	.031	.016
B7	$10g/U_1$	1.440	1.440	.960	.576	.576	.576	.424	.424	.424	.310	.396	.413	.641	.266	.267	.369	.277	.208	.166	.144	.103	.096	.072	.090	.106	.089	.085	.083	.088	.074
B8	$10M_\delta/57.3$	.036	.036	.053	.090	.090	.090	.123	.123	.123	.183	.145	.145	.090	.163	.221	.163	.221	.297	.374	.151	.123	.104	.095	.103	.121	.102	.093	.101	.100	.091
B9	$\theta_R/200$	0	0	0	.250	.250	.250	.250	.250	.250	.250	.250	.250	.250	.250	.250	.250	.250	.250	.250	.412	.508	.599	.652	.599	.508	.599	.652	.599	.599	.652
B10	$\theta_R/200$	0	0	0	.500	.500	.500	.500	.500	.500	.500	.500	.500	.500	.500	.500	.475	.475	.475	.475	.320	.320	.320	.306	.300	.300	.300	.300	.300	.300	.300
B11	$\theta_{TR}/200$	0	0	0	.050	.050	.050	.050	.050	.050	.050	.050	.050	.050	.050	.050	.052	.052	.052	.052	.090	.090	.090	.100	.100	.100	.100	.100	.100	.100	.100
A1'	$\delta_e/10$	.045	.045	.045	.045	.045	.045	.045	.045	.045	.087	.083	.072	.045	.098	.125	.045	.151	.213	.261	.287	.349	.408	.436	.373	.246	.352	.388	.505	.357	.554
A2'	$\delta_L/10$	0	0	0	0	0	0	0	0	0	0	0	0	0	0	0	0	0	0	0	.500	.500	.500	.500	.500	.500	.500	.500	.500	.500	.500
A3'	$\delta_R/10$	.100	.100	.100	.100	.100	.100	.025	.025	.025	.025	.098	.10	.10	.084	.025	.10	.10	.040	.025	.072	.025	.025	.025	.064	.100	.090	.069	.100	.100	.100
A4'	$\frac{1}{10}\frac{d\alpha_W(R-T)}{dM}$	1.00	1.00	.726	.465	.465	.465	.357	.357	.357	.256	.312	.312	.465	.282	.215	.282	.215	.161	.124	/ .961	.804	.664	.575	.664	.804	.664	.574	.664	.664	.574

FIGURE 5.1 ANALOG COMPUTER DIAGRAM FOR LINEAR DAMPER AND AUTOPILOT STUDIES

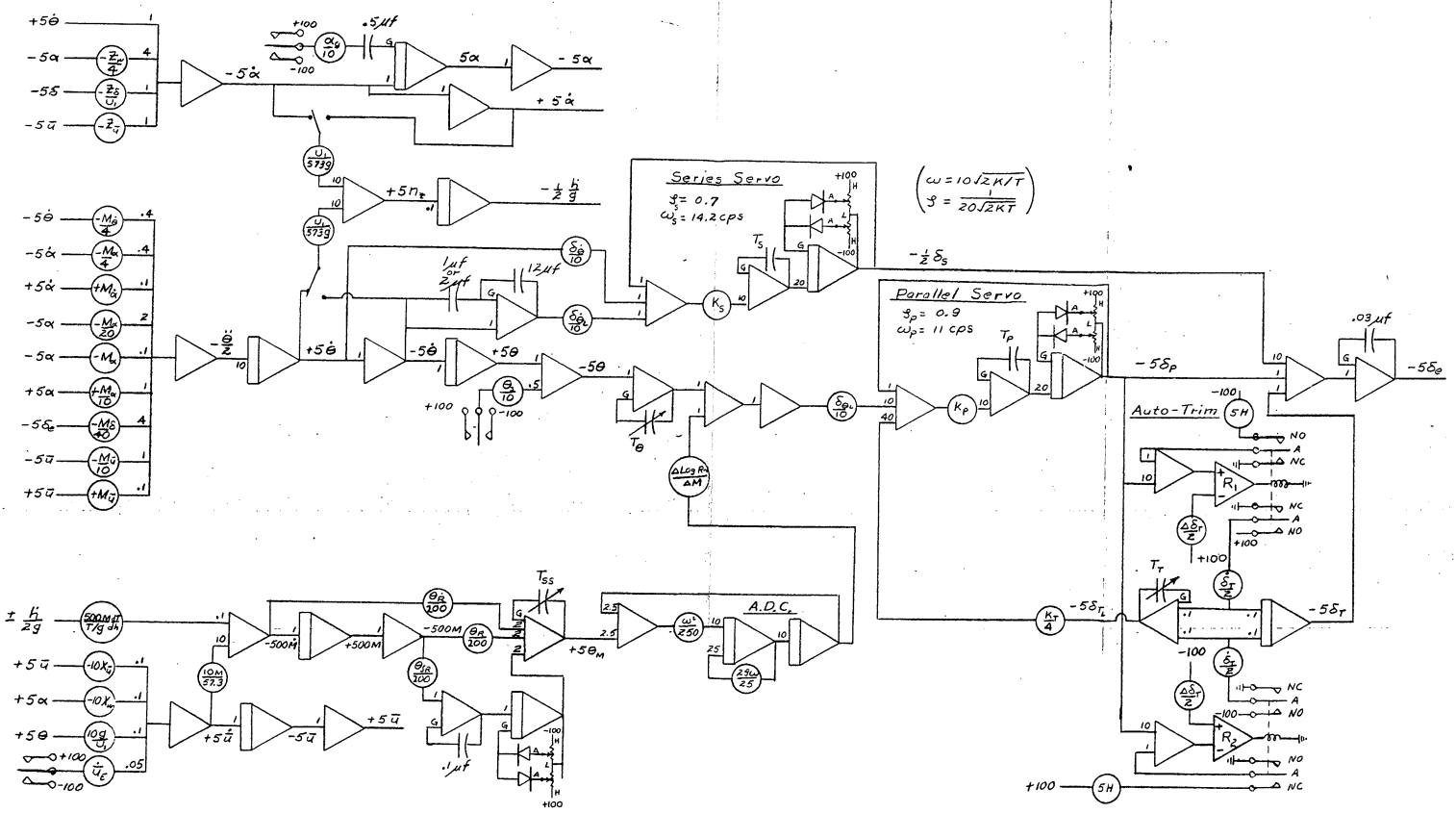

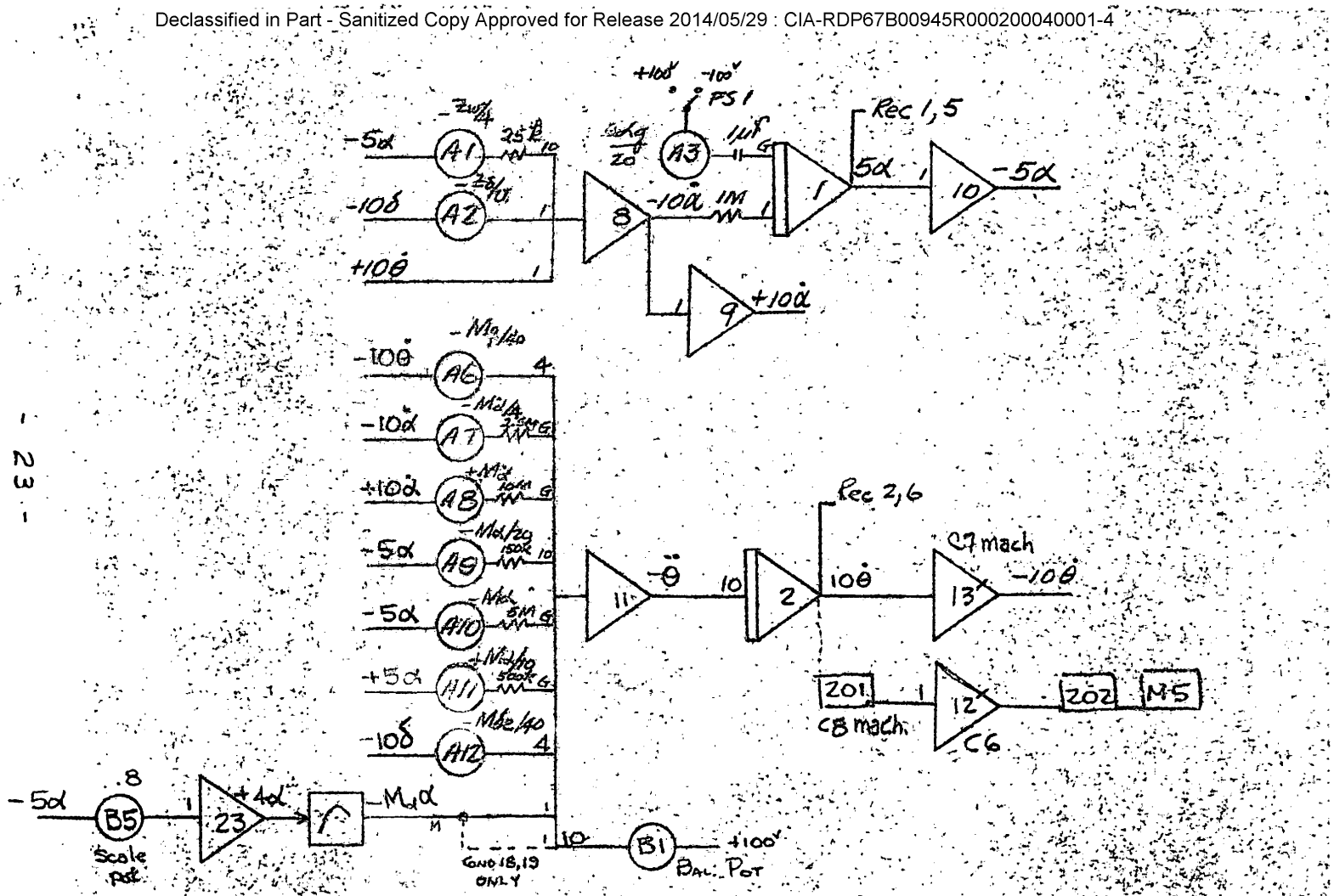

FIGURE 5.2a NONLINEAR PITCH DAMPER SIMULATION

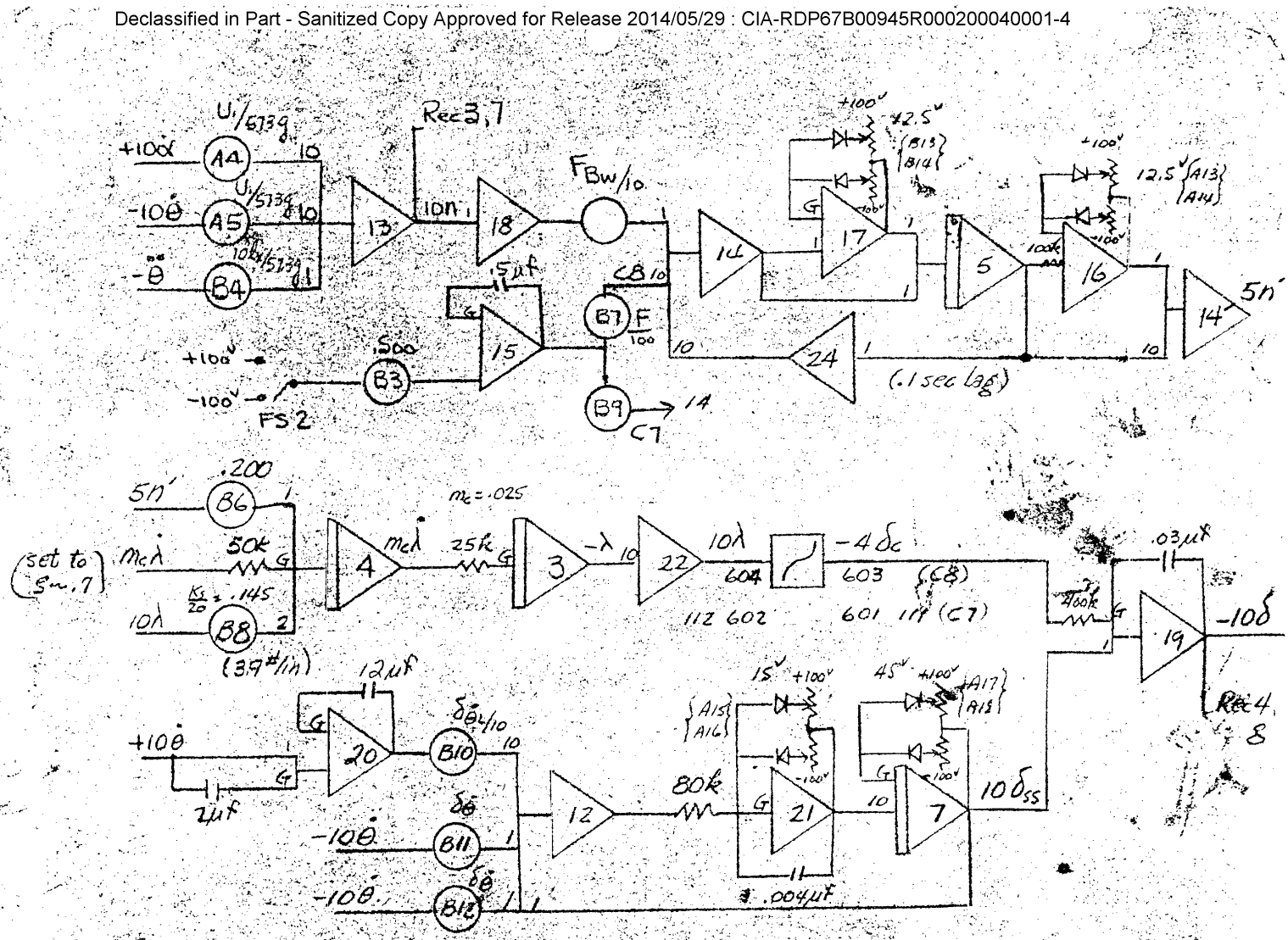

- 24 -

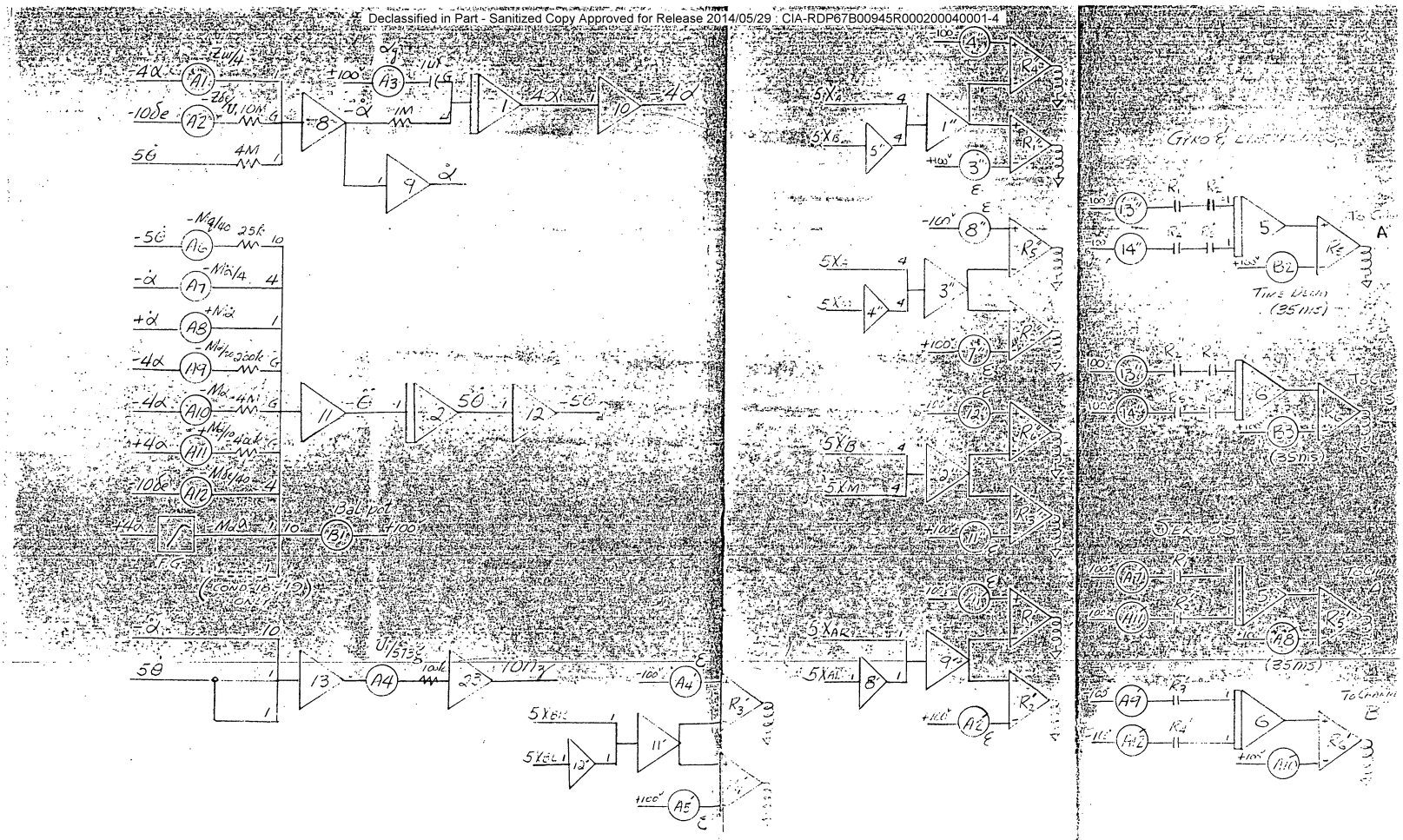

FIGURE 5.3a PITCH AXIS REDUNDANT SYSTEM SIMULATION

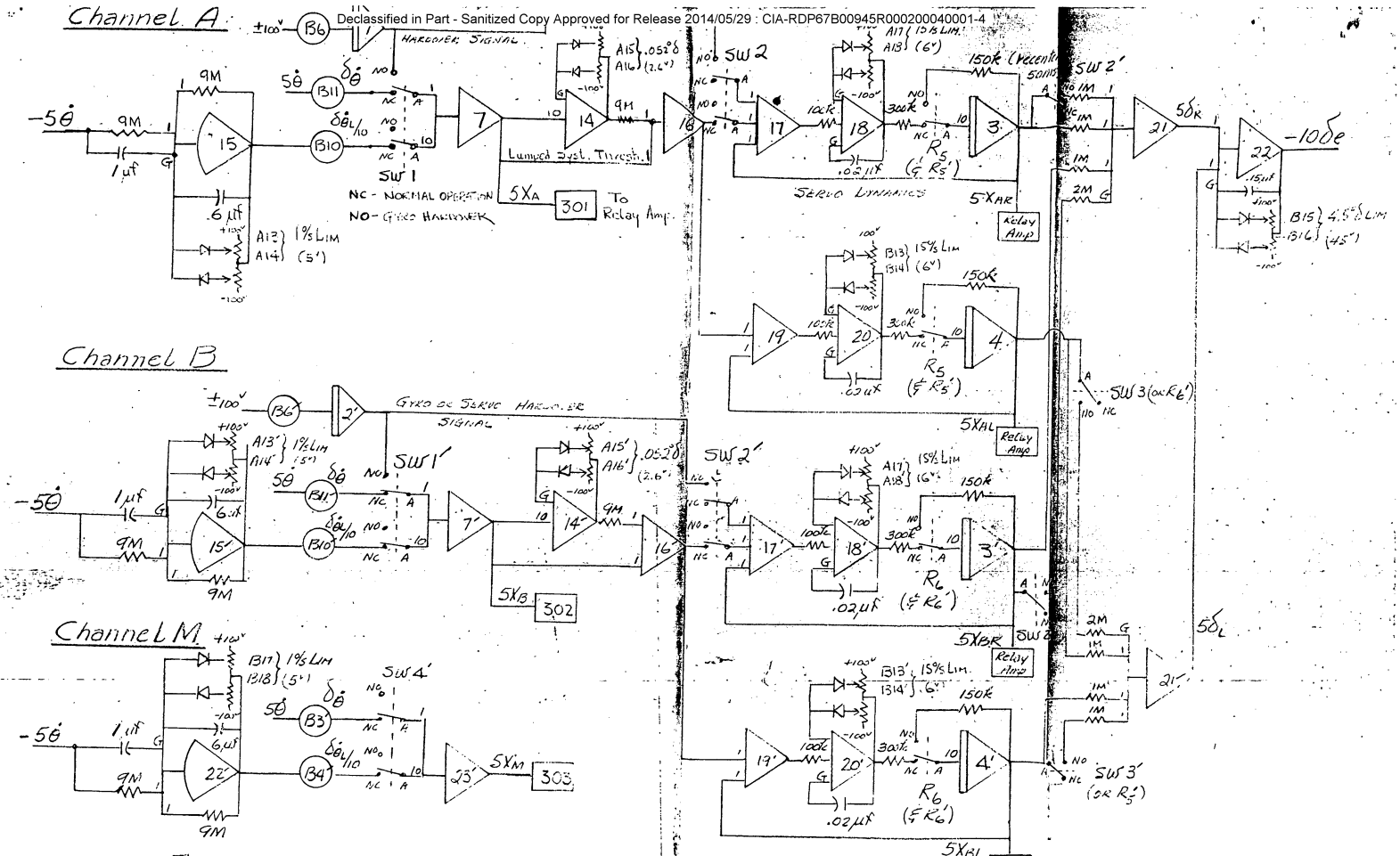

FIGURE 5.3b PITCH AXIS REDUNDANT SYSTEM SIMULATION

SECTION 6

PRESENTATION AND DISCUSSION OF RESULTS

Representative results of the various pitch axis design studies are presented here together with discussions of significant points of interest.

(a) Linear Damper

Figure 6 A shows the free aircraft characteristics for normal acceleration (at the c.g.) response to elevator deflection. Lines of desirable characteristics are superimposed on this plot (dotted lines). The desirable lines are tempered by:

a. the low fundamental structural frequency (which sets an upper limit on augmented frequency)

b. a compromise between system performance and system simplicity.

The resulting modified desirable characteristics for the 129 are plotted as solid lines on Figure 6 A.

When the damper loop is closed with a proportional pitch rate feedback both the natural frequency and damping are increased. In regions where the pitching moment due to elevator (M_{δ_e}) is high and the aerodynamic time constant (T_a) is low the frequency is rapidly increased while the damping ratio is, in comparison, slowly increased. In regions where M_{δ_e} is small and T_a large the reverse is true, i.e. damping ratio is rapidly increased in comparison to frequency. If static instability should occur in this second region (imaginary natural frequency) then it sometimes becomes necessary to augment the frequency separately from the damping. Separate frequency augmentation can be obtained from:

a. a lagged pitch rate feedback

b. a normal acceleration feedback

In the case of this vehicle, M_{δ_e} is small and T_a very large for conditions 20 through 30. In addition static instability can occur at several of these flight conditions when the vehicle is pulling normal acceleration below the limit load factor. Thus separate static stability augmentation is required at high altitudes.

Since pitch rate is readily available in the system, lagged pitch rate is used for separate frequency augmentation at altitudes above 62,000 feet. The results for a fixed gain and time constant on this term are shown in Figure 6 B. The proportional gain, $\delta_{\dot{\theta}}$, is scheduled with q'_c. The schedule is shown in the inset.

Many of the flight conditions fall outside of the desired region. However, improving these conditions would require a much more complicated schedule. For example, conditions 4 and 5 are the same Mach number and altitude thus they have the same gain. Since condition 4 has a lower weight than 5, M_{δ_e} is larger and the gain is much more effective than at condition 5. The same is true of conditions 7, 8, and 9.

With the lagged pitch rate term the high altitude conditions fall within the desired region. However, the low damping ratios, while sufficient for manual operation, will not provide an adequate inner loop for autopilot modes. Thus it is desirable to have more proportional pitch rate at the higher altitudes during autopilot operation. A fixed gain of 1 degree per degree per second of pitch rate will provide sufficient additional damping for autopilot operation at altitudes above 62,000 feet. Since the lagged term and the additional pitch rate are fixed and both switched in at the same altitude they are combined into a single term;

$$1 + \frac{5}{1 + 12s} = \frac{6\ (1 + 2s)}{1 + 12s}$$

which converts the lagged term to a lag-lead term.

The results of this configuration are shown in Figure 6 C. The hexagonal boxes show the characteristics of perturbations from trimmed 2g ($\Delta n = 1$ g) flight for the conditions where M_α is non-linear. (Conditions 18-30)

Figures 6.1 through 6.12 show the transient responses for α gusts and δ steps. The free and augmented aircraft are shown together for the purpose of direct comparison. For brevity, only the landing, takeoff, refueling, and design flight conditions are shown. Data on other flight conditions are available upon request.

Since the landing and takeoff characteristics are of extreme importance the pitch rate response to an elevator step for conditions 1, 2, and 3 are shown separately in Figure 6 D.

The analog computer studies (both damper and autopilot) show that the lag-lead term can be reduced to $\frac{5\,(1+s)}{1+12s}$ without noticeable effects. The results shown in Figures 6.1 through 6.12 include this modification. The damper control equation then becomes:

$$\delta_e = \dot{\theta}\left\{\delta_{\dot{\theta}} + \left[\frac{5\,(1+s)}{1+12s}\right]_{h \geq 62{,}000'}\right\}$$

where: $\delta_{\dot{\theta}} = f\,(q'_c)$

The damper gain schedule, $\delta_{\dot{\theta}} = f\,(q'_c)$, is shown in Figure 6 E. Transient results for both 1 g and 2 g (primed conditions) at high altitudes are shown in Figures 6.5 through 6.12.

A better evaluation of the damper is obtained by studying the acceleration response due to stick force. This type of study can include the effects of non-linear gearing, bobweight, and fuel system. In addition the non-linear characteristic of M_{α} at high altitudes can also be simulated more exactly. This type of study has been done. The results are given in Section 6 e.

(b) Pitch Attitude Hold

The principal objective of attitude hold analysis was to define scheduling curves for the pitch attitude gain $\delta_{\theta L}$ and the filter time constant T_{θ}, and at the same time, minimize any damper changes. The selected criteria for pitch attitude response to step commands were a response time to 90%, t_{90}, of 3 to 5 seconds and a maximum overshoot of 25%. It was soon apparent that sufficient damping was not available to meet these criteria at the higher altitude flight conditions. As a result an additional 1 deg/deg/sec of straight-through pitch rate gain was added to the pitch damper (discussed in Item a of this section). Resulting performance, with the $\delta_{\theta L}$ and T_{θ} schedules of Figures 3.2 and 3.3, gave response times of from 1.5 to 6 seconds and overshoots of less than 20%. At a constant altitude, both response time and overshoot tend to be larger for the lower Mach numbers. Some representative time histories of attitude hold responses are shown in Figures 6.13 through 6.18. These responses for the "starred" design flight conditions only. Responses to both attitude step commands and vertical gusts are shown. In computing these responses, ±2 degree displacement limits were placed on the parallel servo. Figures 6.17 and 6.23 show the effect of these limits if inputs are large enough to "bottom" the servo. In practice, the parallel servo will be force limited rather than displacement limited. Further analysis will determine a safe level of force limiting.

Figures 6.1 through 6.12 include responses of the dampered airplane with the revised pitch rate network $5\ \frac{(1 + s)}{1 + 12s}$. Although the autopilot responses shown here do not include this network, sufficient analysis has been conducted to determine that the change does not seriously harm autopilot performance.

(c) Mach Hold

Determination of suitable Mach displacement, integral, and rate gains has been based upon the following criteria:

> "Following a step input command of pitch attitude, the resulting Mach error should decrease from its maximum value to 10% of that value in from 5 to 25 seconds and reduce each overshoot by at least 60%."

Experience has shown that the longer response time is more desirable from the pilot's viewpoint and that zero overshoot should be an objective if not a requirement.

It was found that the Mach gains most suitable for the high altitude conditions resulted in responses at lower altitude which were too fast and exhibited too much overshoot. After applying the gain schedules as shown in Figure 3.4, response times over the flight envelope varied from 15 to 28 seconds and overshoots were less than 30%. Mach rate gain was included primarily for its effect on conditions in the left half of the flight envelope. Transient responses for the "starred" flight conditions are given in Figures 6.19 through 6.24.

(d) Automatic Trim

The configuration of the auto-trim system is based on the capability of the vehicle to change flight condition and on the stability requirements of the auto-trim loop. Maximum rates of change of altitude and Mach number dictate that a trim rate of 0.1 deg/sec is necessary. Since the trim actuator and the parallel servo displacements sum in parallel to drive the power actuator, recentering of the parallel servo during the trimming process would be accomplished entirely by feedback through the airplane pitch axis if a stability compensator was not employed. Without compensation, the phase lag through the airplane and back to the parallel servo is such that the stability of the attitude and Mach hold modes is significantly altered by the auto-trim loop.

The compensator, however, begins to recenter the servo immediately upon activation of the trim actuator. As a result the net perturbed surface motion during the trimming process is greatly reduced together with subsequent aircraft motion. It can be seen from the block diagram (Figure 3.1) that, once the parallel servo stabilizes within the switch deadband, the compensator output decays to zero and has no effect on steady-state trim. The effects of the auto-trim loop on attitude and Mach hold responses to disturbances are illustrated by Figures 6.13 through 6.24. It will be noted in Figures 6.13 through 6.18 that the commanded value of θ is not always attained with auto-trim operation. These static errors result because integral control is not used on attitude hold. The maximum error is proportional to the auto-trim switch deadspot and inversely proportional to pitch attitude gain. At the design flight conditions, where attitude gain is high, the maximum attitude error is less than 0.1 degree with a 0.25 degree switch deadspot. Selection of the deadspot size was affected to some extent by parallel servo motion during a disturbance. Smaller

values of deadspot (more desirable from an accuracy viewpoint) resulted in higher frequency on-off cycling of the trim system as the trim condition was approached. It was reasoned that less frequent stick motions of somewhat larger amplitude would be more desirable.

(e) Non-Linear Damper Study

The results of the non-linear damper study, utilizing a non-linear slope for the variable M_α at conditions 18 and above, and including the non-linear effect of the manual control system, indicated that

(1) Rescheduling of the pitch rate parameter, $\delta_{\dot{\theta}}$, to break at 800 q'_c instead of 750 q'_c had little, if any, effect on the damper performance. This change makes all q'_c scheduling potentiometers in the damper identical and thus interchangeable.

(2) The fixed lagged pitch rate term, $\frac{5\ (1 + s)}{(1 + 12s)}$, could be switched into the damper configuration at an altitude between 50,000 feet and 70,000 feet.

The transient normal acceleration responses to stick force commands with the bobweight set at 5 #/g were very similar to those obtained with the linear damper simulation at conditions 17 and below. At conditions 18 and above, the transient normal acceleration responses to large stick force commands with the bobweight set at 5 #/g did differ from that of the linear damper primarily as a result of the non-linear slope of M_α. Representative responses at conditions 26 and 27 are shown for stick force commands near one g in Figure 6.25. A pilot lag of 0.5 seconds was used. Here, stable g commands can be held to the limit of the series servo authority at condition 26. However, lack of adequate stability augmentation allows pitch up to occur at condition 27 although the series servo is not saturated prior to pitch up. Additional responses in Figure 6.26 indicate the effect of changing the lagged pitch rate term at these conditions.

The bobweight will add a normal acceleration feedback (destabilizing) to the damper configuration. The effects of this feedback vary with the bobweight size, the force deadspots in the control system, and the amount of damping provided by the pilot.

If the bobweight is held within the force deadspots of the control system then the destabilizing feedback to the damper will only be "seen" at conditions where the incremental load factor exceeds 1g. Analog computer runs were made with the bobweight set at 5 lbs/g and 10 lbs/g. The loss of damping resulting from the 10 #/g bobweight is quite noticeable with pilot lags up to 0.2 sec. The 5 #/g bobweight shows no detrimental performance with "g" commands up to the limit load factor and no pilot lag. Since it is very difficult to evaluate the bobweight without a pilot in the loop, it is recommended that the bobweight be held to 5 #/g until the final value can be determined through simulator tests.

(f) Failsafety, Redundant System

The results of the analog computer analysis of the redundant pitch damper system indicate that automatic failsafe protection is provided for the first damper failure throughout the mission profile. In addition, automatic failsafe protection is provided for the second damper failure at all inherently statically stable conditions in the profile. At statically unstable flight conditions, such as condition 13, the vehicle will slowly pitch up upon disengagement of the damper system. Since the incremental load factor resulting from the damper failure does not exceed the maximum allowable load factor of 1.5 g's until 14 seconds have elapsed at condition 13, recovery by the pilot is possible. The term "damper failure" is defined as ramp type failures in the series servo, pitch rate gyro or electronic circuitry. In this study, only failures occurring in straight and level flight were considered. Thus, the second damper failures simulated at conditions in the non-linear $M_\alpha \alpha$ region were failsafe because the low surface effectiveness yielded small angle of attack changes from trim within the statically stable portion of the $M_\alpha \alpha$ slope.

The logic equations used in the failsafe analysis to detect and disengage a malfunctioning channel are described below:

Let $\mathcal{E}$ = allowable difference between channel displacements.

A' represents $|X_{AR} - X_{AL}| \leq \mathcal{E}$ Normal operation in Channel A

A represents $|X_{AR} - X_{AL}| > \mathcal{E}$, either right servo, X_{AR}, or left servo, X_{AL}, failed in channel A

B' represents $|X_{BR} - X_{BL}| \leq \varepsilon$, normal operation in channel B

B represents $|X_{BR} - X_{BL}| > \varepsilon$, either right servo, X_{BR}, or left servo, X_{BL}, failed in channel B

C' represents $|X_A - X_B| \leq \varepsilon$, normal operation in gyro channels A and B

C represents $|X_A - X_B| > \varepsilon$, gyro and electronics of either channel A or B failed

E' represents $|X_A - X_M| \leq \varepsilon$ normal operation in channels A and M

E represents $|X_A - X_M| > \varepsilon$ gyro and electronics of either channel A or M failed

F' represents $|X_B - X_M| \leq \varepsilon$, normal operation in channels B and M

F represents $|X_B - X_M| > \varepsilon$, gyro and electronics of either channel B or M failed

The malfunctioning channel is detected and disengaged by the following discrimination:

F_A = A or C and E, channel A failed

F_B = B or C and F, channel B failed

F_M = E and F, channel M failed

In the event of multiple failures, the combination of one gyro channel failure plus a monitor failure will disengage the remaining good channel. However, the combination of one channel servo failure plus a monitor failure will not disengage the remaining good channel. The remaining channel will continue operating until a third failure disengages that channel.

The failure types considered in the failsafe analysis are described below:

a. First Failure: servo

$\mathcal{E}$ = 2.18 degrees = $\delta_R - \delta_L$, differential

Here three servos can oppose the malfunctioning servo. The malfunctioning servo can drive the right actuator, δ_R, (or the left, δ_L) up to the full authority of 15 degrees/s and ±4.5 degrees as commanded by the ramp failure. The mating servo in the δ_R channel (or the δ_L channel) can oppose the malfunctioning servo up to the full authority as commanded by the feedback parameters $\delta_{\dot{\theta}}$ and $\delta_{\dot{\theta}L}$. The two servos in the opposite δ_L (or δ_R) channel track together to drive that actuator at full authority as commanded by the feedback parameters $\delta_{\dot{\theta}}$ and $\delta_{\dot{\theta}L}$. When the error signal $\mathcal{E}$ is exceeded, condition A or B exists and the malfunctioning channel A (or B) servos are disengaged and recentered. The remaining channel B (or A) servos continue to drive δ_R and δ_L at full authority as commanded by the damper feedback parameters.

b. Second Failure: servo

$\mathcal{E}$ = 2.18 degrees = $\delta_R - \delta_L$, differential

Here, one servo can oppose the malfunctioning servo as one operating channel has been previously disengaged. The malfunctioning servo can drive its actuator at full authority as commanded by the ramp failure and the remaining good servo can oppose it by driving its actuator at full authority as commanded by the damper feedback parameters. When the error signal $\mathcal{E}$ is exceeded, condition A or B exists, the damper servos are disengaged and recentered, and the unaugmented vehicle remains.

c. First Failure: Gyro

$\mathcal{E}$ = 1.09 degrees = $\delta_R - \delta_L$

Here, a gyro or electronic failure drives one servo in each right and left actuator channel at full authority as commanded by the ramp failure. The remaining servo in each δ_R and δ_L channel can oppose the gyro malfunction at up to full authority as commanded by the damper feedback parameters. When the error signal $\mathcal{E}$ is exceeded, condition C and E or F exists; the faulty gyro channel is disengaged, and the servos are recentered. The remaining channel carries on at full authority.

d. Second Failure: Gyro

$\mathcal{E}$ = 1.09 degrees = $\delta_R = \delta_L$

Here, one channel is disengaged and a gyro or electronic malfunction in the remaining channel can drive each surface actuator as commanded by the ramp failure with no opposition. The gyro monitor, M, although not an operative channel, does emit a voltage proportional to the damper feedback parameters times the pitch rate generated by the failure. Thus, the error signal $\mathcal{E}$ is exceeded and conditions C, E and F exist, before the surface moves the full error amount. The damper is disengaged and only the unaugmented vehicle remains operative.

Various failure combinations, such as a servo failure in one channel followed by a monitor failure which is then followed by a gyro failure in the remaining channel, are covered by the preceding failure conditions. Here, the gyro and electronics of the first channel (servo failure) would still be available to serve as a monitor for the third channel gyro failure.

The failsafe analysis used the nominal values of

$\mathcal{E}$ = 2.18 degrees = $\delta_R - \delta_L$ for servo failures,

$\mathcal{E}$ = 1.09 degrees = $\delta_R = \delta_L$ for gyro and electronic failures, servo recentering time of $t_{63\%}$ = 50 milliseconds and system dead time of 35 milliseconds. An increased dead time of 115 milliseconds was used on slow, creeping failures. Variations in the nominal values were checked at three critical flight conditions.

The transient responses to a series of ramp inputs to the four failure types previously described are shown at flight conditions 7, 8 and 10 in figures 6.27 through 6.32. Peak failure load factors up to 1.1 incremental are obtained at these flight conditions because of the high surface effectiveness. The peak failure load factors are plotted against pitot differential pressure, q'_c, at the flight conditions checked for ramp inputs of 15 degrees/s, the maximum series servo rate, and 0.3 degrees/s, a typical slow creeping type of failure, for four failure types in figures 6.33 through 6.36. These figures indicate that peak failure load factors are predicted in the pitot differential pressure region of 800 to 1000 psf.

The peak failure load factors at the critical conditions 7, 8 and 10 are plotted against the ramp inputs for four failure types in figure 6.37. For servo failures, the ramp input is the rate at which either the right or left surface would be driven if no pitch rate feedbacks were present. For gyro or electronic failures, the ramp input is the rate at which the right and left surfaces would be driven if no pitch rate feedbacks were present. Thus, it can be seen that the gyro failures produce a surface rate roughly twice that of the servo failures. In addition, the allowable error signal for servo failures is 2.18 degrees = $\delta_R - \delta_L$. That is, if no pitch rate feedbacks are considered, one surface would have to move a full 2.18 degrees displacement before the relay logic would disengage the channel. In the case of gyro failures, the allowable error is 1.09 degrees = $\delta_R = \delta_L$. Here, if no pitch rate feedbacks are considered, each surface would move 1.09 degrees displacement before the relay logic would disengage the channel. As a result, a gyro failure at a ramp of 0.3 degrees/s would cause a total surface motion nearly equivalent to that of a servo failure at four times 0.3 degrees/s or 1.25 degrees/s. This can be checked by referring to figure 6.37. Since the peak failure load factors occur at the slow, creeping failure rates, the servo failures naturally would produce the highest load factors for a given slow ramp input.

The peak failure load factors at the critical flight conditions 7, 8 and 10 are plotted in figures 6.38 through 6.40 for variations in $\mathcal{E}$ for four types of failures. The maximum allowable $\mathcal{E}$ caused by tolerance deviations can be 3 degrees = $\delta_R - \delta_L$ for servo failures and 1.5 degrees = $\delta_R = \delta_L$ for gyro failures without exceeding the peak load factor of 1.5 g incremental.

The effect of varying the system dead time and the servo recentering time on the peak gyro failure load factors at condition 7 is plotted in figure 6.41. As would be expected, large system dead times greatly increase the peak load factors at the fast failure rates; whereas the effect is negligible at the slow, creeping failure rates. The mitigating effect of the pitch rate feedback on the surface motion can be seen by comparing the peak g's obtained with a 200 millisecond dead time on the first gyro channel failure with that of the second gyro channel failure. Variations in servo recentering time have far less effect on the peak g's than system dead time variations.

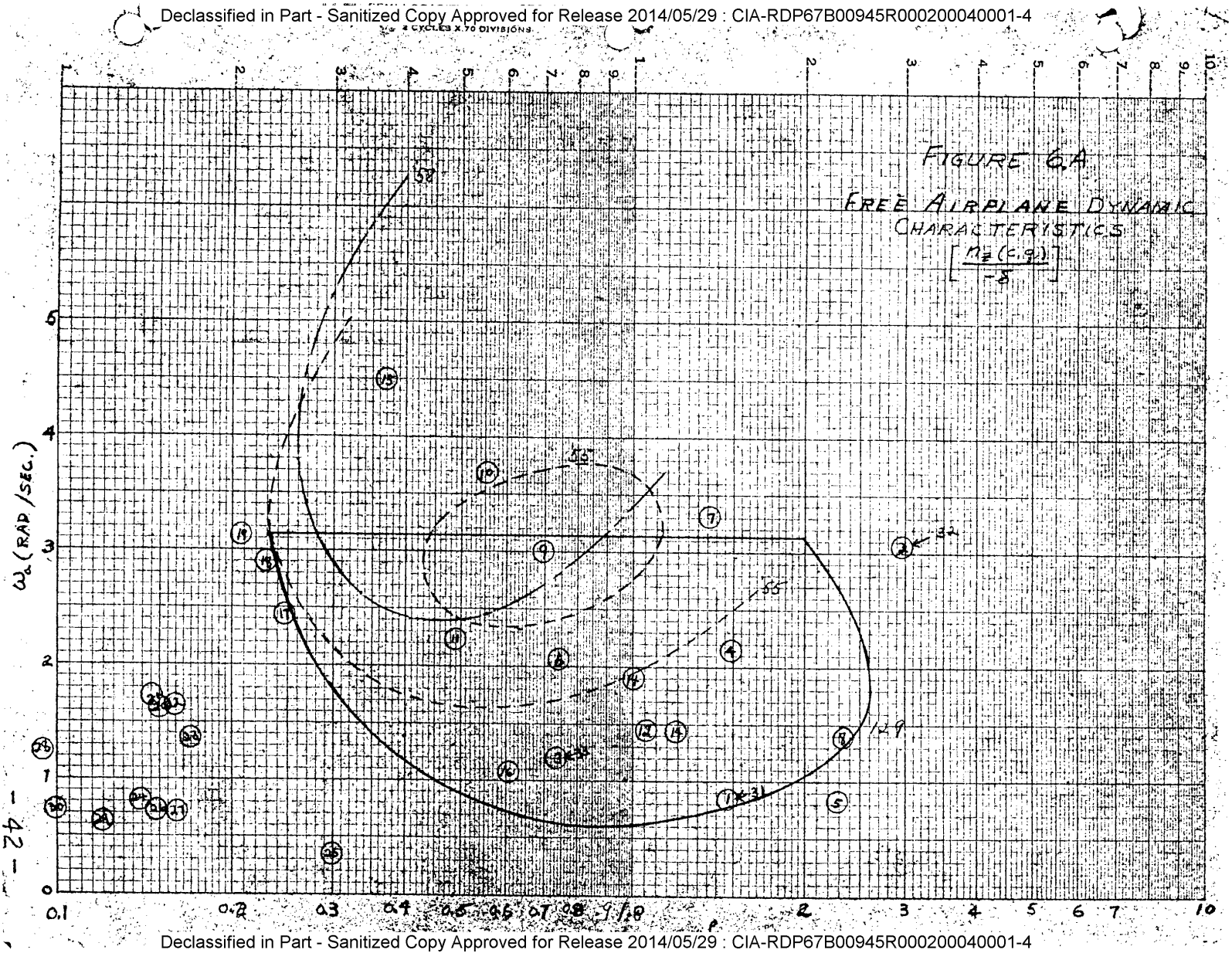

FIGURE 6A

FREE AIRPLANE DYNAMIC CHARACTERISTICS

$\left[\frac{n_z\,(c.g.)}{\alpha}\right]$

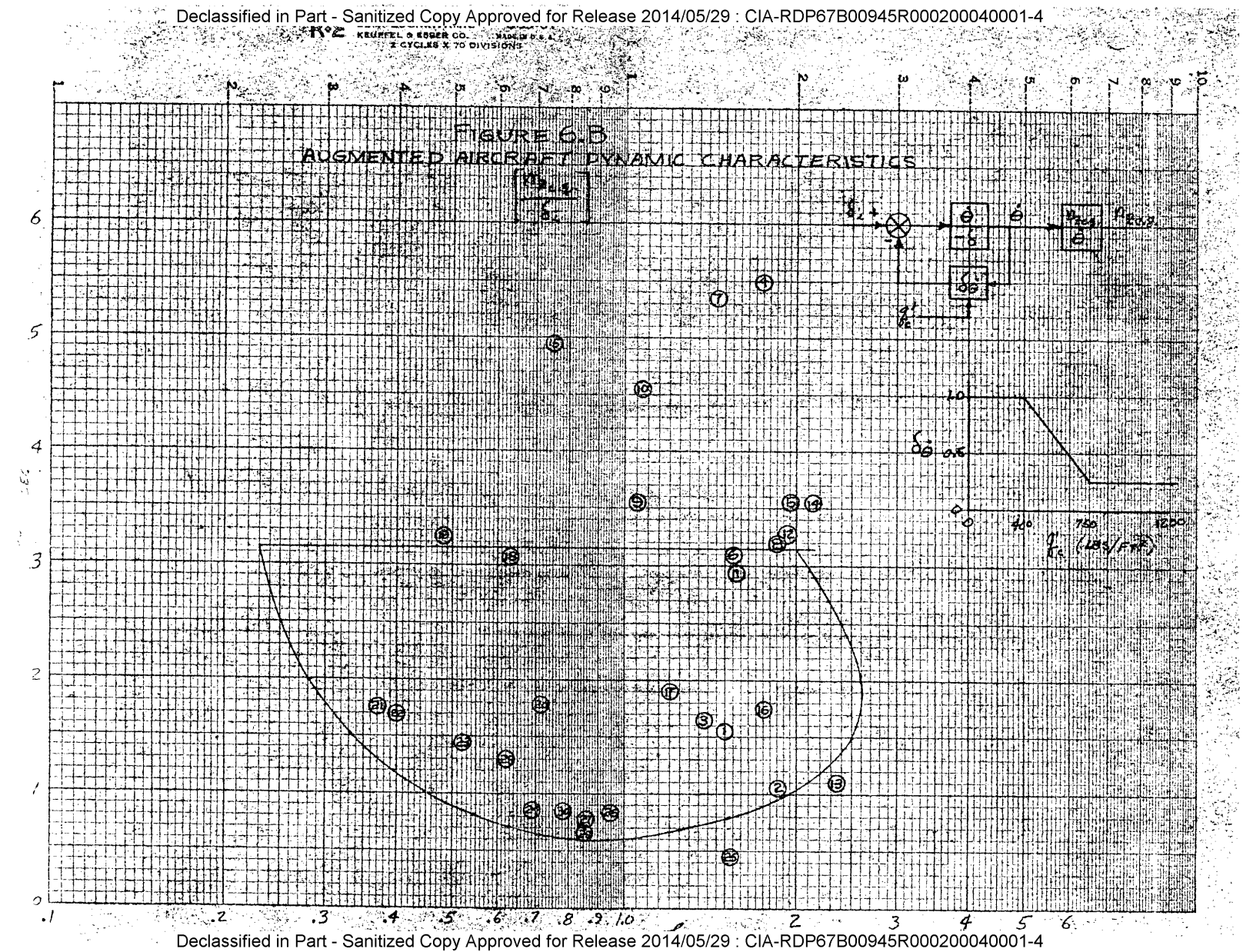

FIGURE 6.C

AUGMENTED AIRCRAFT DYNAMIC CHARACTERISTICS

$\left[\frac{n_z\ (c.g.)}{\delta_e}\right]$

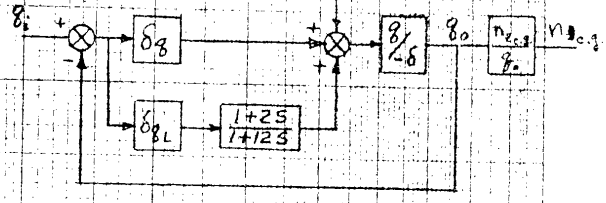

$\delta_{q_L} = 6$ @ COND 20 → 30

$= 0$ @ COND 1 → 19

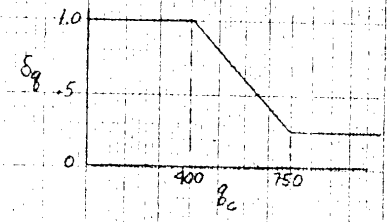

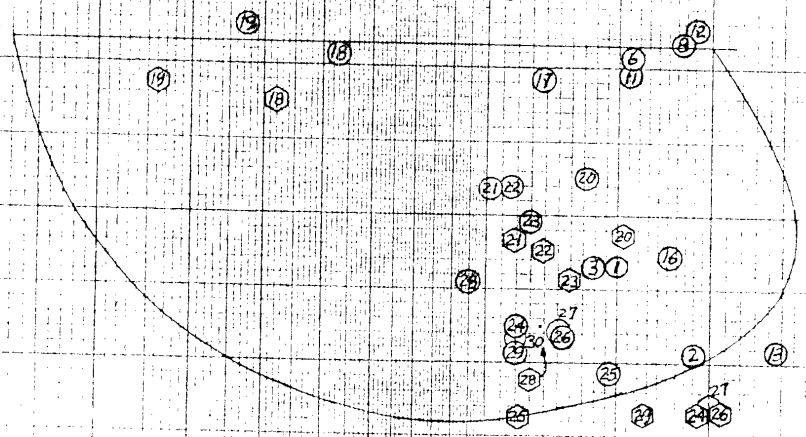

○ 1 g FLIGHT

⬡ 2 g FLIGHT

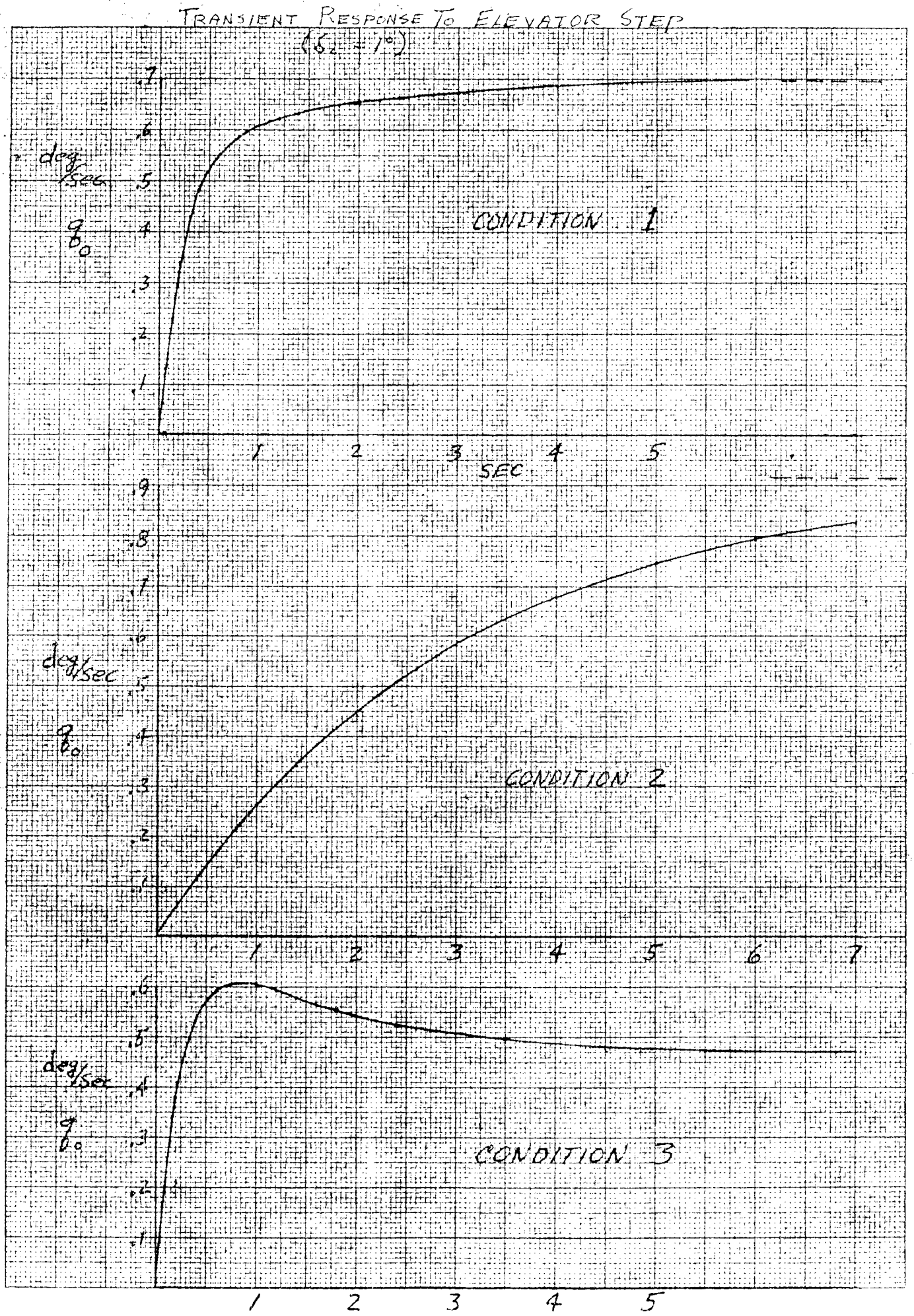

FIGURE 6.E
PROPORTIONAL PITCH RATE GAIN SCHEDULE

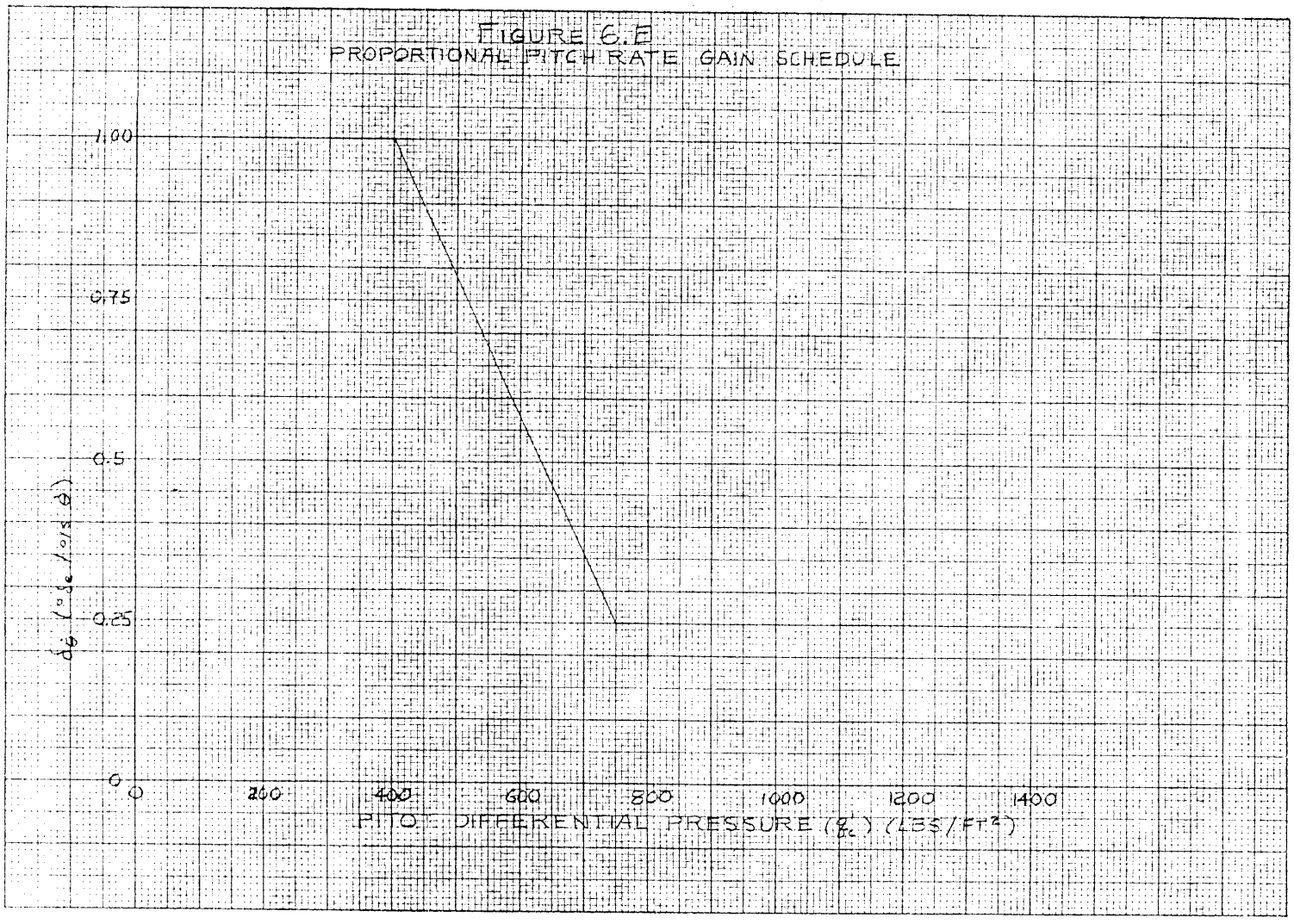

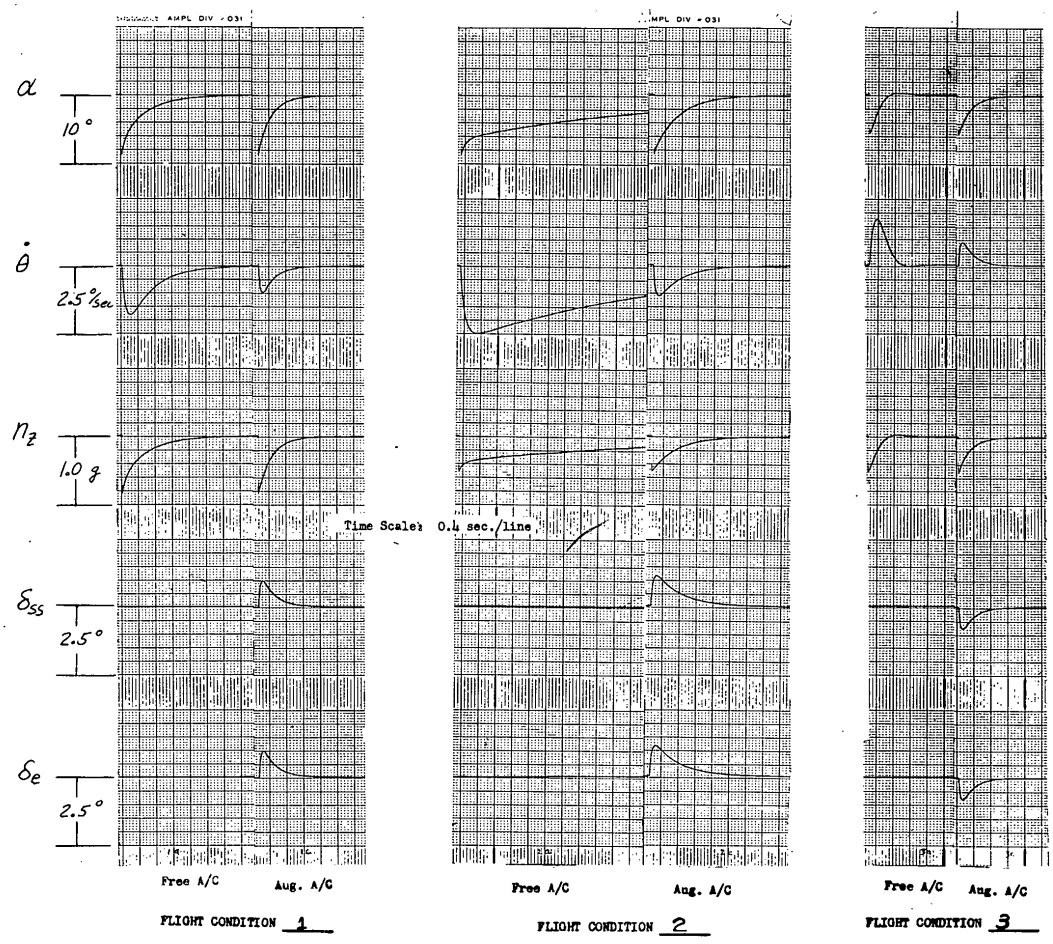

FLIGHT CONDITION 1

FLIGHT CONDITION 2

FLIGHT CONDITION 3

FIGURE NO. 6.1

α Gust - 30 fps

WLO-72-60

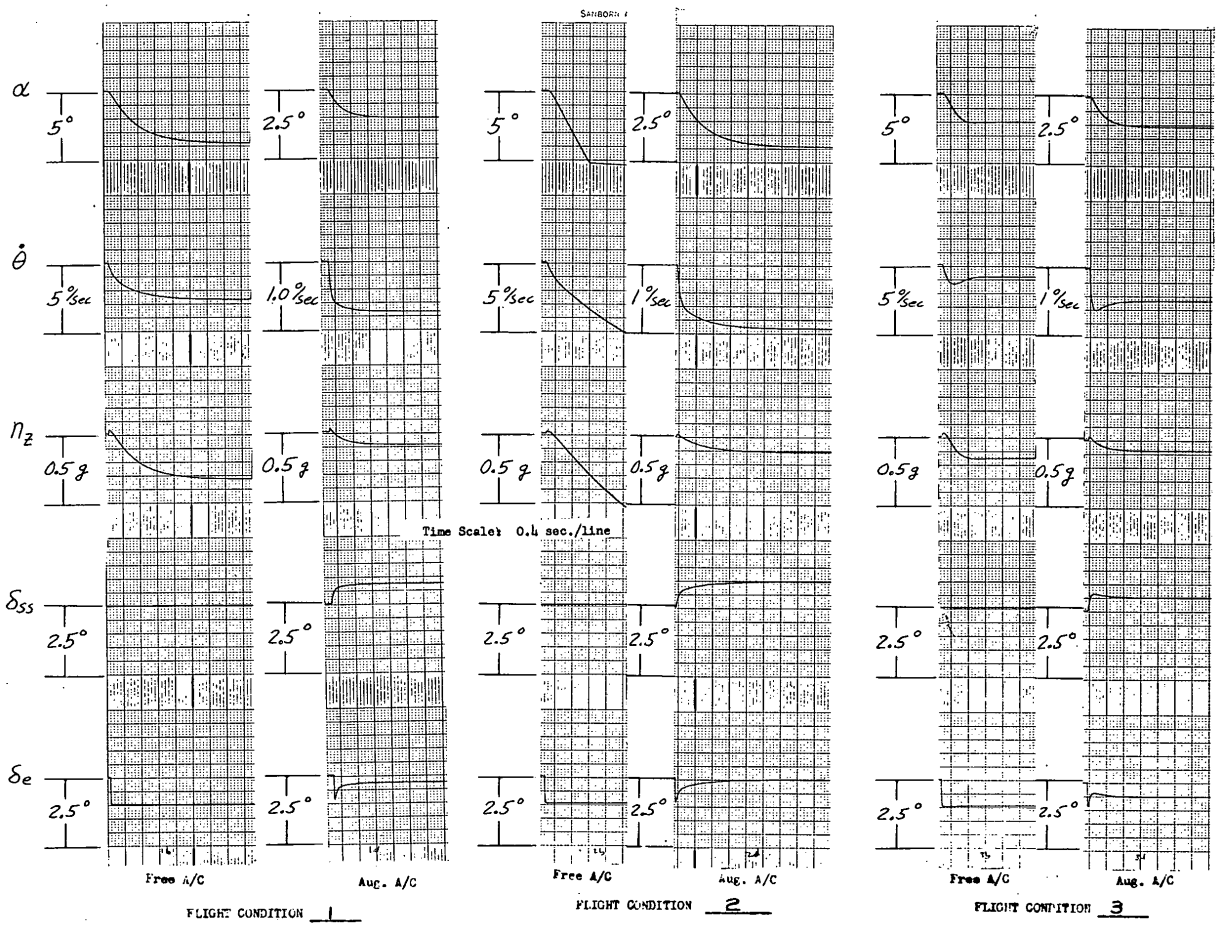

$\int$ Step = 1°

FIGURE NO. 6.2

WLO-72-60

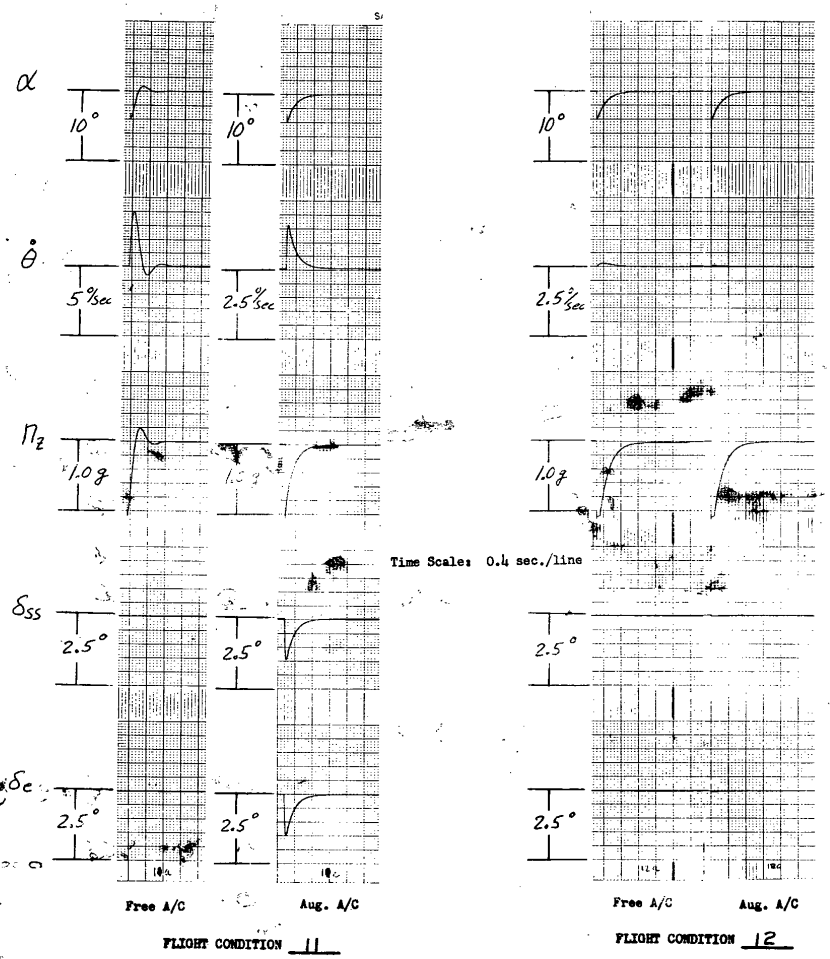

FLIGHT CONDITION 11

FLIGHT CONDITION 12

FIGURE NO. 6.3

α Gust = 50 fps

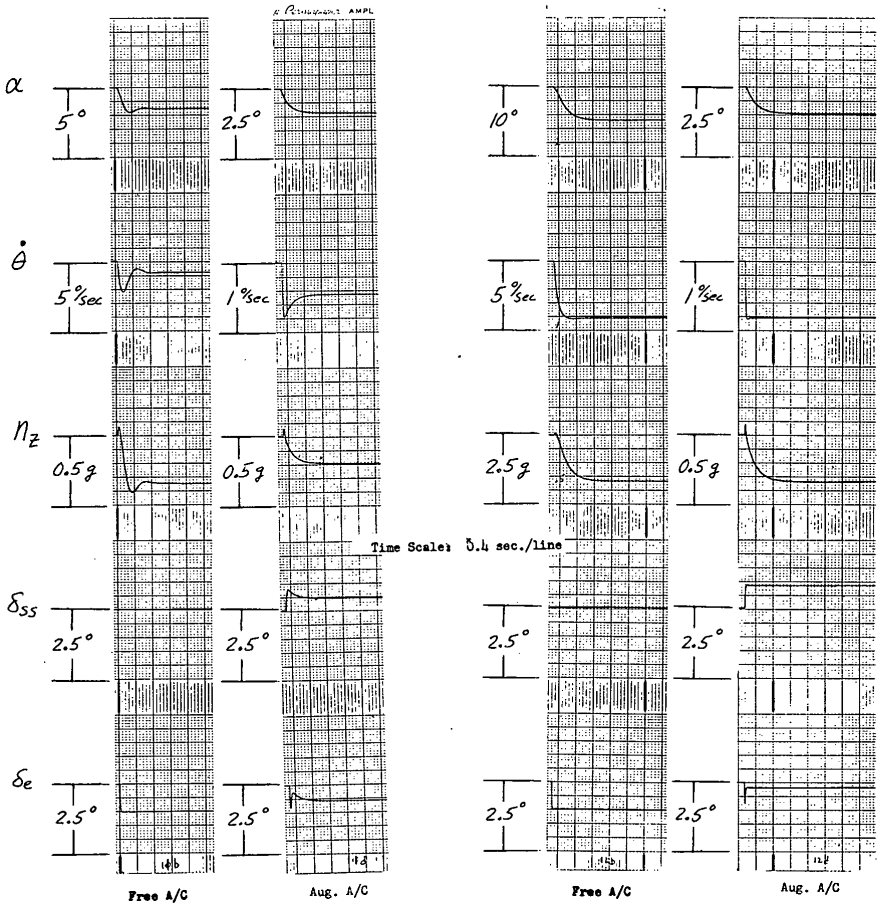

FLIGHT CONDITION 11

FLIGHT CONDITION 12

FIGURE NO. 6.4

δ Step - 1°

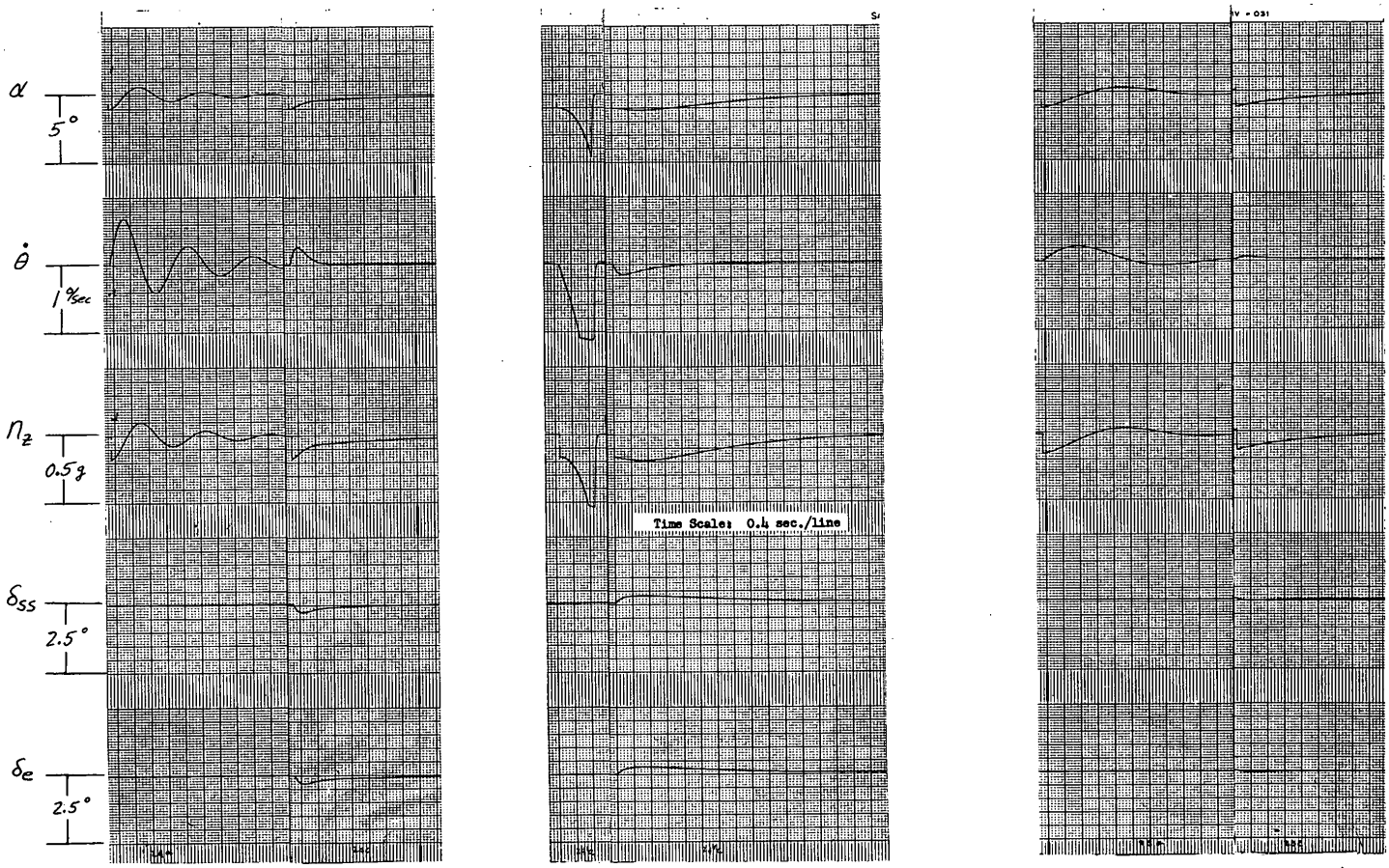

Free A/C Ang. A/C
FLIGHT CONDITION 24

Free A/C Ang. A/C
FLIGHT CONDITION 24'

Free A/C Ang. A/C
FLIGHT CONDITION 25

FIGURE NO. 6.5

WLO-72-60

∝ Gust = 50 fps

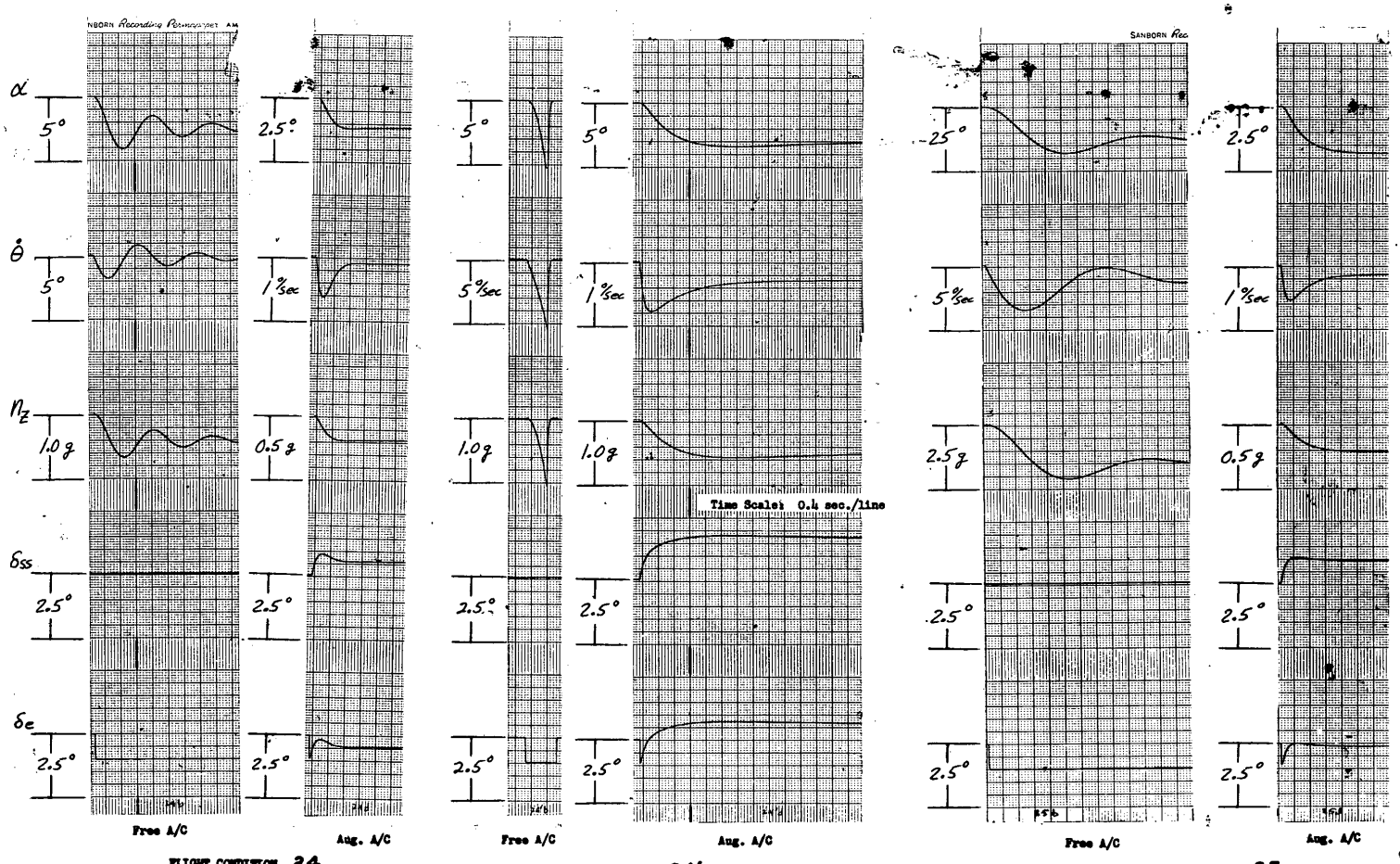

FLIGHT CONDITION 24

FLIGHT CONDITION 24'

FLIGHT CONDITION 25

FIGURE NO. 6.6

δ Step = 1°

WLO-72-60

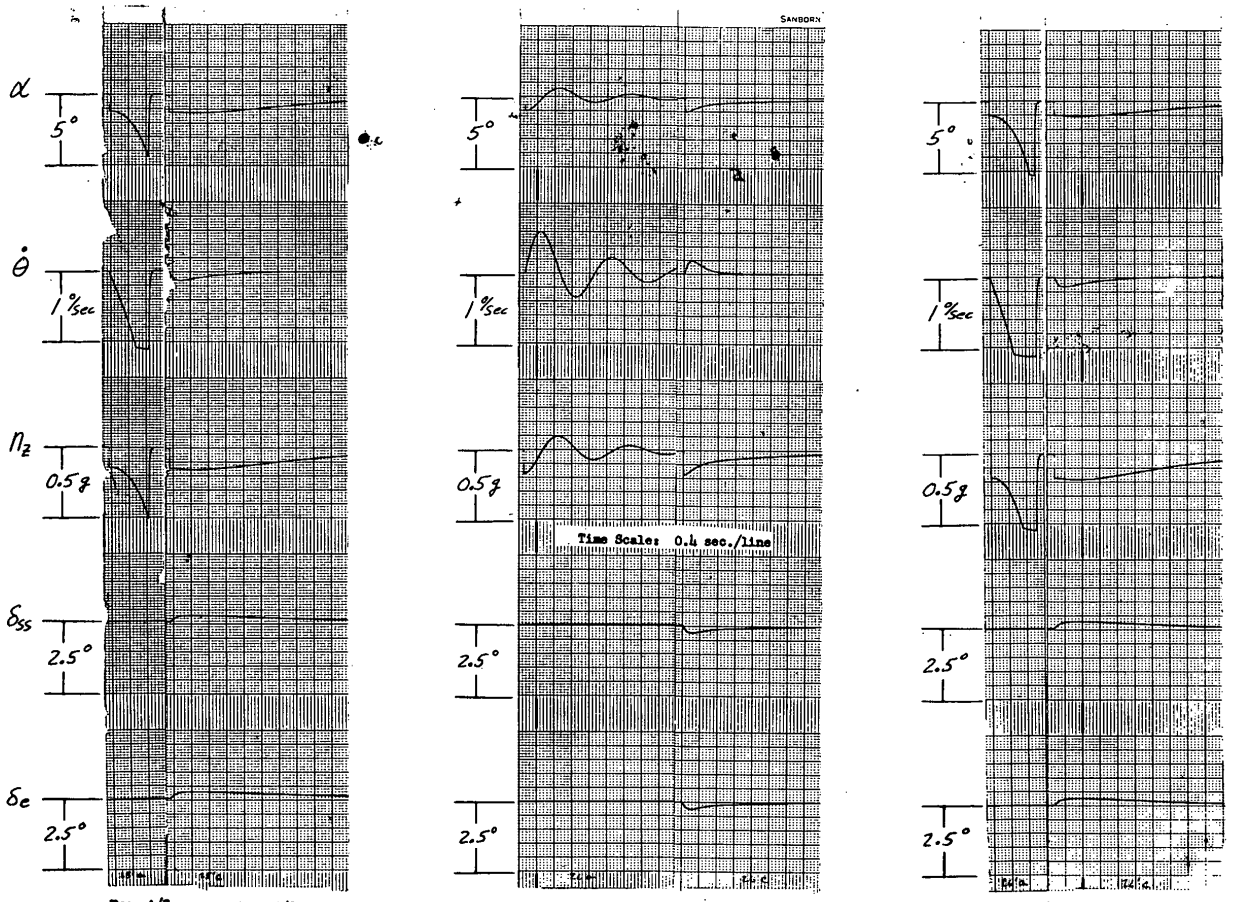

FLIGHT CONDITION 25'

FLIGHT CONDITION 26

FLIGHT CONDITION 26'

FIGURE NO. 6.7

WLO-72-60

α Gust = 50 fps

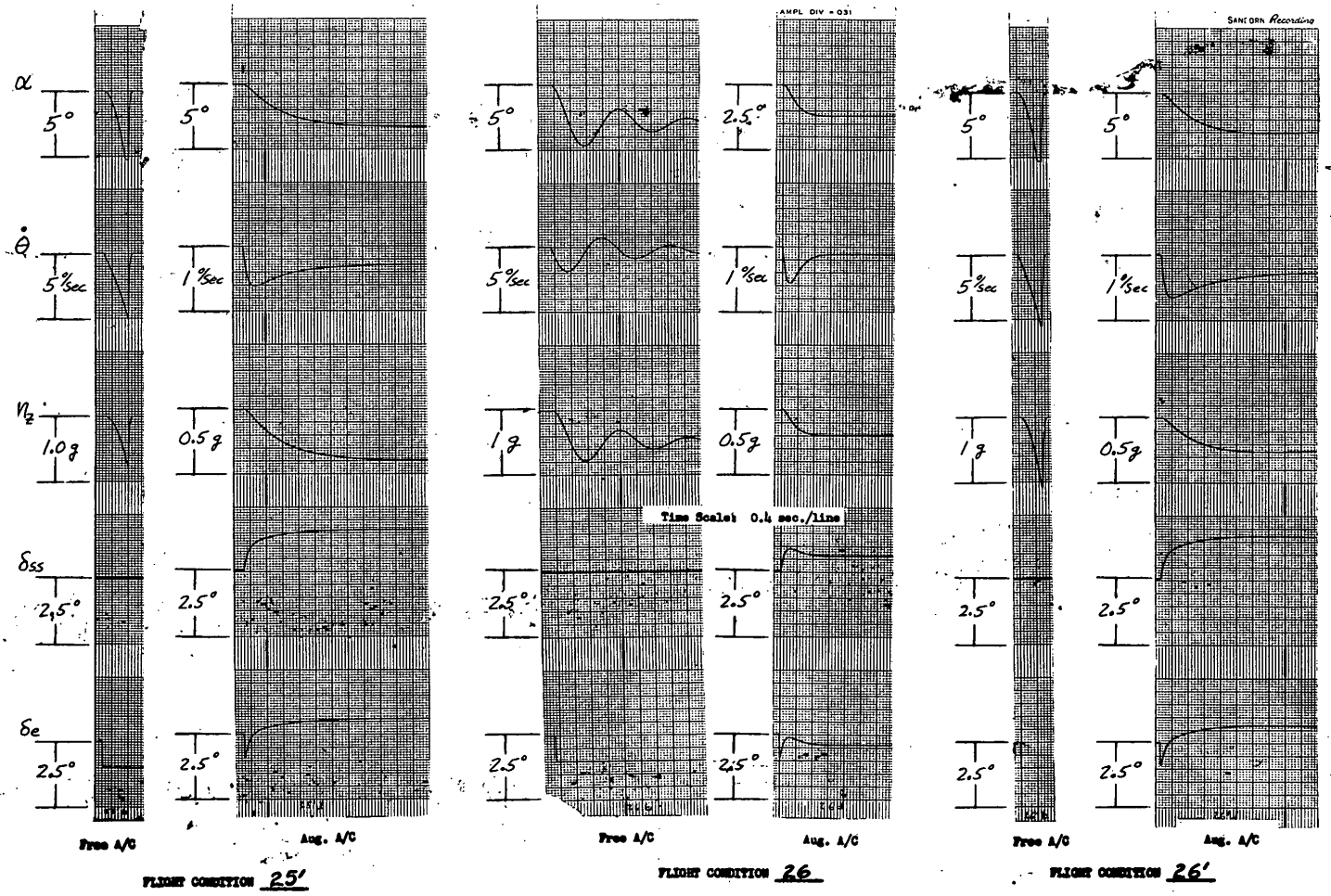

FLIGHT CONDITION 25'

FLIGHT CONDITION 26

FLIGHT CONDITION 26'

FIGURE NO. 6.8

MLO-72-60

δ Step = 1°

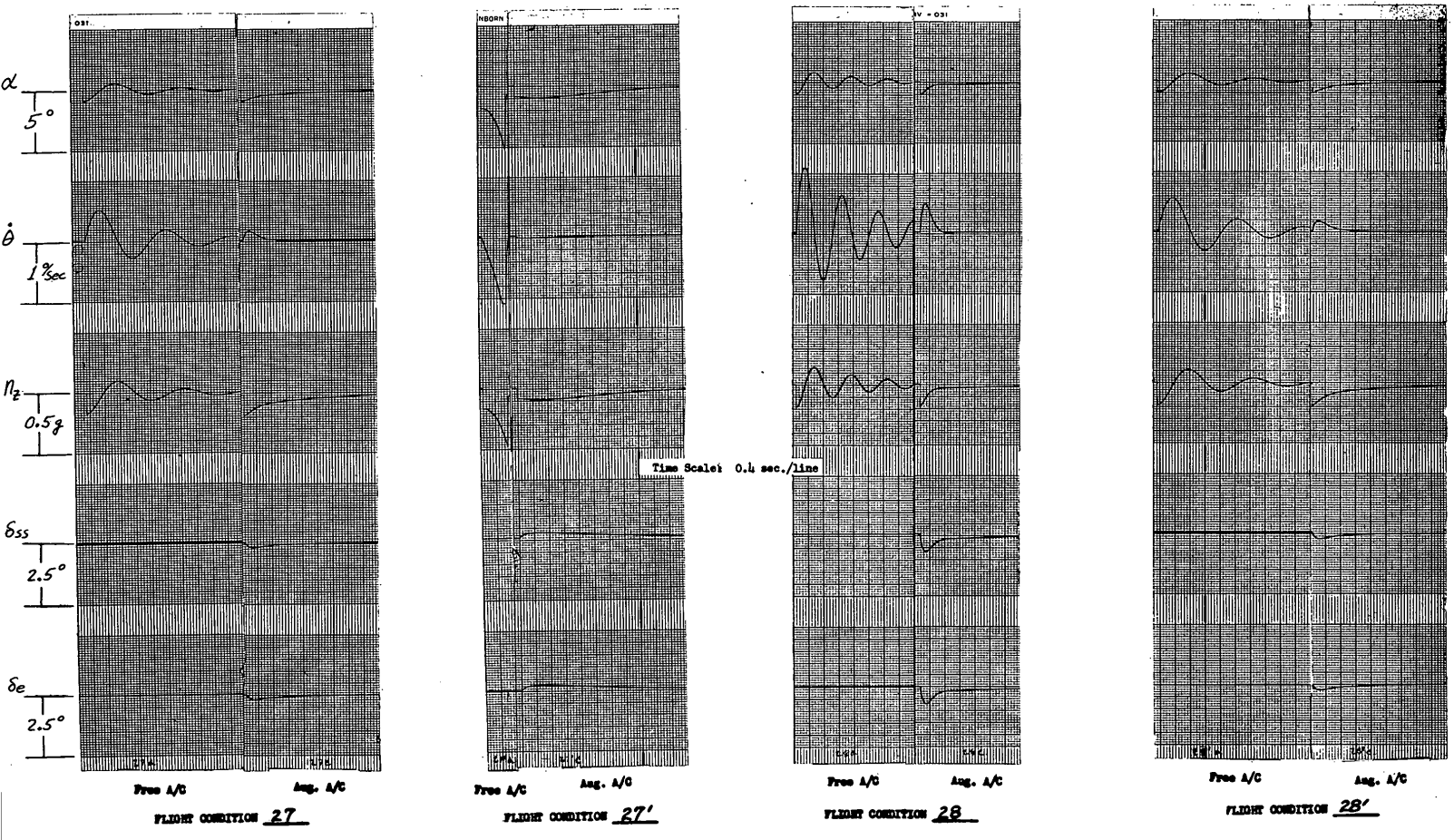

FIGURE NO. 6.9

WLO-72-60

α Gust = 50 fps

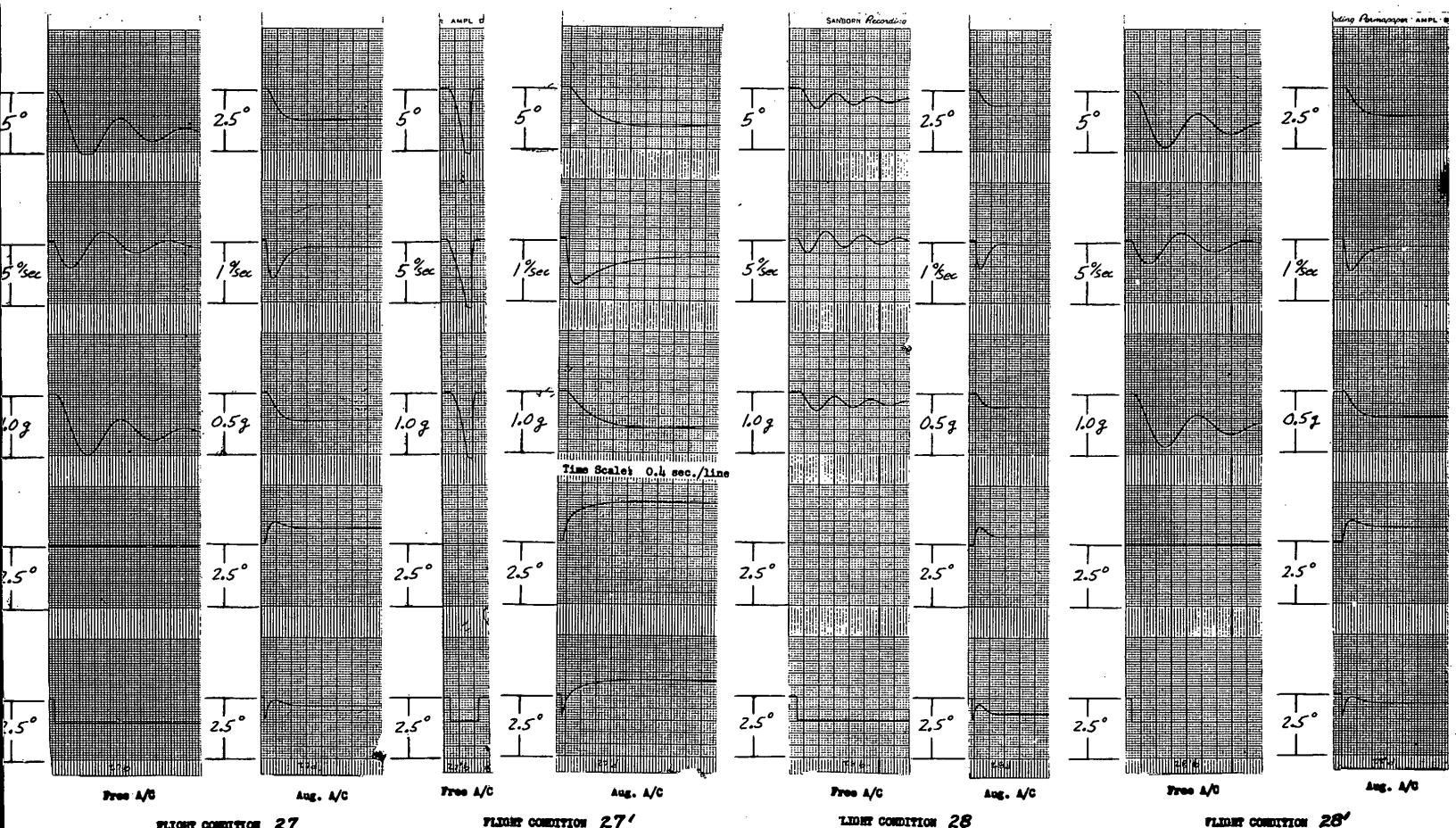

FLIGHT CONDITION 27 FLIGHT CONDITION 27' FLIGHT CONDITION 28 FLIGHT CONDITION 28'

FIGURE NO. 6.10

WLO-72-60

δ Step = 1°

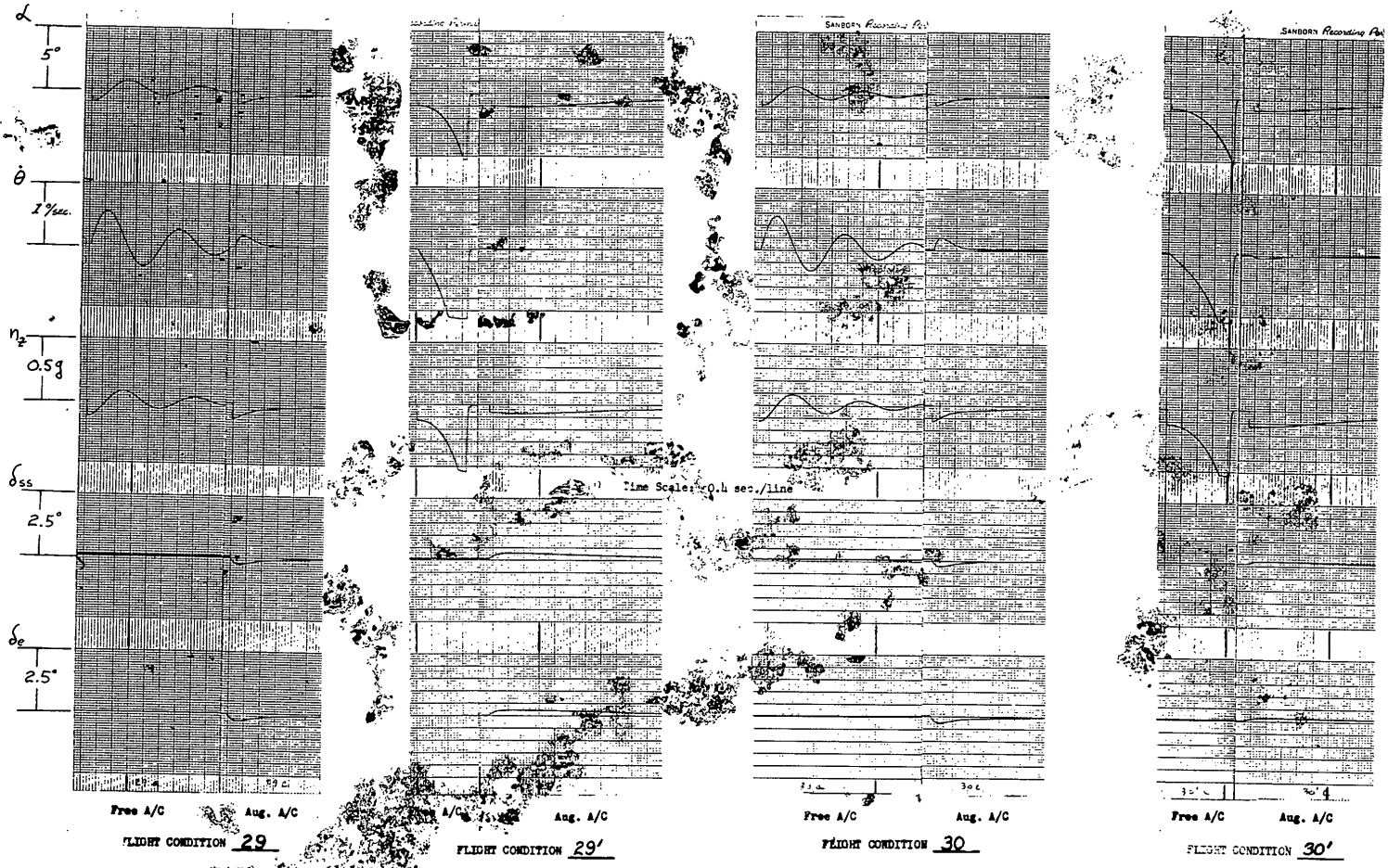

FIGURE NO. 6.11

α Gust = 50 fps

WLO-72-60

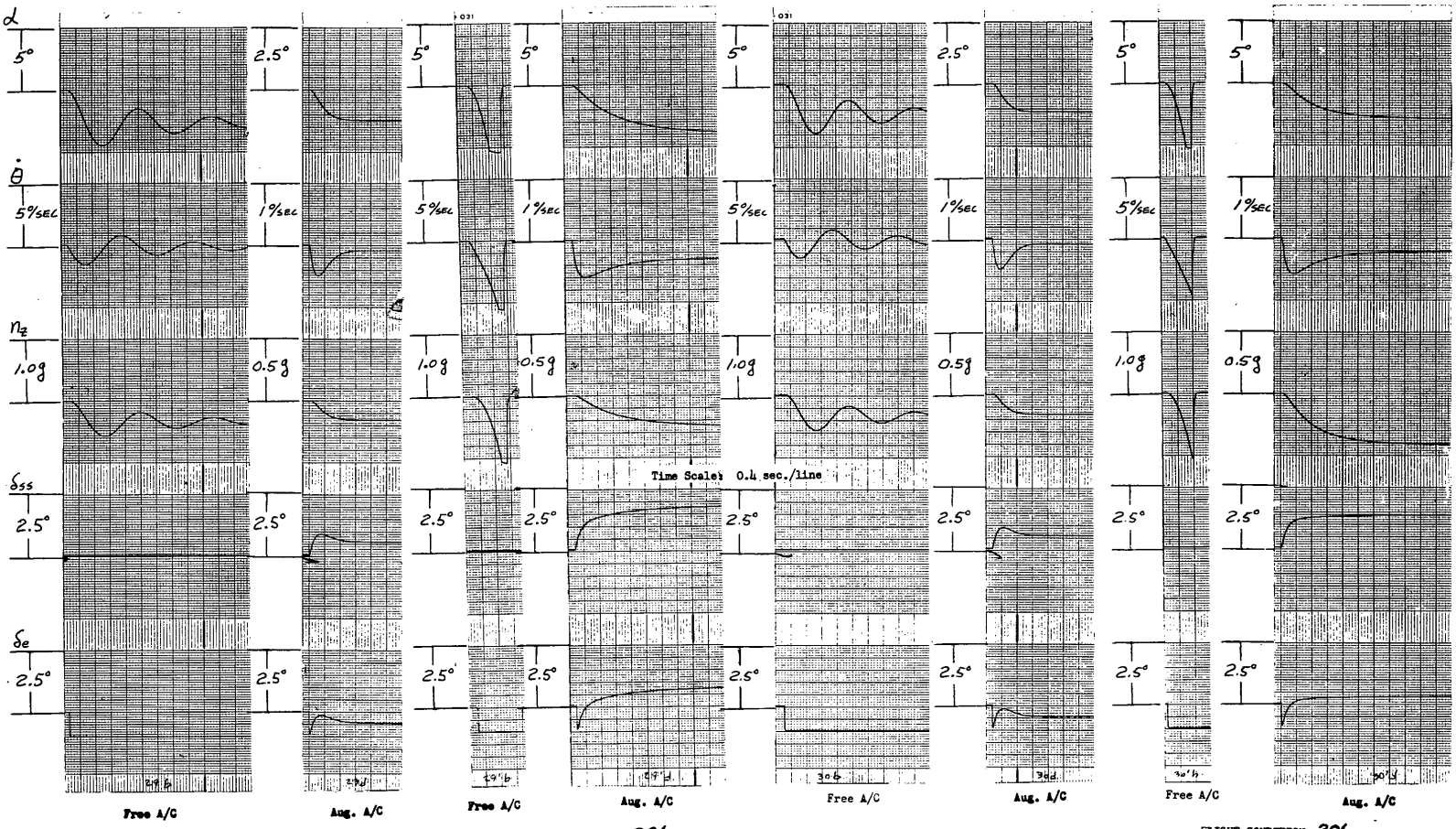

FIGURE NO. 6.12

WLO-72-60

δ Step = 1°

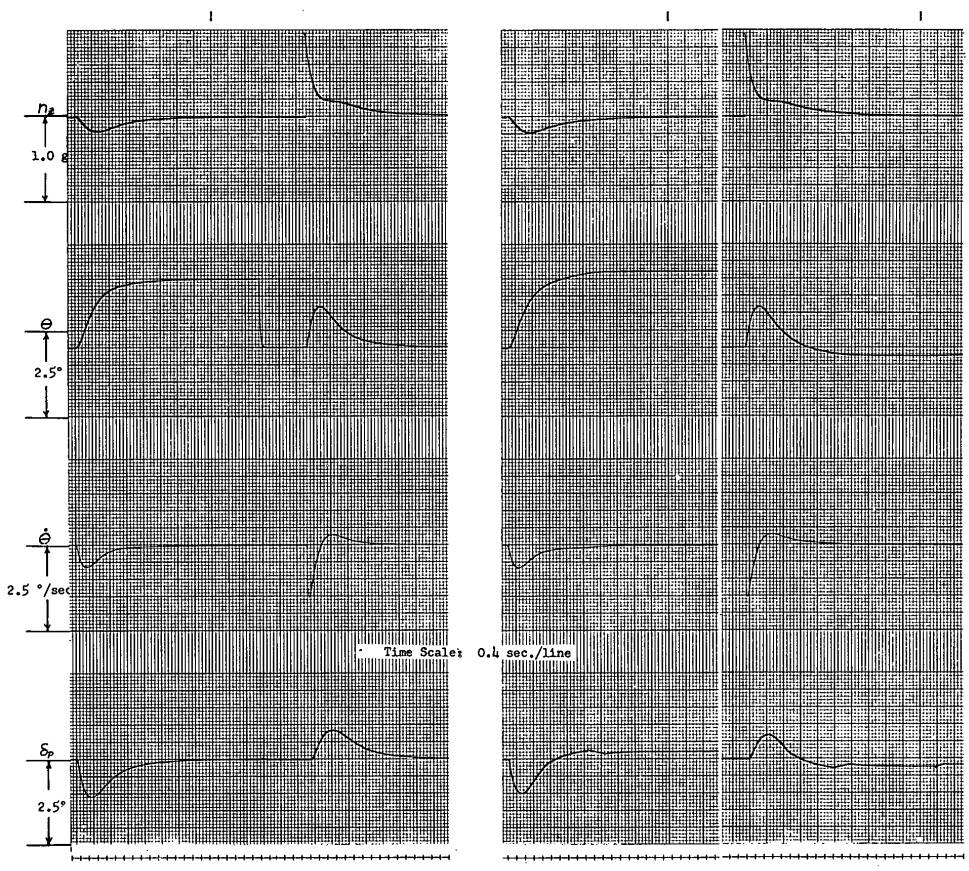

Pitch Attitude Hold

CONDITION 11

WLO-72-60

FIGURE NO. 6.13

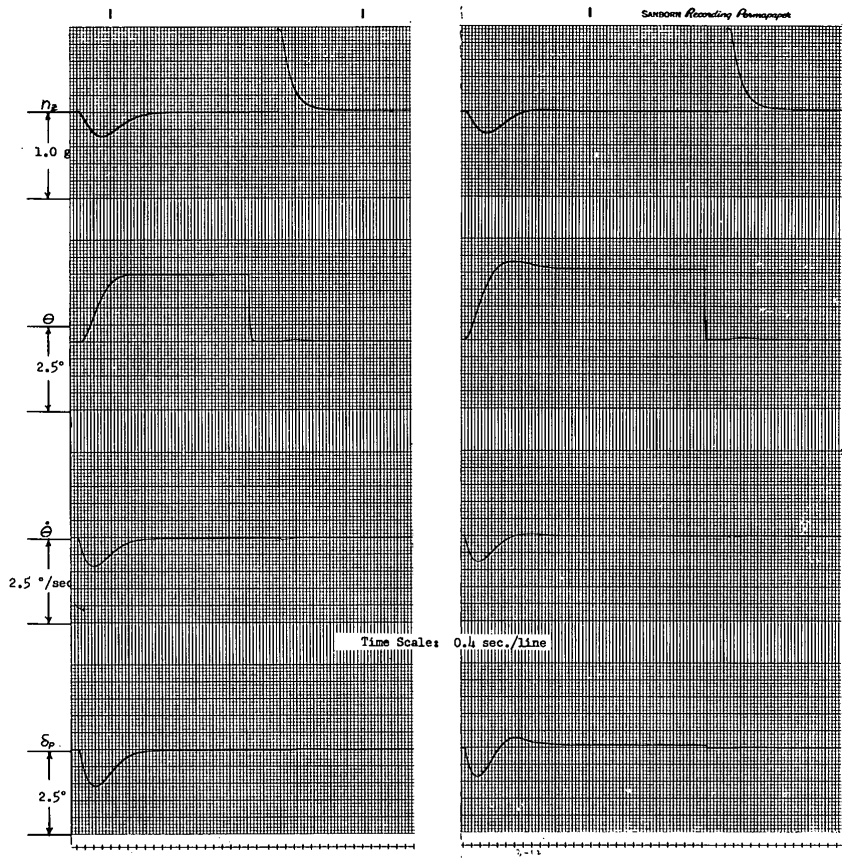

Pitch Attitude Hold

CONDITION 12

WLO-72-60

FIGURE NO. 614

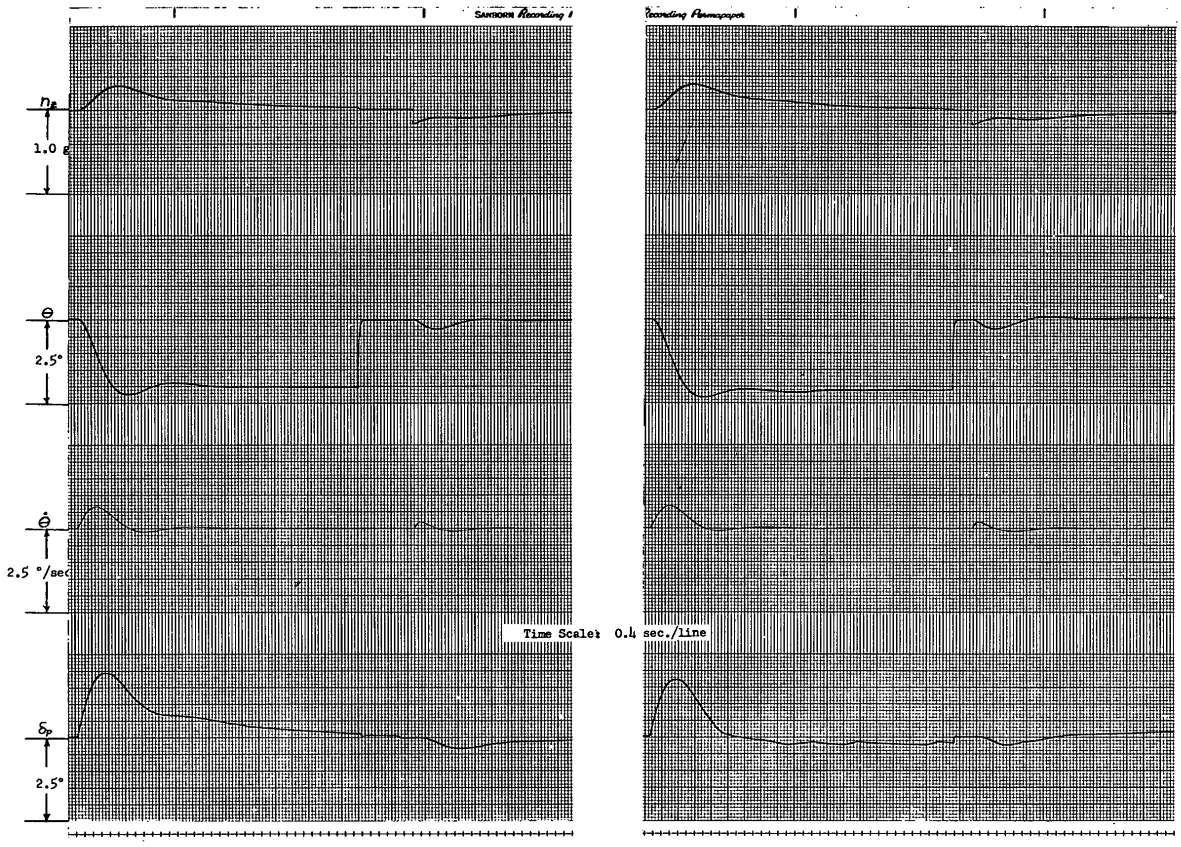

Pitch Attitude Hold

CONDITION 24

WLO-72-60

FIGURE NO. 6.15

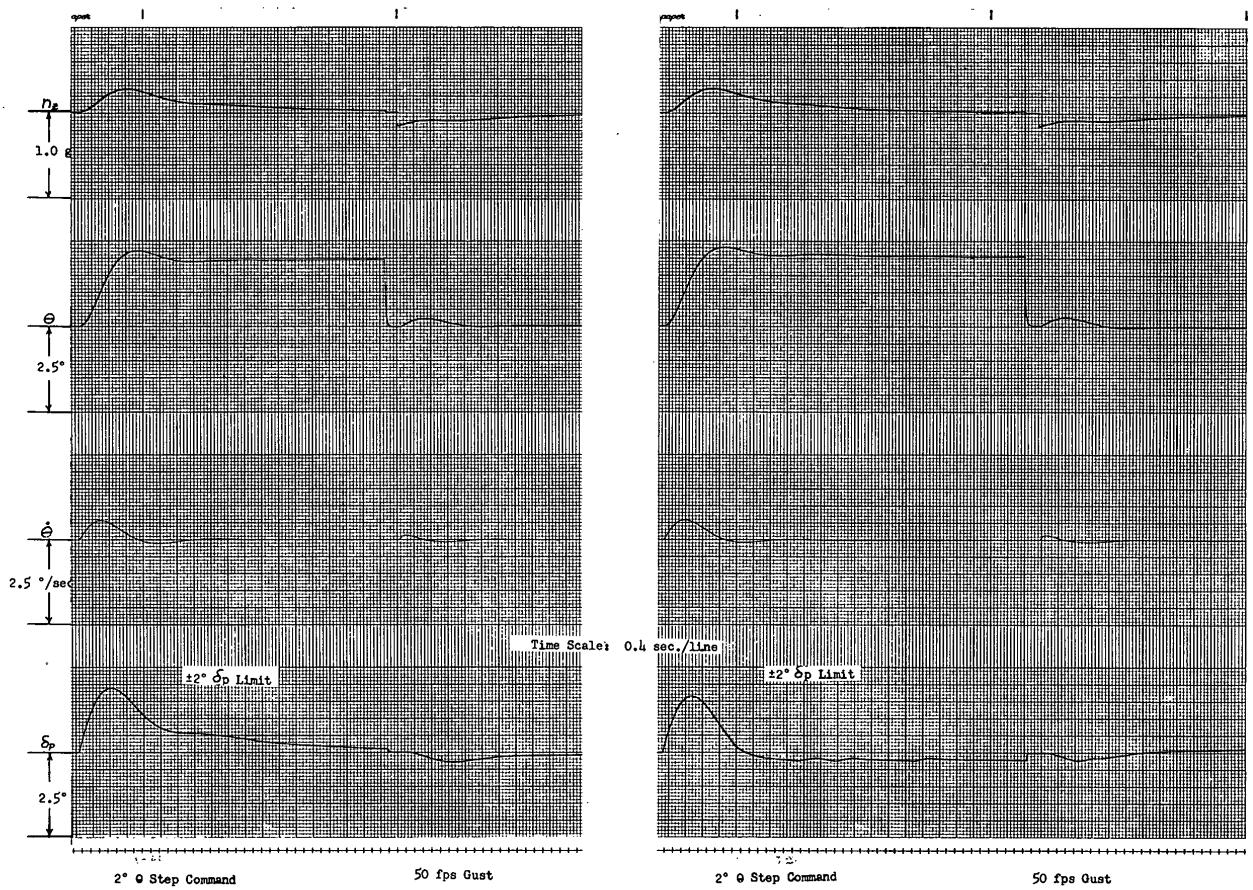

Pitch Attitude Hold

CONDITION 26

WLO-72-60

FIGURE NO. 6.16

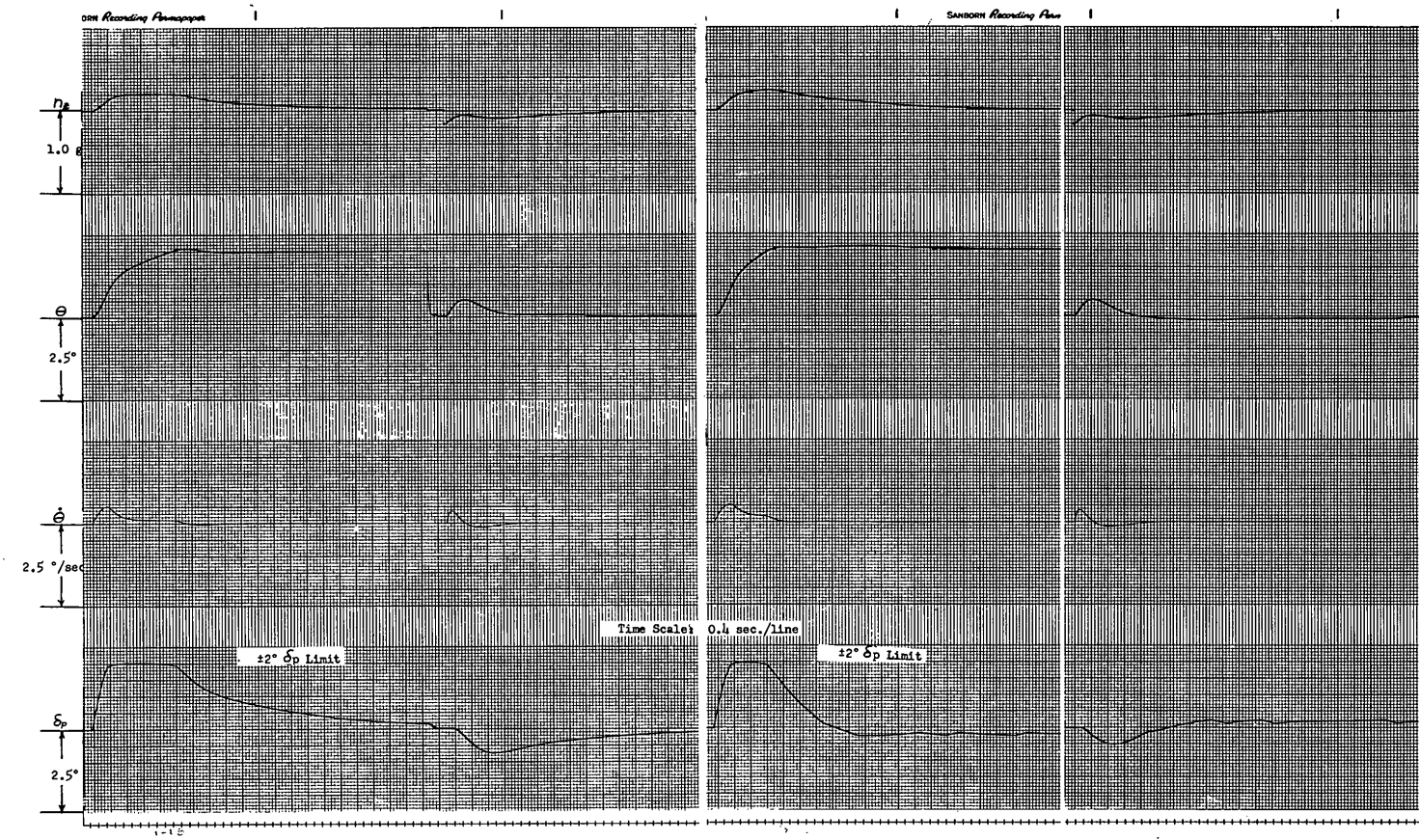

Pitch Attitude Hold

CONDITION 28

WLO-72-60

FIGURE NO. 6.17

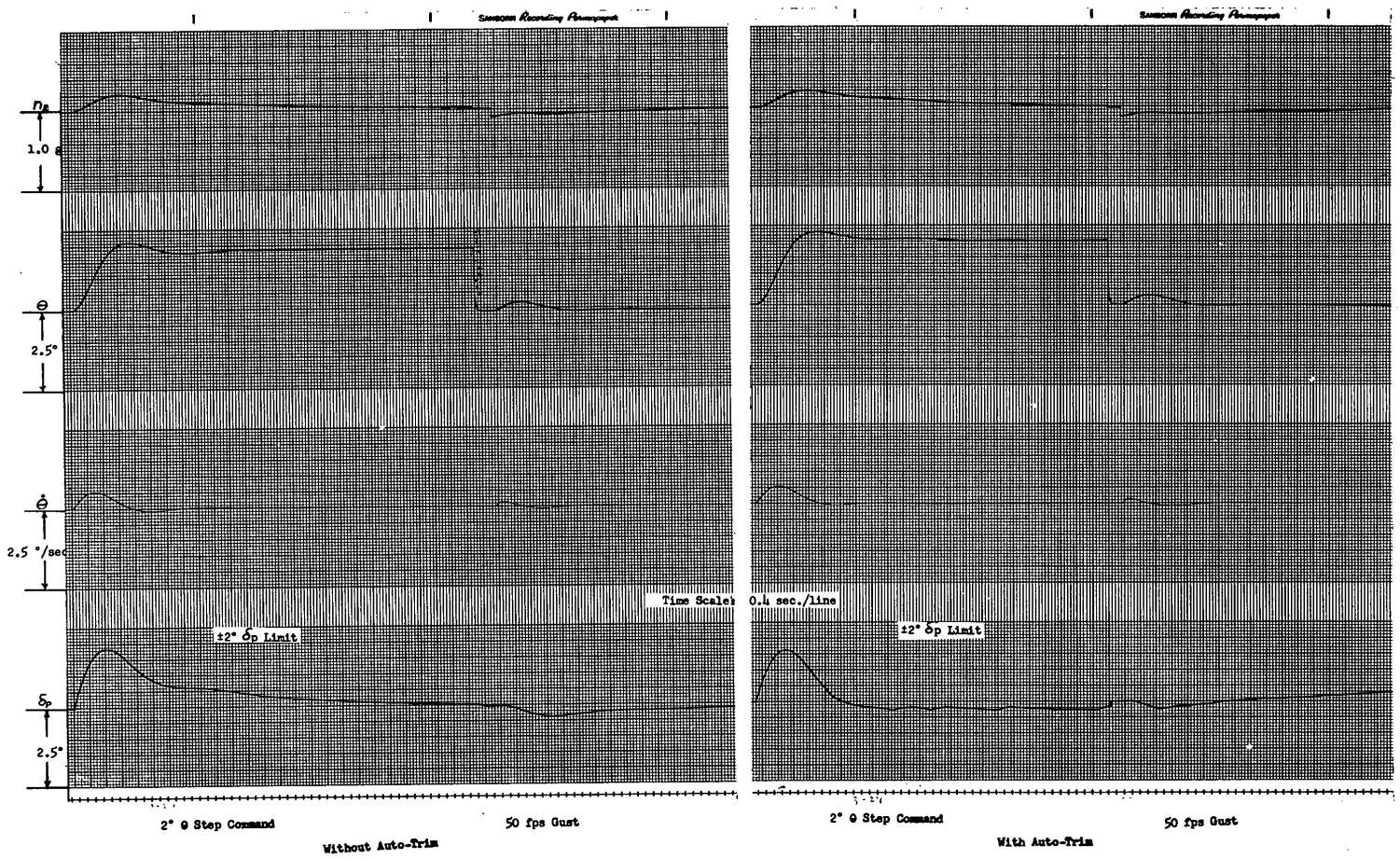

Pitch Attitude Hold

MLO-72-60

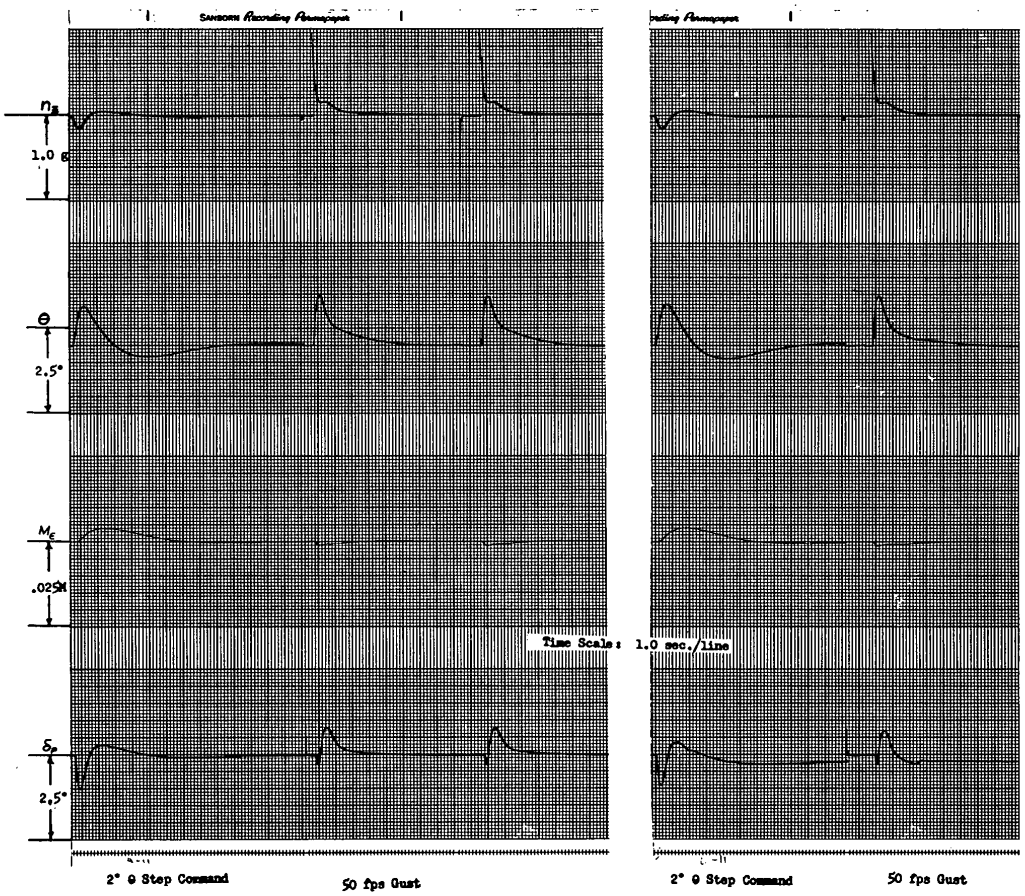

Mach Hold

CONDITION 11

WLO-72-60

FIGURE NO. 6.19

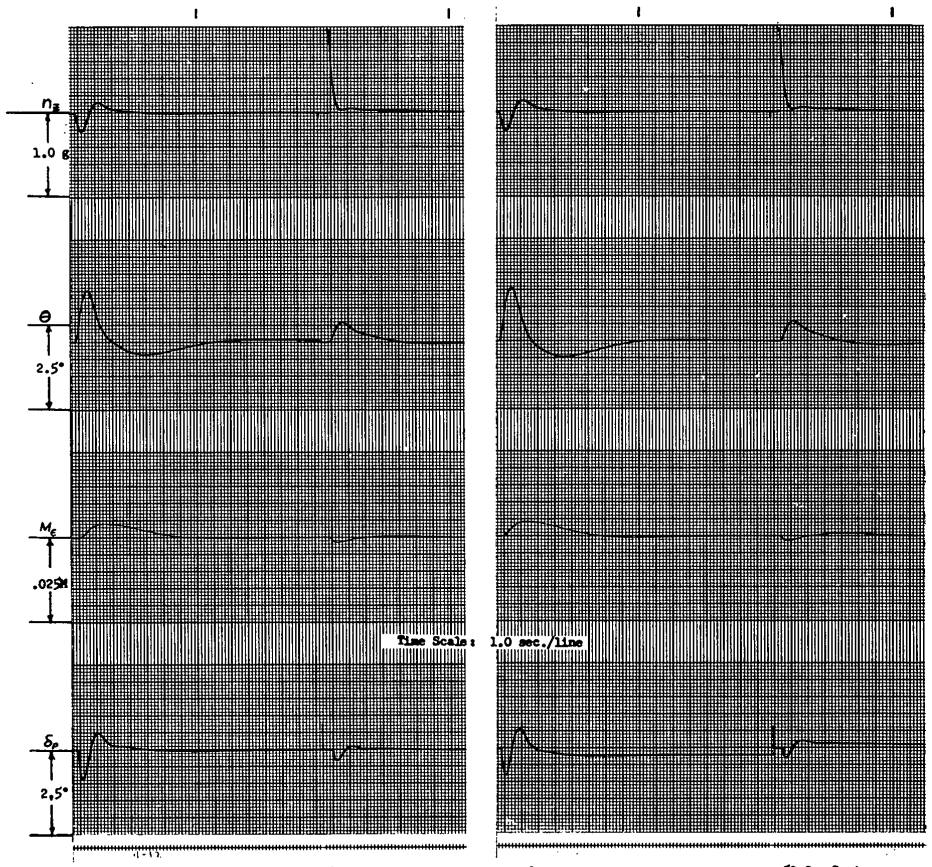

FIGURE NO. 6.20

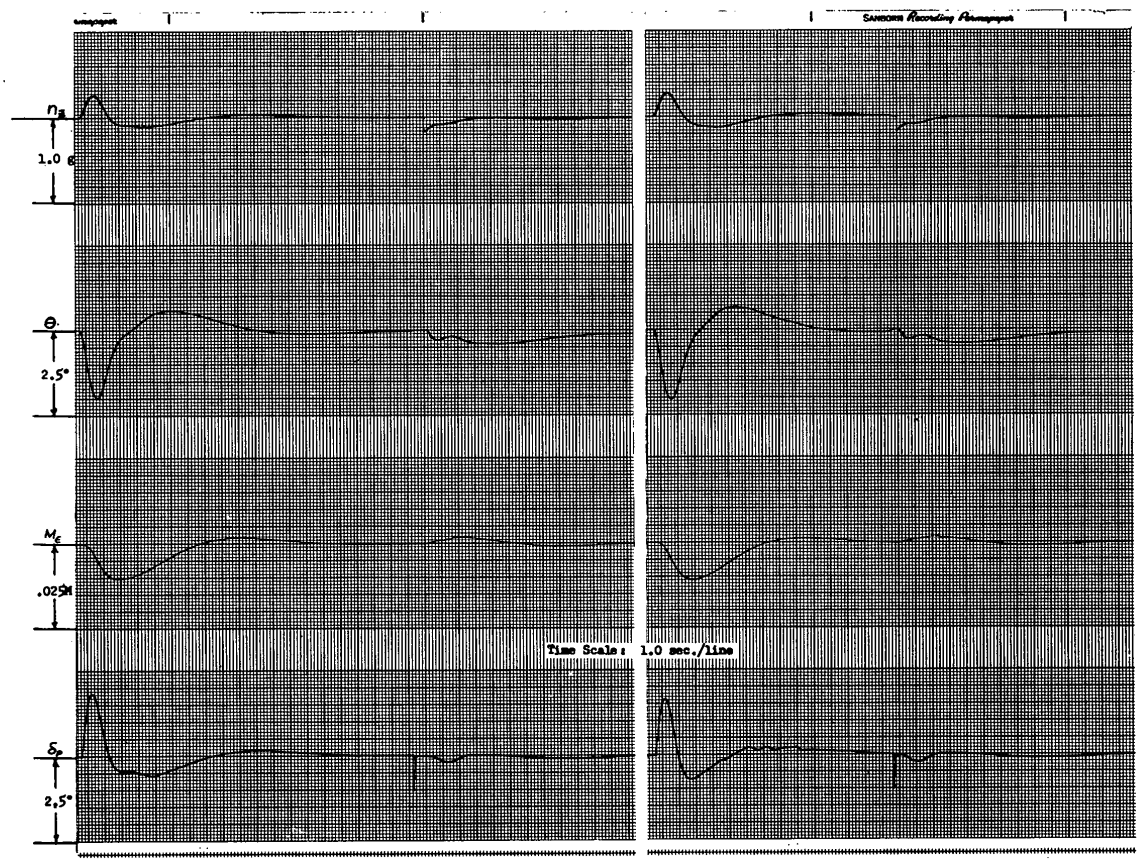

Mach Hold

CONDITION 24

WLO-72-60

FIGURE NO. 6.21

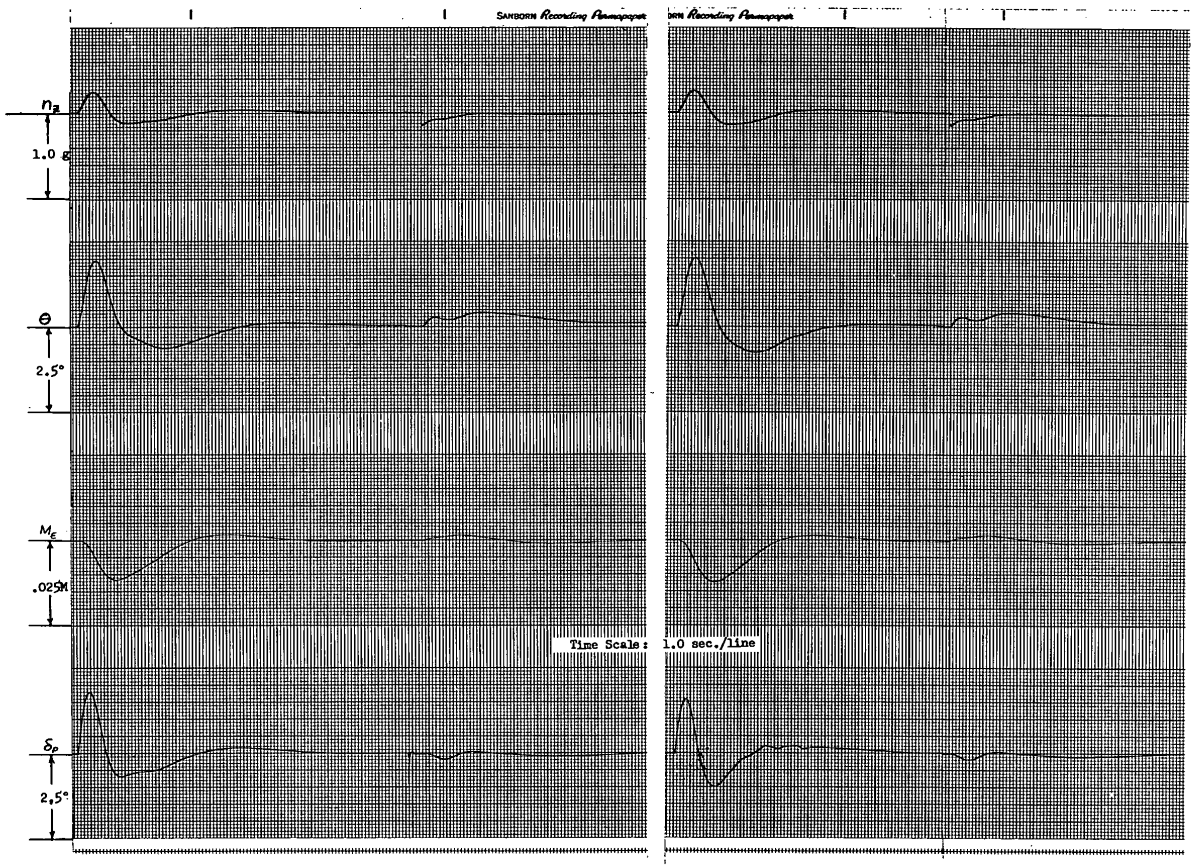

Mach Hold
CONDITION 26

WLO-72-60

FIGURE NO. 6.22

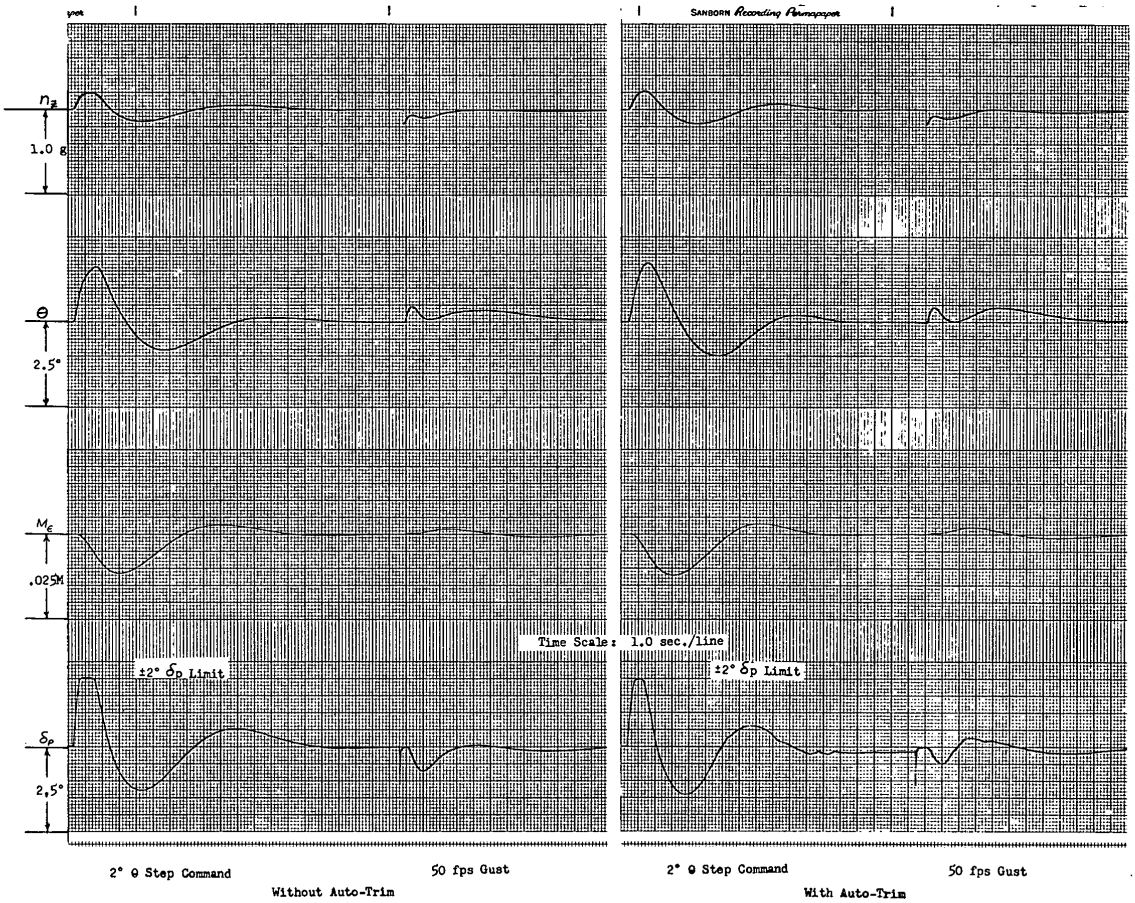

CONDITION 28

FIGURE NO. 6.23

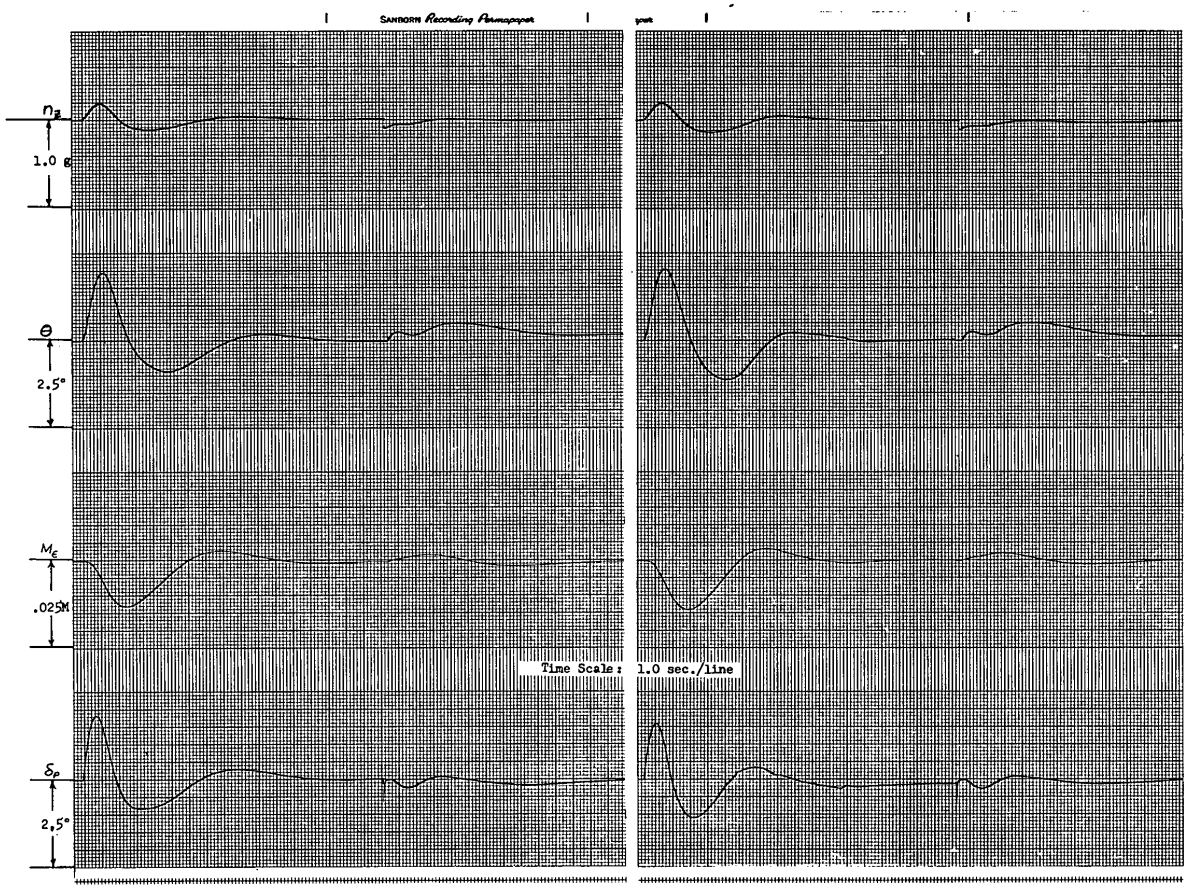

CONDITION 29

FIGURE NO. 6.24

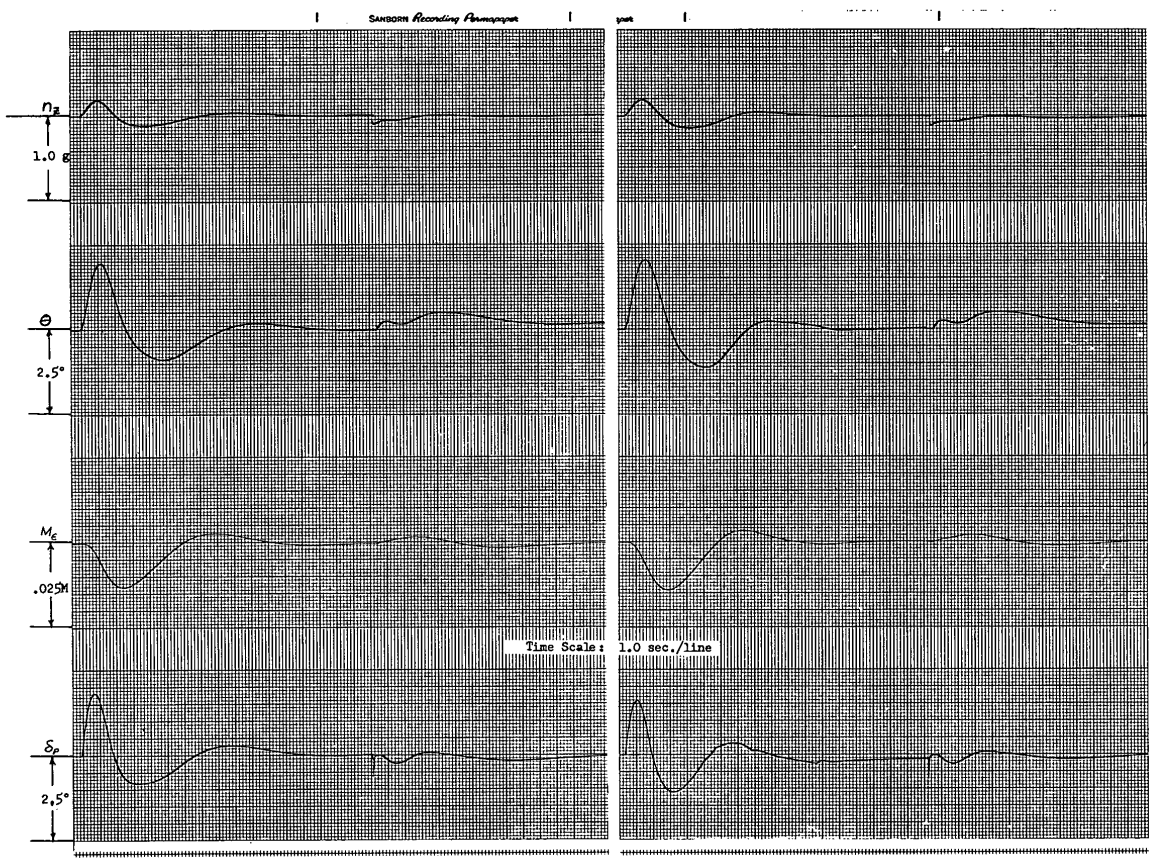

CONDITION 29

FIGURE NO. 6.24

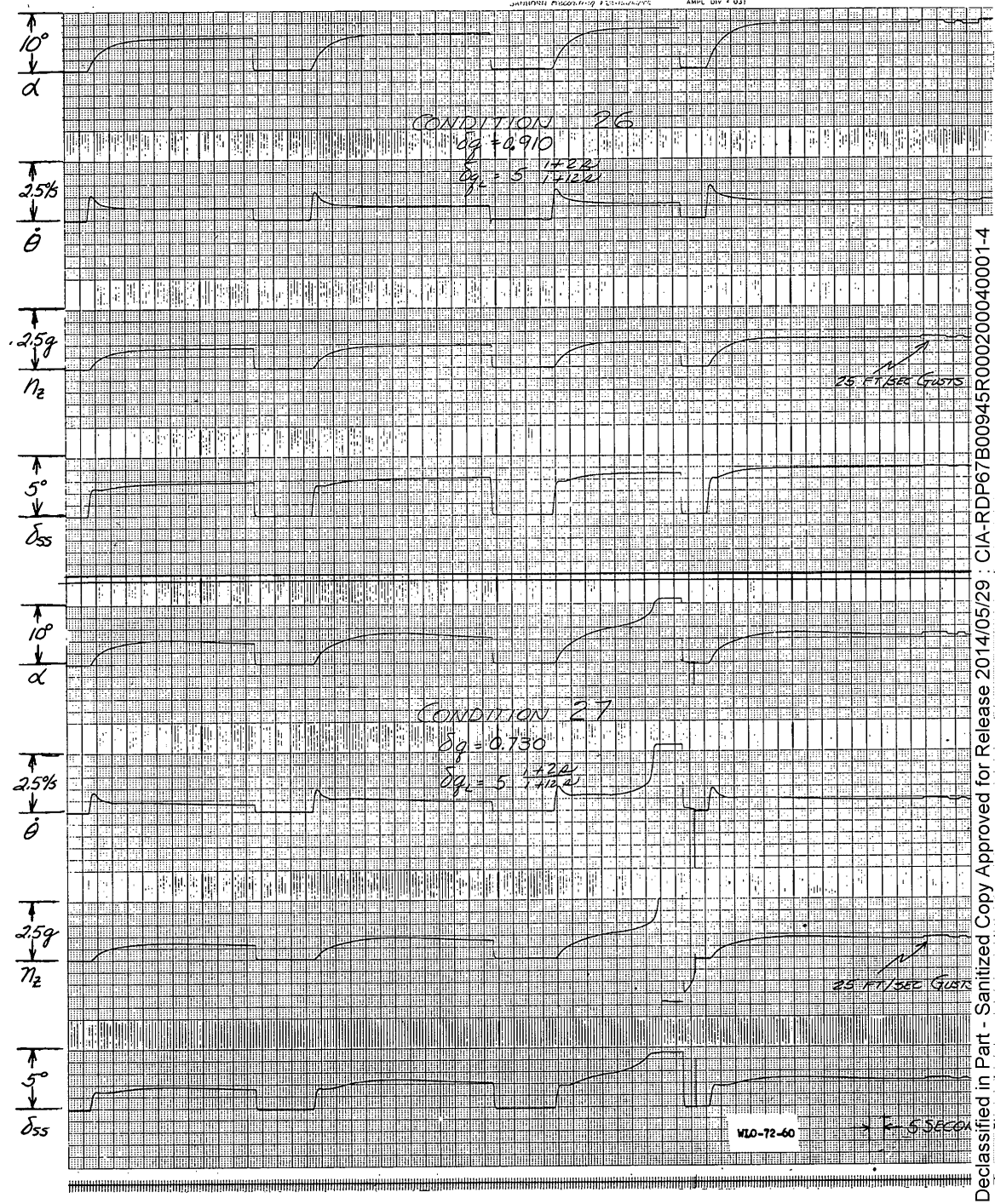

FIGURE 6.25 NONLINEAR DAMPER RESPONSES TO STICK FORCE COMMANDS NEAR IG, CONDITIONS 26 & 27

Declassified in Part - Sanitized Copy Approved for Release 2014/05/29 : CIA-RDP67B00945R000200040001-4

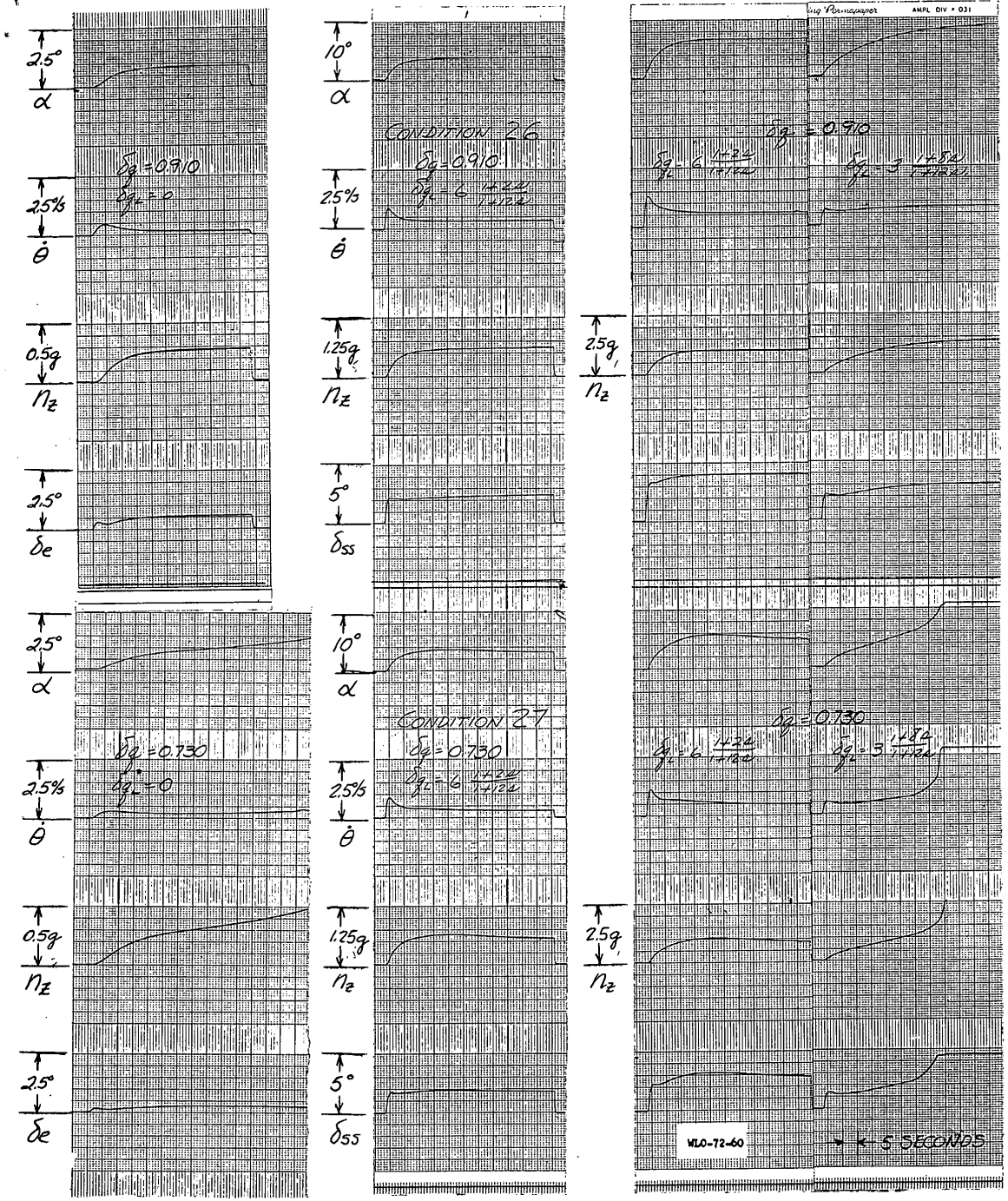

FIGURE 6.26 EFFECT OF LAGGED PITCH RATE FEEDBACK ON NONLINEAR DAMPER RESPONSE TO STICK FORCE COMMANDS, COND. 26 & 27

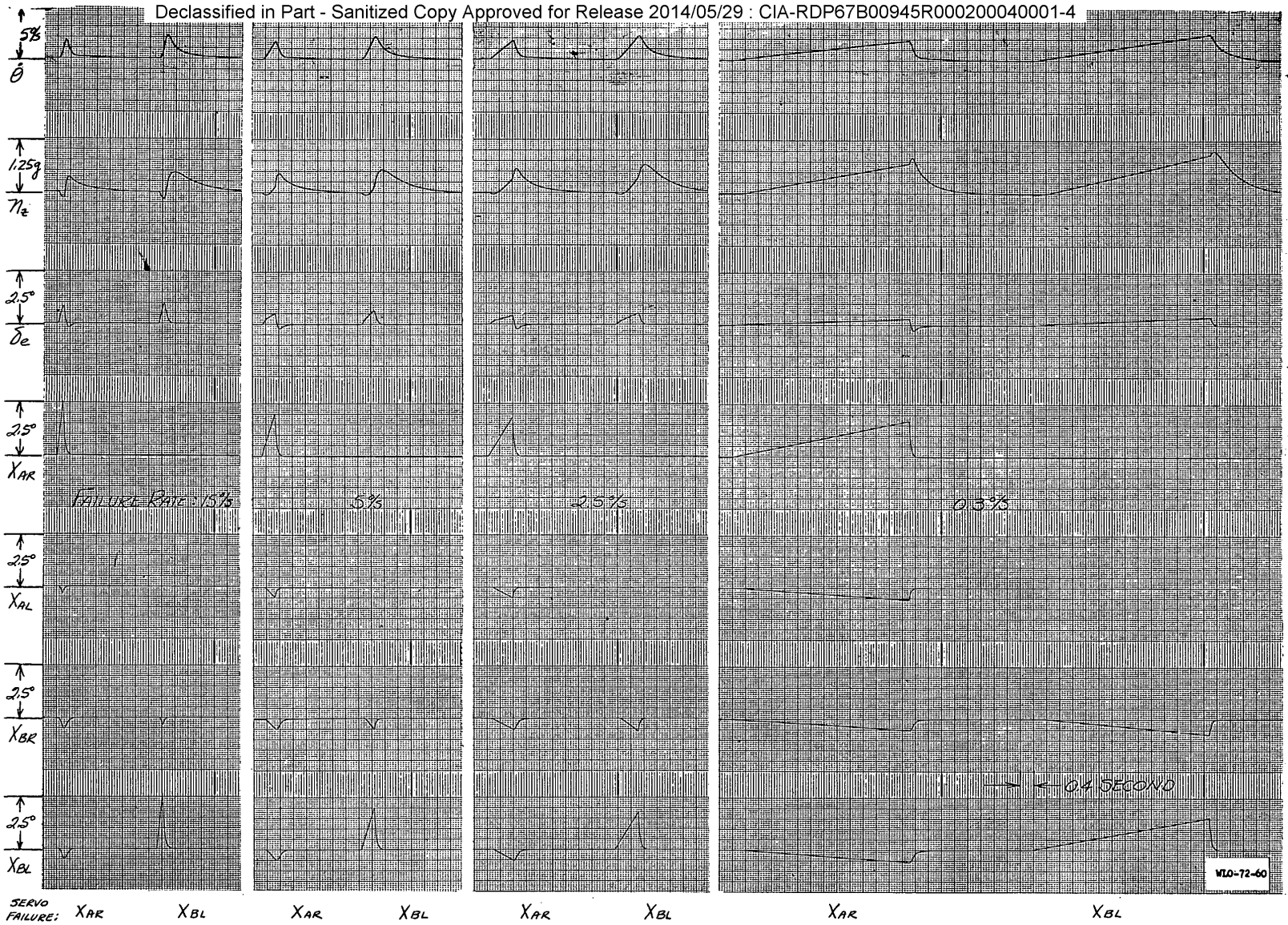

FIGURE 6.27 REDUNDANT PITCH DAMPER, FIRST AND SECOND CHANNEL SERVO FAILURES AT VARIOUS RATES, CONDITION 7

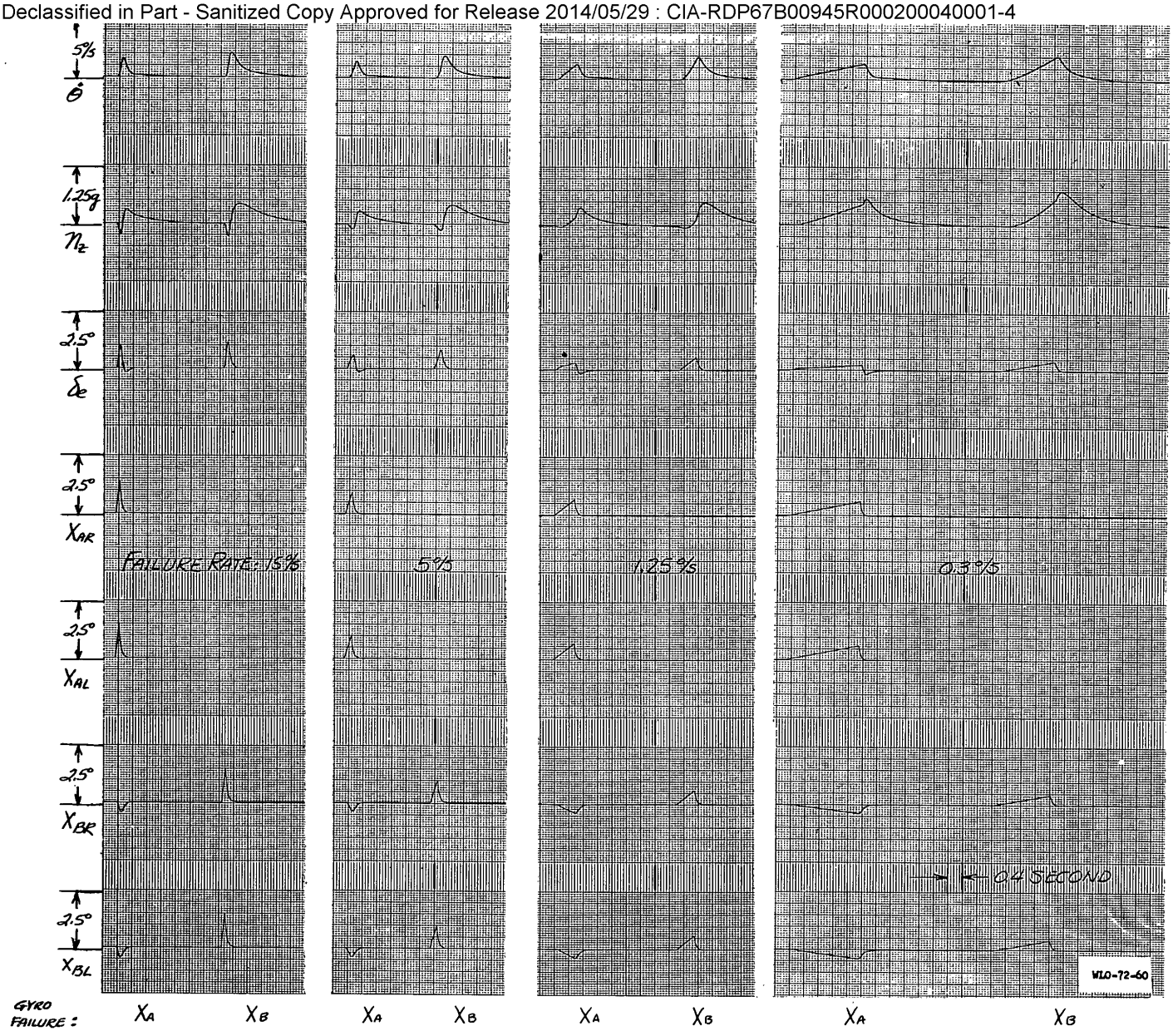

FIGURE 6.28 REDUNDANT PITCH DAMPER, FIRST AND SECOND CHANNEL GYRO FAILURES AT VARIOUS RATES, CONDITION 7

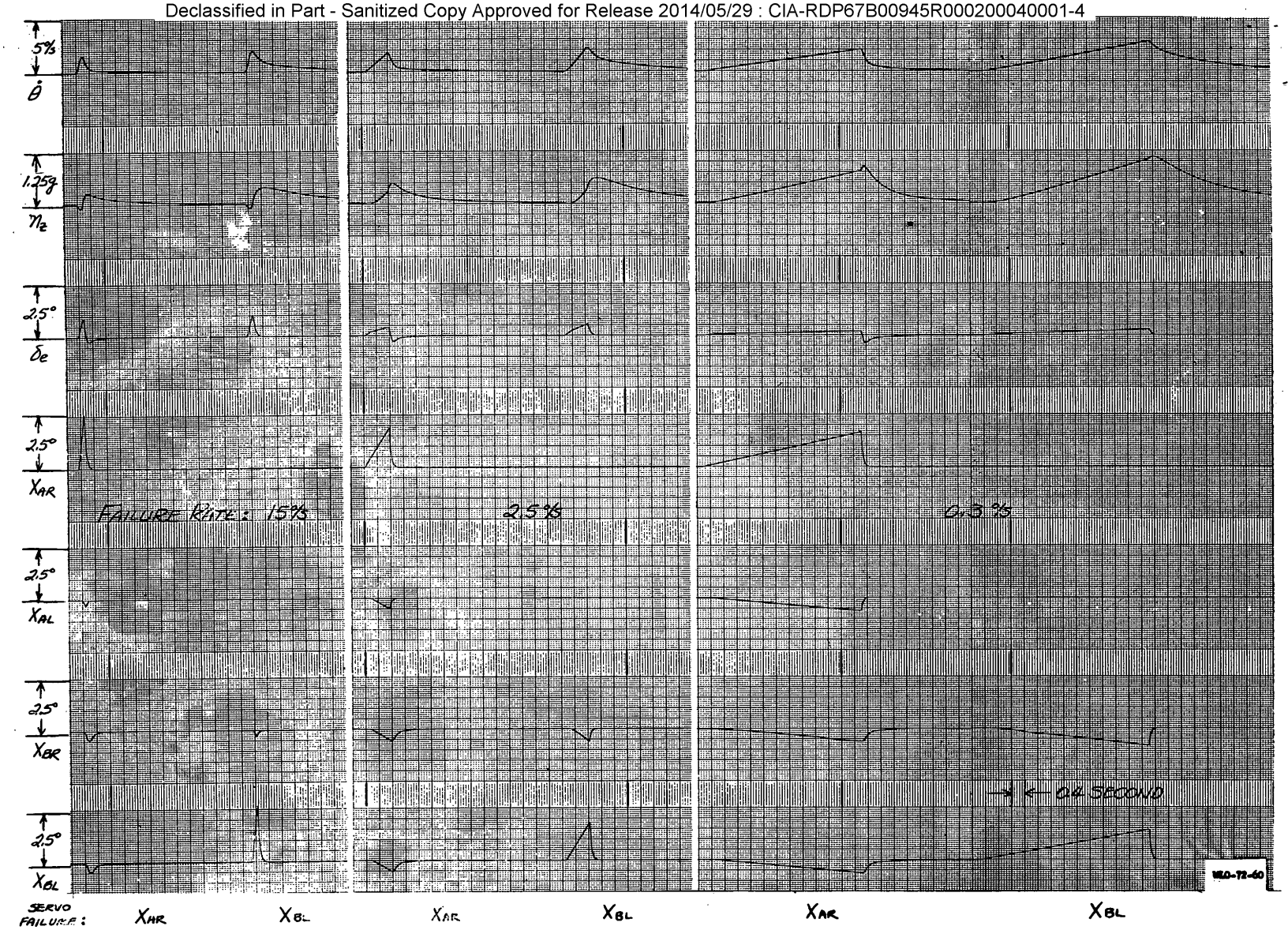

FIGURE 6.29 REDUNDANT PITCH DAMPER, FIRST AND SECOND CHANNEL SERVO FAILURES AT VARIOUS RATES, CONDITION 8

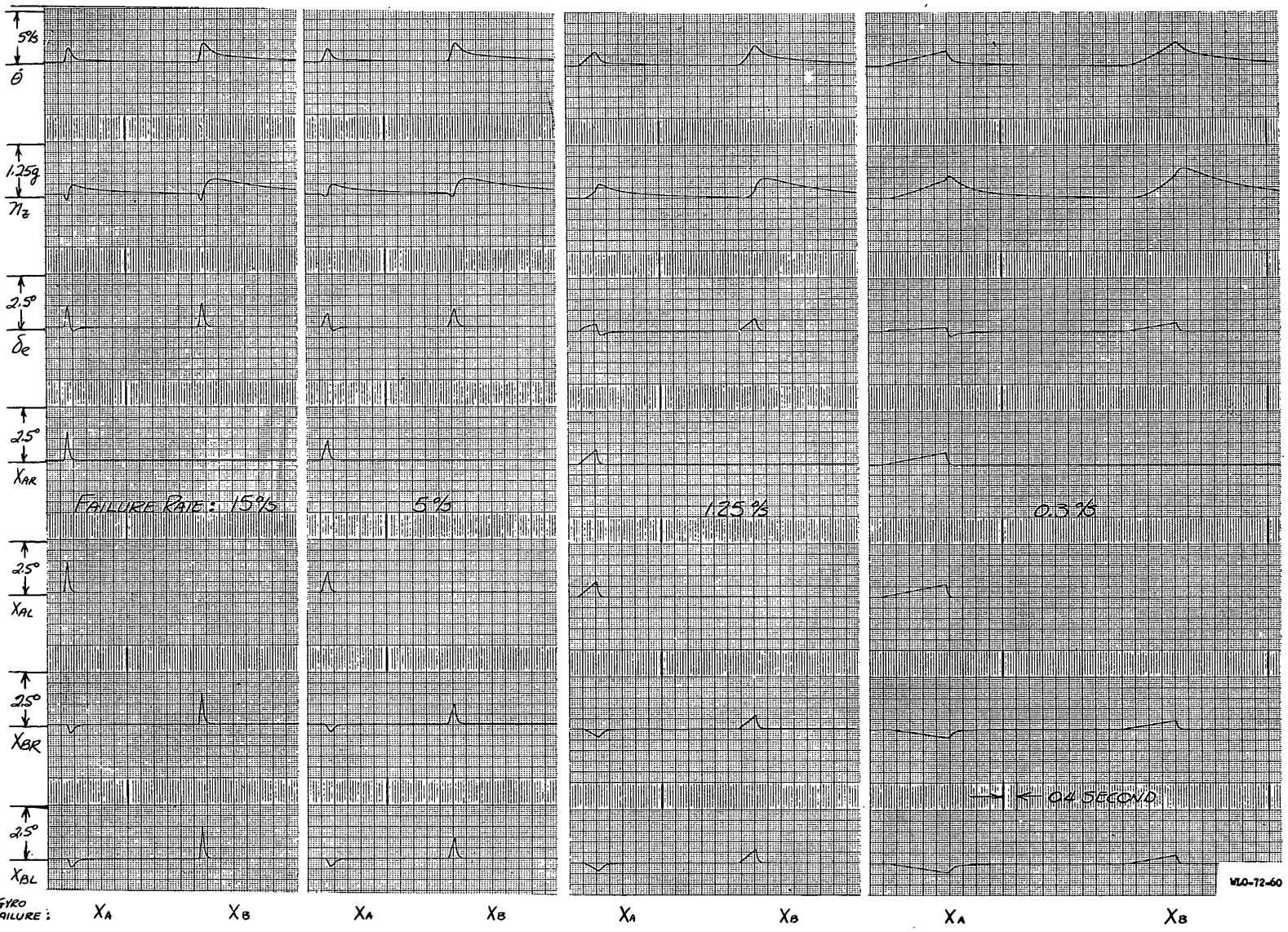

FIGURE 630 REDUNDANT PITCH DAMPER, FIRST AND SECOND CHANNEL GYRO FAILURES AT VARIOUS RATES, CONDITION 8

Declassified in Part - Sanitized Copy Approved for Release 2014/05/29 : CIA-RDP67B00945R000200040001-4

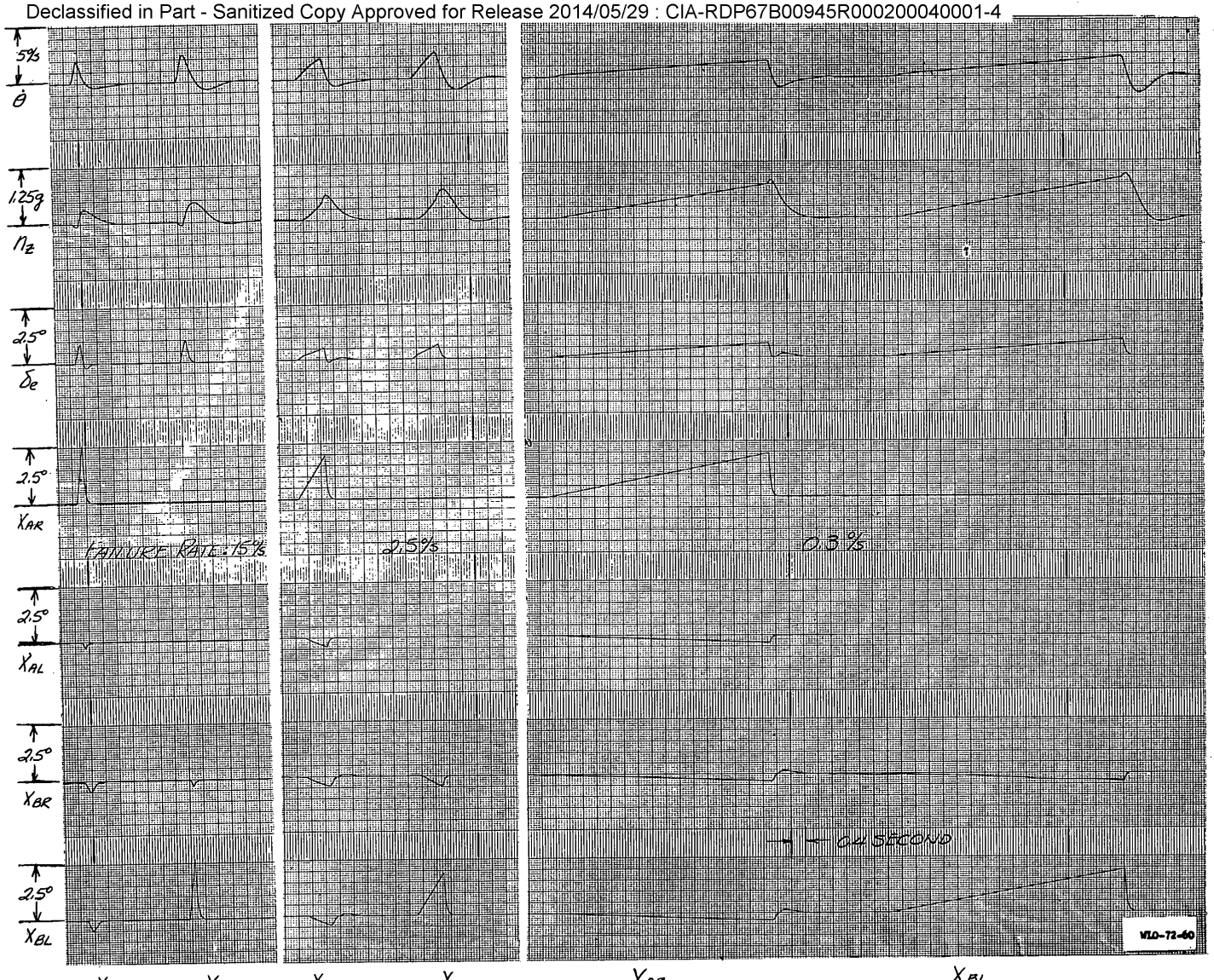

FIGURE 6.31 REDUNDANT PITCH DAMPER, FIRST AND SECOND CHANNEL SERVO FAILURES AT VARIOUS RATES, CONDITION 10

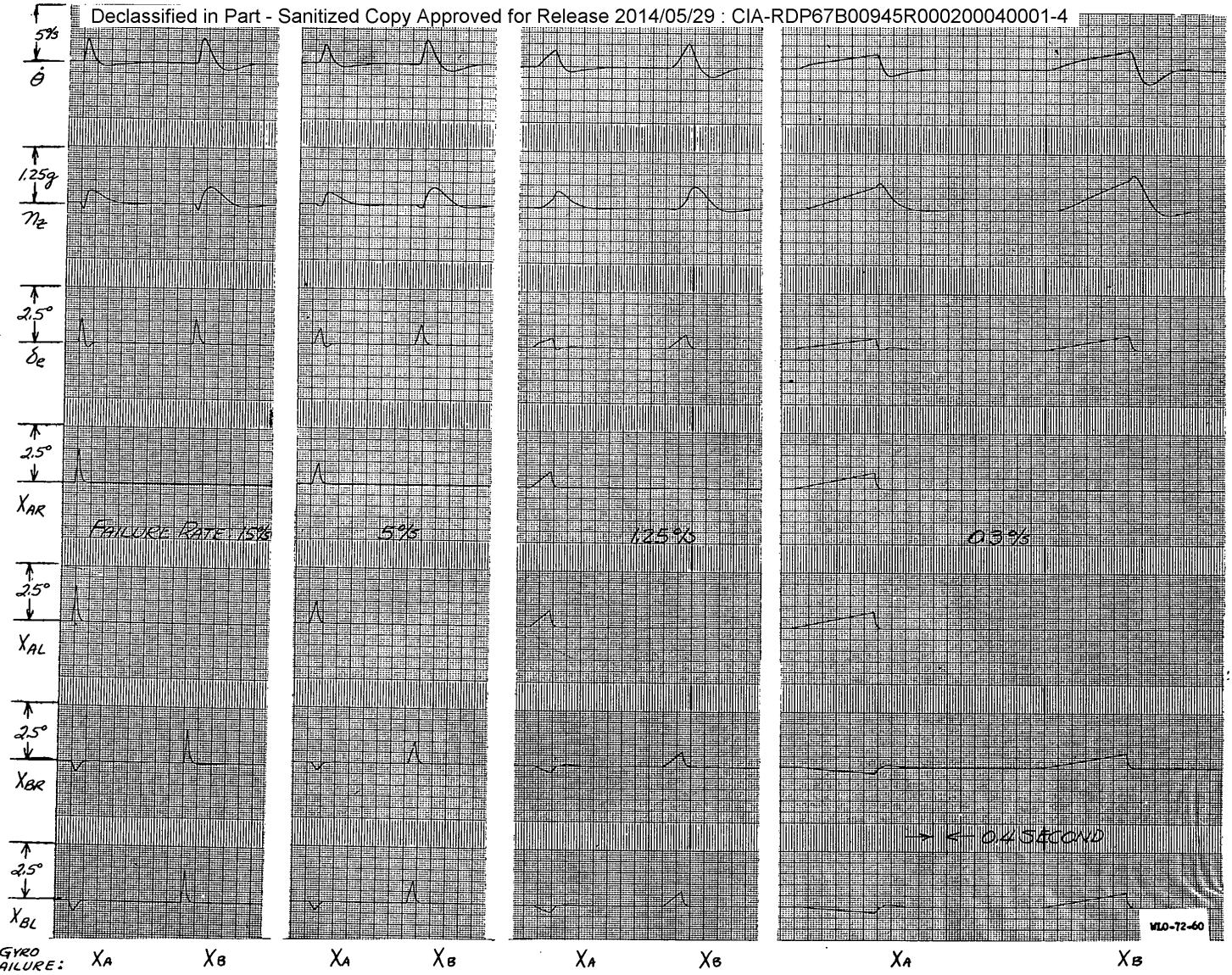

FIGURE 632 REDUNDANT PITCH DAMPER, FIRST AND SECOND CHANNEL GYRO FAILURES AT VARIOUS RATES, CONDITION 10

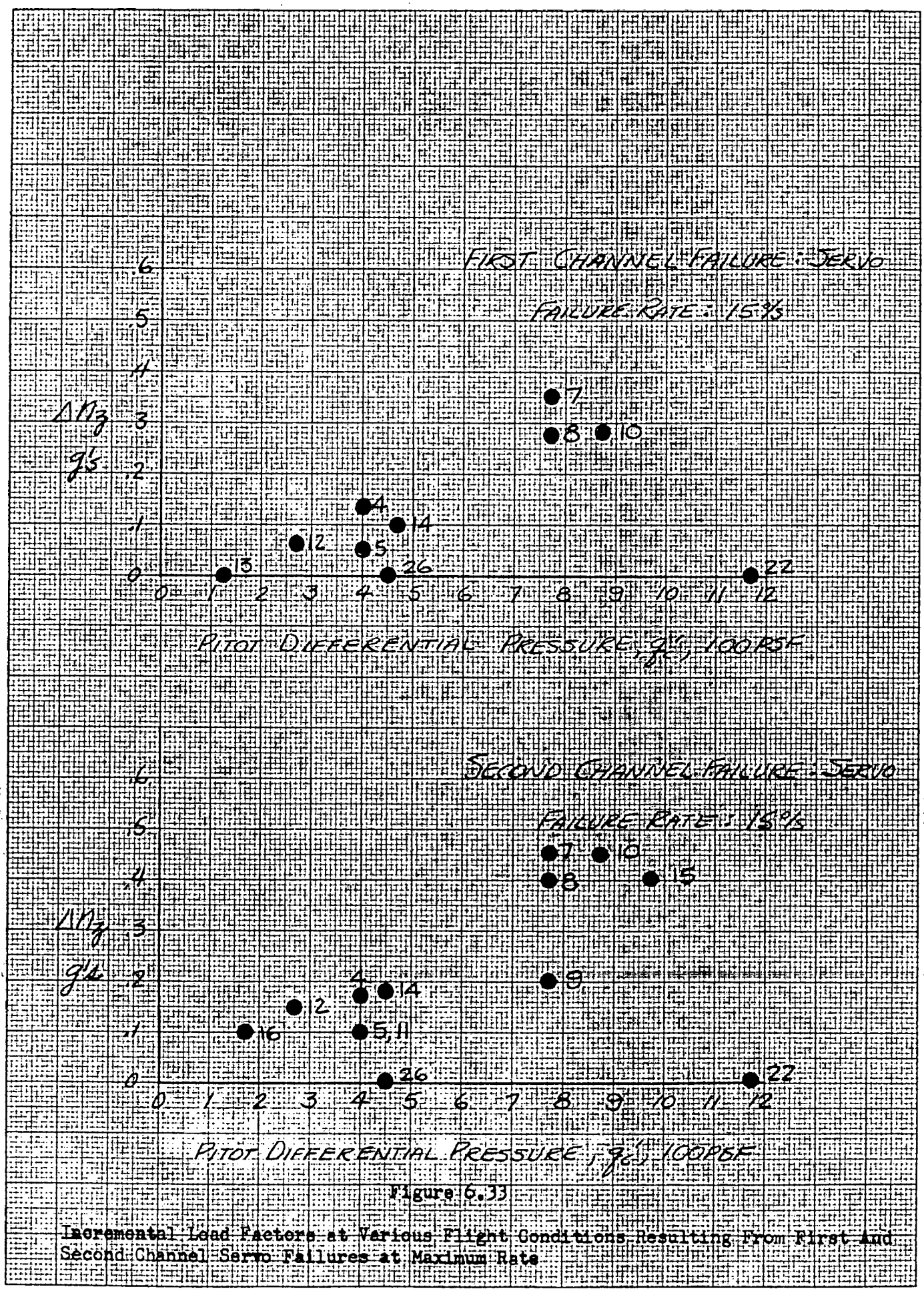

Figure 6.33

Incremental Load Factors at Various Flight Conditions Resulting From First And Second Channel Servo Failures at Maximum Rate

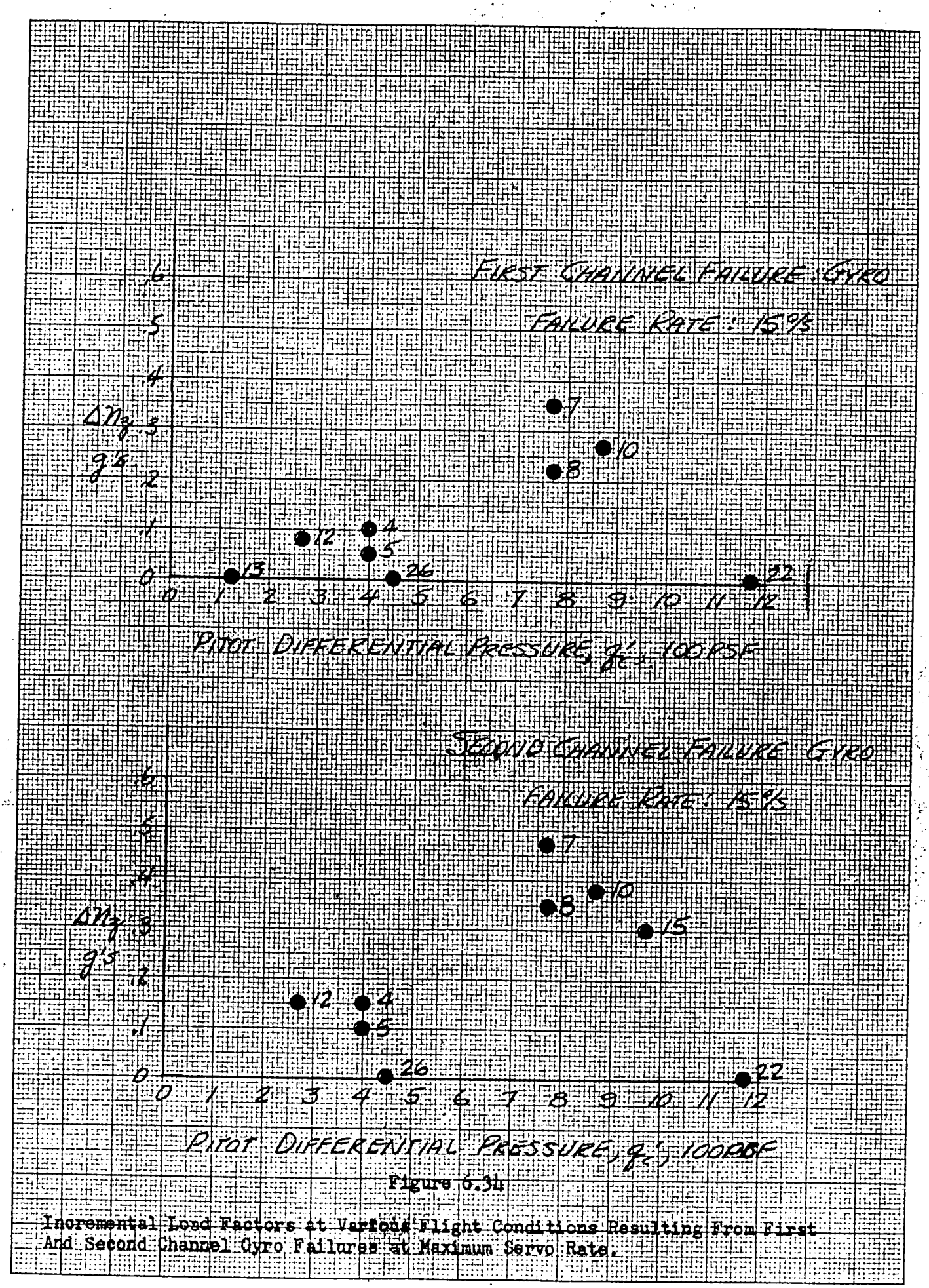

Figure 6.34

Incremental Load Factors at Various Flight Conditions Resulting From First And Second Channel Gyro Failures at Maximum Servo Rate.

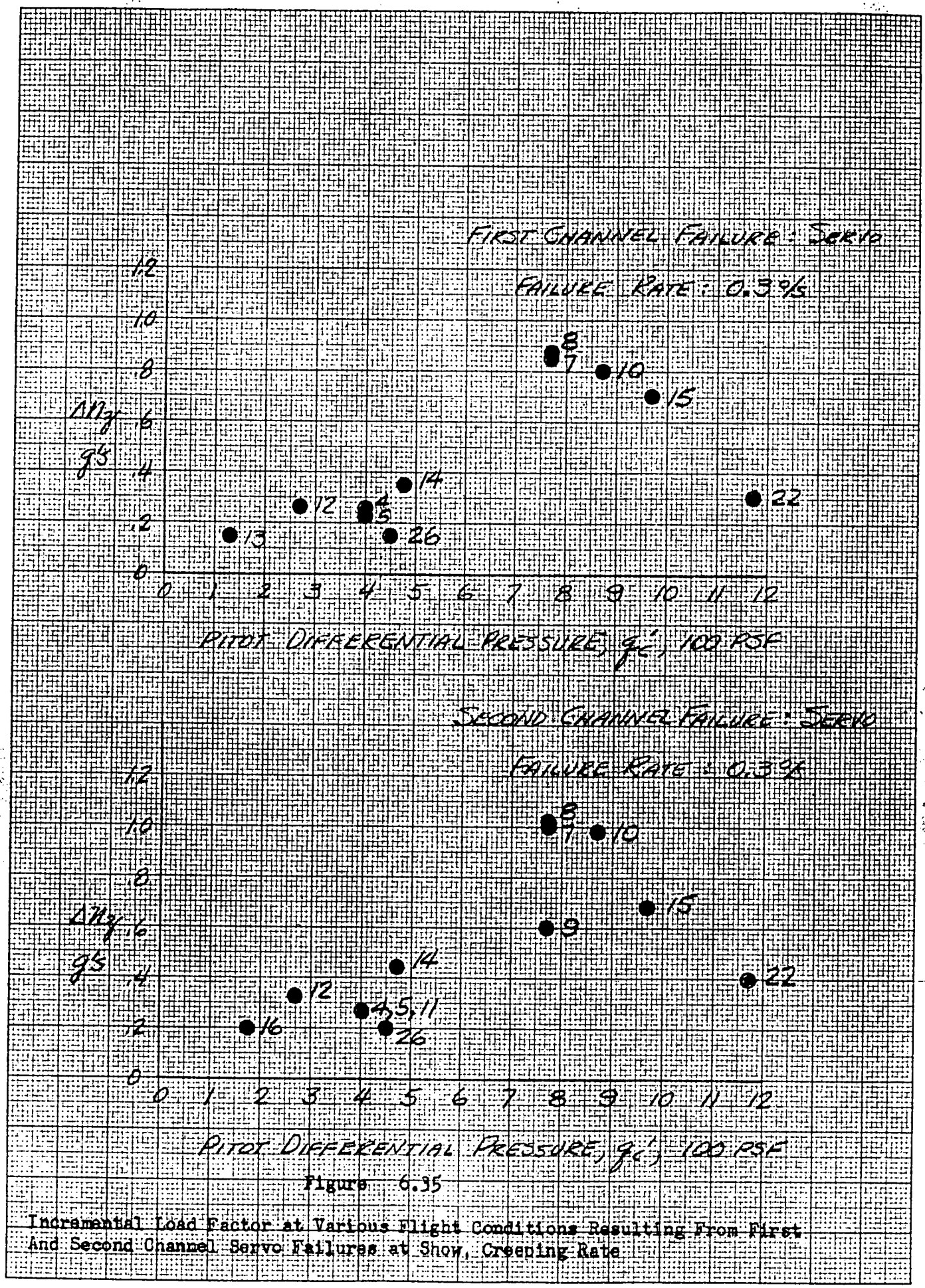

Figure 6.35

Incramental Load Factor at Various Flight Conditions Resulting From First And Second Channel Servo Failures at Show, Creeping Rate

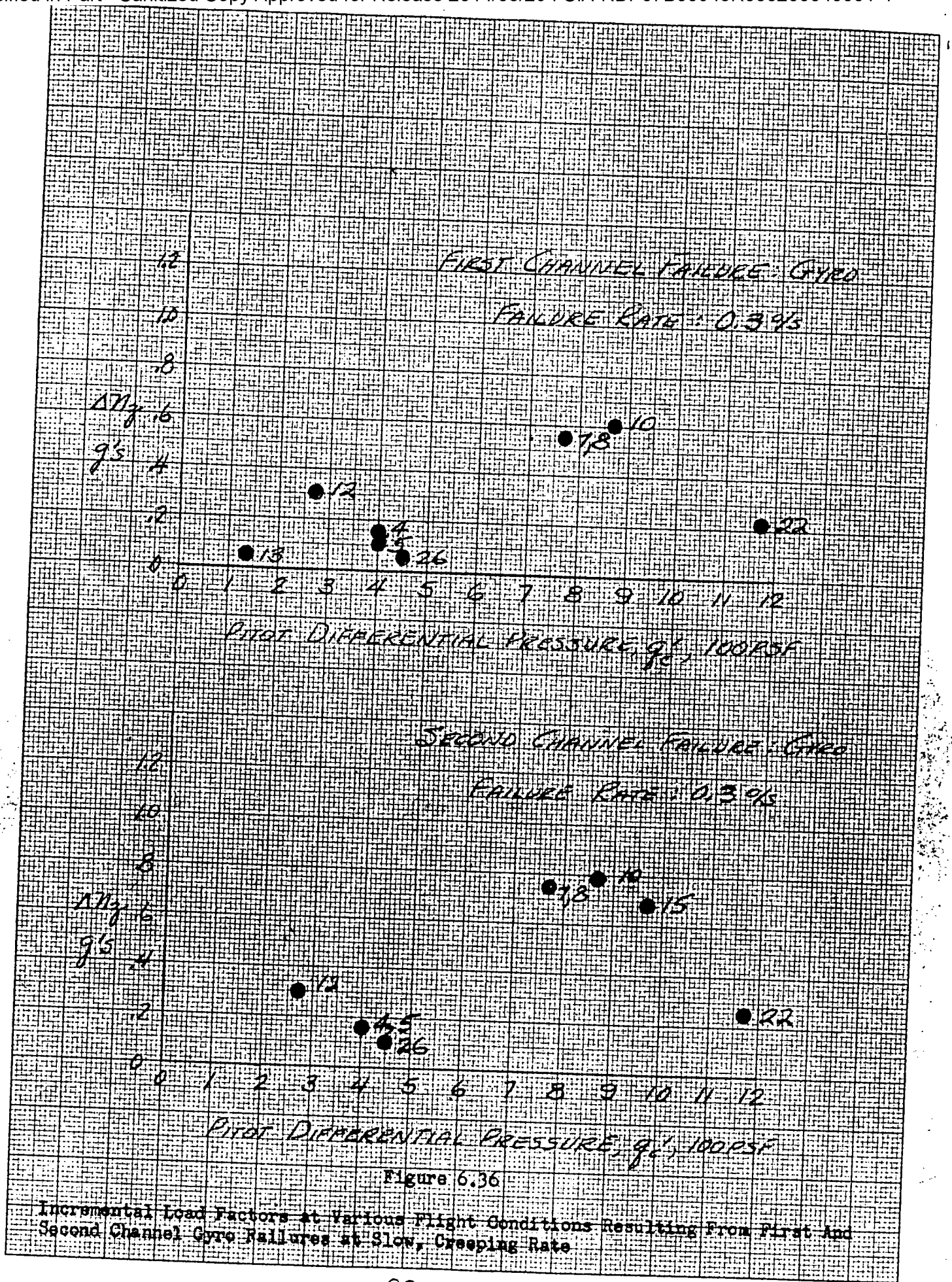

Figure 6.36

Incremental Load Factors at Various Flight Conditions Resulting From First And Second Channel Gyro Failures at Slow, Creeping Rate

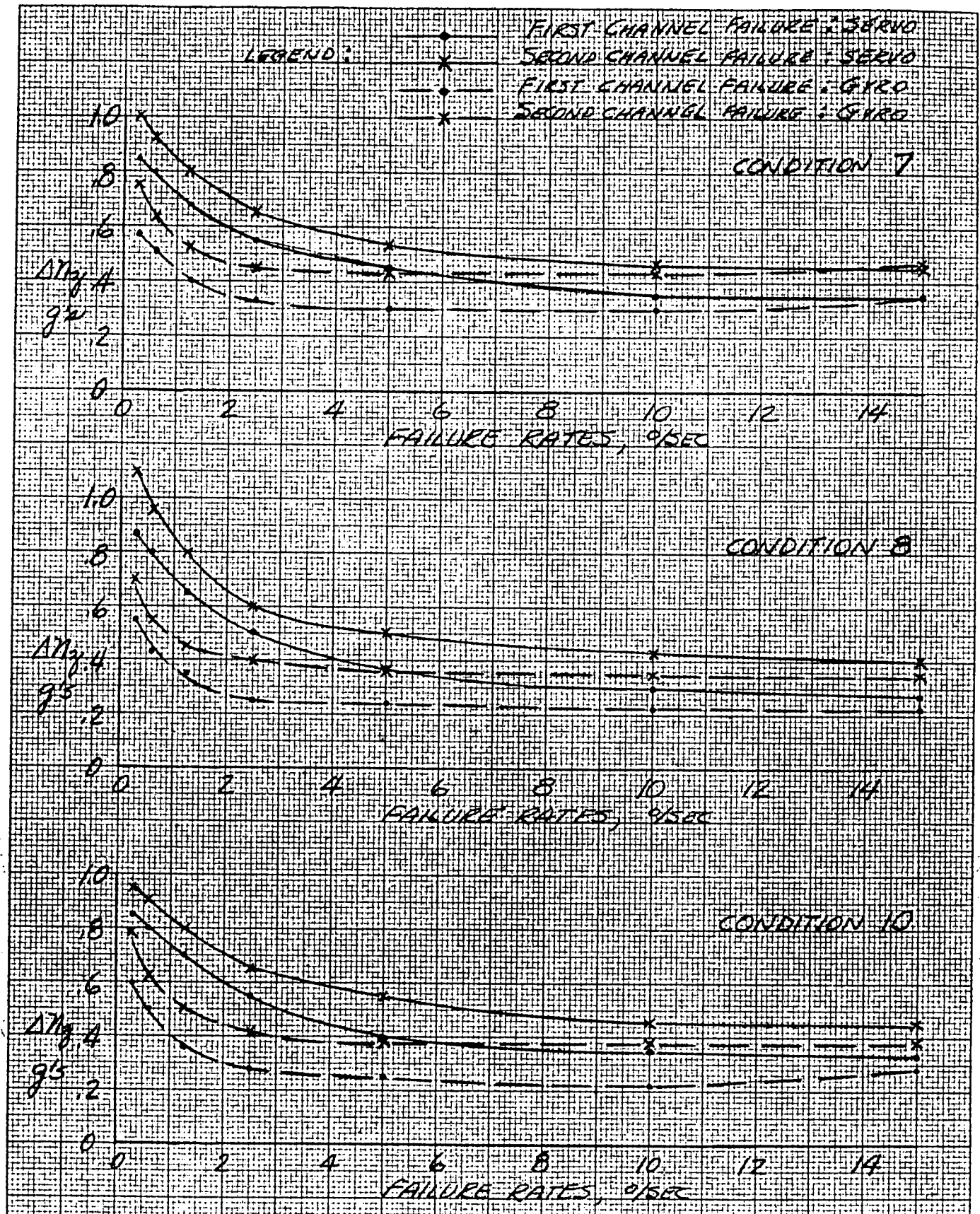

Figure 6.37

Comparison of Load Factors Resulting From First and Second Channel Servo and Gyro Failures at Critical Flight Conditions 7, 8, and 10

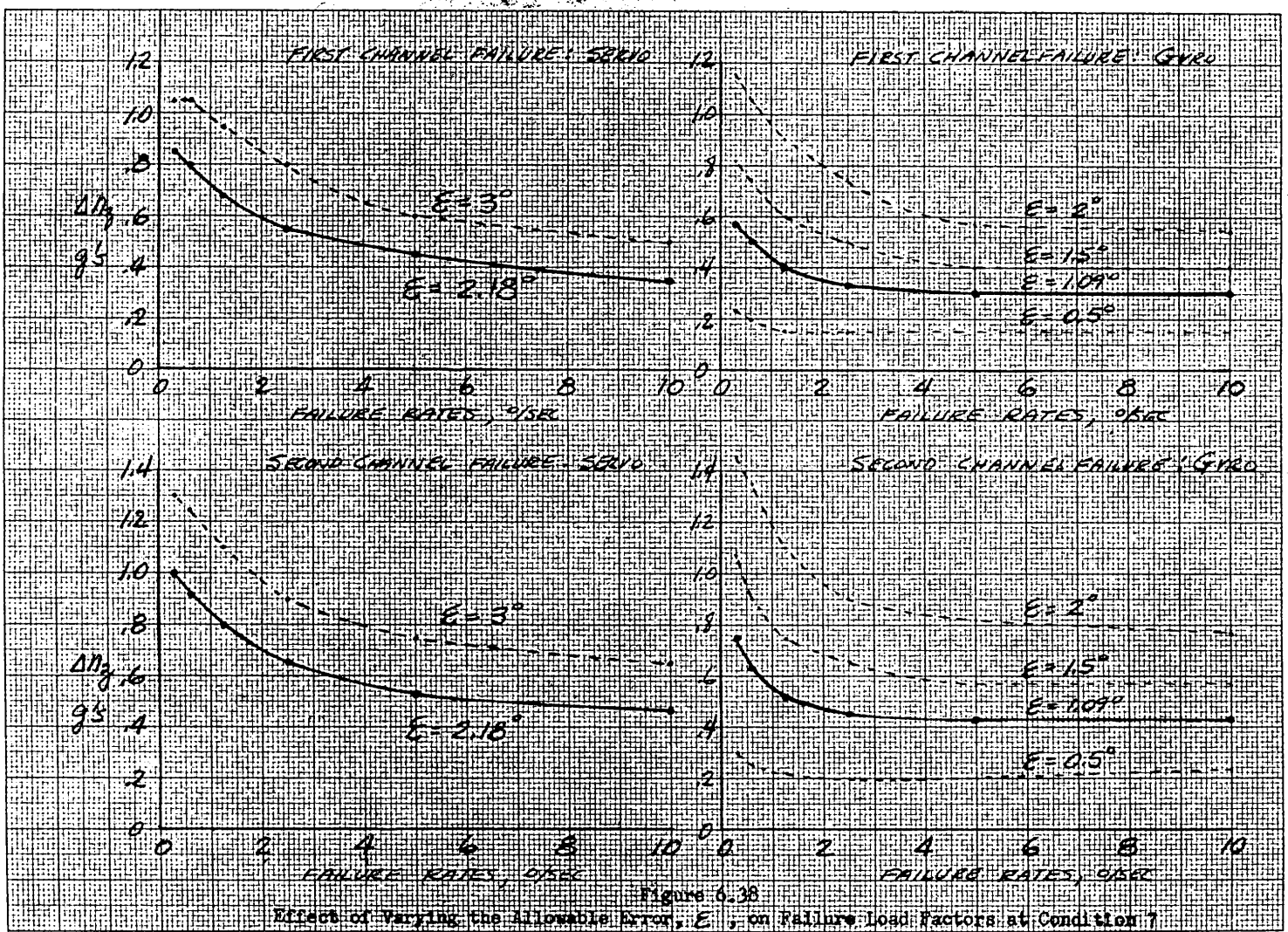

Figure 6.38
Effect of Varying the Allowable Error, ε, on Failure Load Factors at Condition 7

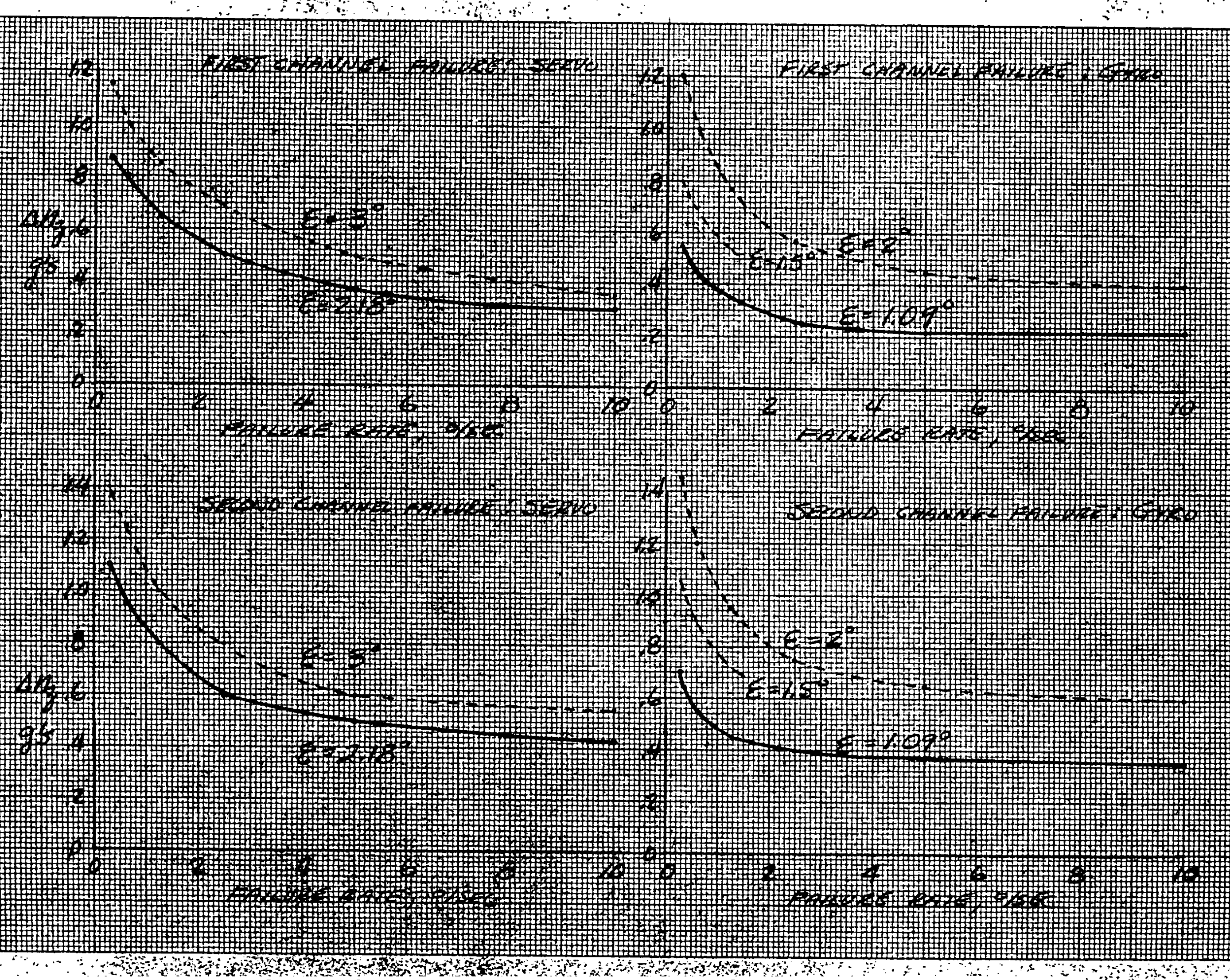

Figure 6.39

Effect of Allowable Error, ε, Variations on Failure Load Factors at Condition 8

Declassified in Part - Sanitized Copy Approved for Release 2014/05/29 : CIA-RDP67B00945R000200040001-4